Monitoring and Predicting Forest Growth and Dynamics

Three Dimensional — Coupled Model Carbon Cycle — Forest Ecosystem Module's Theoretical Bases

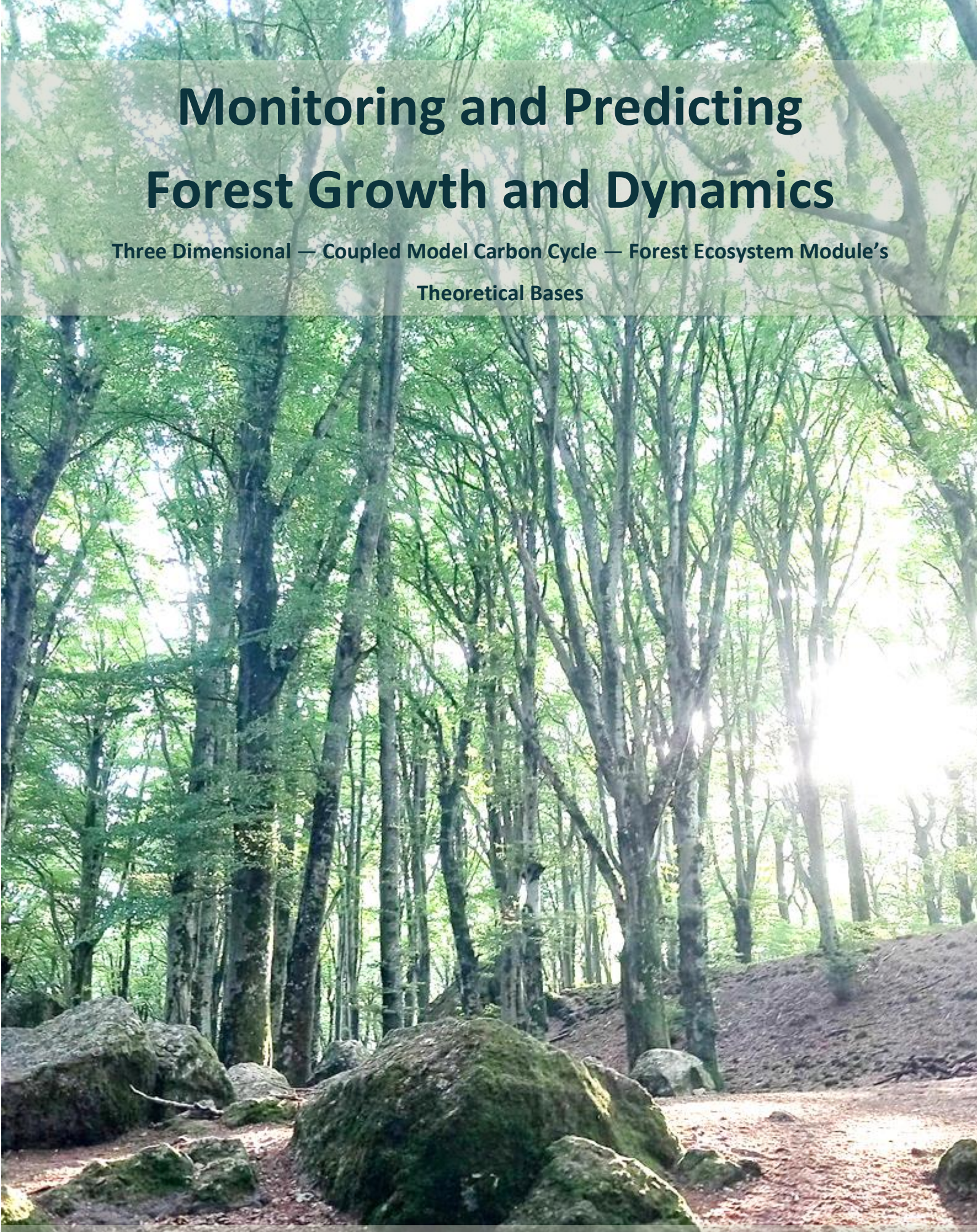

Forest Modelling Laboratory
National Research Council of Italy
Institute for Agriculture and Forestry Systems in the Mediterranean (CNR-ISAFOM)
Via Madonna Alta 128 – 06128 Perugia (PG), Italy

Monitoring and Predicting Forest Growth and Dynamics

Three Dimensional – Coupled Model Carbon Cycle – Forest Ecosystem Module's Theoretical Bases

A. COLLALTI, D. DALMONECH, E. VANGI, G. MARANO, P.F. PUCHI, M. MORICHETTI, V. SAPONARO, M.R. ORRICO, E. GRIECO

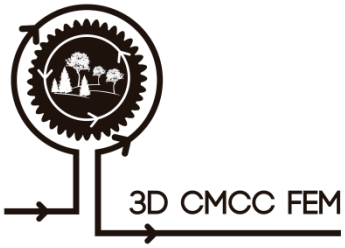

edizioni
Consiglio Nazionale delle Ricerche

National Research Council of Italy

Institute for Agricultural and Forestry Systems in the Mediterranean (CNR-ISAFOM)

Piazzale Aldo Moro, 7 - 00185 Roma

ISBN: 978 88 8080 655 4 (electronic edition)

DOI: https://doi.org/10.32018/ForModLab-book-2024

Consiglio Nazionale delle Ricerche

CNR - ISAFOM

Cover image: Old growth beech forest of Monte Cimino, Viterbo (Italy). Photo credit: A. Collalti

To our parents,

and to our children

Alessio Collalti

alessio.collalti@cnr.it

Institute for Agriculture and Forestry Systems in the Mediterranean of the National Research Council of Italy (CNR- ISAFOM)
Via della Madonna Alta, 128 - 06128 Perugia (PG) Italy; *National Biodiversity Future Centre (NBFC)*, Piazza Marina, 61 - 90133 Palermo (PA) Italia

https://www.forest-modelling-lab.com/alessio-collalti

Alessio Collalti has a Master's in Natural Sciences from ''La Sapienza'' University of Rome and a Ph.D. in Forest Ecology at the University of Tuscia (Viterbo). His background concerns Forest Ecology, Carbon and Nitrogen Cycle, and Forest and Vegetation Modelling, particularly concerning vegetation numerical modelling and response under natural and anthropogenic stress, including climate change impacts and forest management scenarios. He has been working at the University 'La Sapienza' (Rome), University of Tuscia (Viterbo), at the Foundation euro-Mediterranean Centre on Climate Change (CMCC), and at the National Research Council of Italy (CNR), where he developed the 3D-CMCC-FEM ('*Three Dimensional — Coupled Model Carbon Cycle — Forest Ecosystem Module*'). He is currently a senior researcher and the Forest Modelling Laboratory Head at the National Research Council of Italy (CNR) at the Institute for Agricultural and Forestry Systems in the Mediterranean (CNR-ISAFOM) and is now jointly with the National Biodiversity Future Centre (NBFC).

Daniela Dalmonech

daniela.dalmonech@cnr.it

Institute for Agriculture and Forestry Systems in the Mediterranean of the National Research Council of Italy (CNR- ISAFOM)
Via della Madonna Alta, 128 - 06128 Perugia (PG) Italy; *National Biodiversity Future Centre (NBFC)*, Piazza Marina, 61 - 90133 Palermo (PA) Italia

https://www.forest-modelling-lab.com/daniela-dalmonech

Daniela Dalmonech has a Master in environmental engineering from the University of Trento with a focus on numerical modelling applied to the environment, she holds a Ph.D. in Forest Ecology attained at the Tuscia University and a postdoctoral grant at the Max Planck Institute for Biogeochemistry in Jena (Germany) within the Innovative Training Networks (ITN) Marie-Skłodowska-Curie actions 'Green cycles II: Global Biosphere Climate Interactions'. She is interested in the dynamics of the carbon and nitrogen cycle at different spatial scales and under anthropogenic and natural stress, through numerical modelling and statistical analyses. In 2019 she started collaborating with the Forest Modelling Laboratory, where she is responsible for the 3D-CMCC-FEM code development and output data analyses. She is a researcher at the Institute for Agricultural and Forestry Systems in the Mediterranean (CNR-ISAFOM) within the National Biodiversity Future Centre (NBFC).

Elia Vangi

elia.vangi@isafom.cnr.it

Institute for Agriculture and Forestry Systems in the Mediterranean of the National Research Council of Italy (CNR- ISAFOM)
Via della Madonna Alta, 128 - 06128 Perugia (PG) Italy

https://www.forest-modelling-lab.com/elia-vangi

Elia Vangi has a master's degree in Forest Systems Sciences and Technologies from the University of Florence. His interest includes but is not limited to forest modelling through remote sensing data, and spatialization of environmental variables, particularly in growing stock volume trends and the carbon cycle. He completed a Ph.D. in Environmental Ecology at Molise University, where his main focus was the development of a spatial approach for the high-resolution yearly prediction of forest growing stock volume and above-ground carbon pool. Other interests include the analysis of the new data from the Global Ecosystem Dynamics Investigation (GEDI), a high-resolution laser ranging of Earth's forests, and topography from the International Space Station (ISS). At the CNR-ISAFOM Forest Modelling Lab, he is engaged in the assimilation of remotely sensed and inventory data for the development, implementation, and use of the 3D-CMCC-FEM forest model. He is an R enthusiastic user.

Gina Marano

gina.marano@usys..ethz.ch

Forest Ecology, Institute of Terrestrial Ecosystems, Department of Environmental Systems Science, ETH Zurich, Universitätstrasse 16, 8290, Zurich, Switzerland; Institute for Agriculture and Forestry Systems in the Mediterranean of the National Research Council of Italy (CNR- ISAFOM) Via della Madonna Alta, 128 - 06128 Perugia (PG) Italy

https://www.forest-modelling-lab.com/gina-marano

Gina Marano is currently a Ph.D. student in Forest Ecology at ETH Zürich. Her research work focuses on developing alternative formulations of soil water dynamics to better represent drought impacts on long-term forest dynamics, in particular on stand growth and biomass production, species competition/composition, and mortality. Within the Forest Modelling Laboratory, she focused on studying and assessing soil physical processes in the 3D-CMCC-FEM model and testing the 3D-CMCC-FEM model by simulating different silvicultural interventions under climate change scenarios. In her past work at the University of Napoli Federico II she provided scientific support for the development of informatic tools over geoSpatial Decision Support Systems to support Sustainable Forest Management practices at the local scale. She believes in transparent and open science, gender justice, and the power of the Force.

Paulina F. Puchi

paulina.puchi@isafom.cnr.it

Institute for Agriculture and Forestry Systems in the Mediterranean of the National Research Council of Italy (CNR- ISAFOM)
Via della Madonna Alta, 128 - 06128 Perugia (PG) Italy; *Institute of Bioeconomy, Italian National Research Council (CNR-IBE),* Via Madonna del Piano, 10 - 50019 Sesto Fiorentino (FI) Italy

https://www.forest-modelling-lab.com/paulina-puchi

Paulina F. Puchi is a forest ecologist with a background in eco–hydrology, dendrochronology, and quantitative wood anatomy. Her research has focused on a better understanding of how trees are adapting to climatic

variability and extreme climatic events. She has implemented novel techniques such as retrospective quantification of wood anatomical traits (i.e. lumen area, cell wall thickness) and stable isotope analysis to unravel the mechanism that trees performed during drought at long-time scales. Paulina received her bachelor's degree from Universidad Austral de Chile (Valdivia, Chile) in Conservation of Natural Resources Engineering, and her Ph.D. from the University of Padua (Legnaro, Italy) in Land, Environment, Resources, and Health. In 2016, before she started her Ph.D., she spent one year at the University of La Republica (Montevideo, Uruguay) in the Faculty of Sciences teaching dendrochronology to professors and students. After she finished her Ph.D., she was awarded by the Department of Land, Environment, Agriculture and Forestry (University of Padua) with a postdoctoral Fellowship for studying Eddy Covariance series and woody biomass to investigate carbon sink activity in conifer stands. Currently, she has a joint postdoctoral position at National Research Council of Italy (CNR) - Institute of Bioeconomy (CNR-IBE) and the Institute for Agricultural and Forestry Systems in the Mediterranean (CNR-ISAFOM) to perform modelling and analysis of carbon and water dynamics in forest and pasture systems in response to water stress.

Mauro Morichetti

mauro.morichetti@cnr.it

Institute for Agriculture and Forestry Systems in the Mediterranean of the National Research Council of Italy (CNR- ISAFOM)
Via della Madonna Alta, 128 - 06128 Perugia (PG) Italy

https://www.forest-modelling-lab.com/mauro-morichetti

Mauro Morichetti has a master's degree in Environmental Engineering from the Polytechnic University of Marche (Ancona, Italy), where he developed the basics of CTMs (Chemical Transport Models) at a regional and urban scale; afterward, he obtained a Ph.D. in Industrial Engineering at the Department of Mathematical Sciences and Industrial Engineering (Ancona, Italy). From the first year of his Ph.D., he has been working with the regional WRF-Chem (Weather Research and Forecasting Model with Chemistry-NCAR) model, focusing specifically on biogenic volatile organic compounds, natural aerosols, and the atmospheric interactions between them. Since 2019 he has had a postdoctoral grant at the National Research Council of Italy, Institute of Atmospheric and Climate Sciences, (CNR-ISAC). From January 2024 he has been working at the Institute for Agricultural and Forestry Systems of the Mediterranean (CNR-ISAFOM) as modeller.

Vincenzo Saponaro

vincenzo.saponaro@isafom.cnr.it

Institute for Agriculture and Forestry Systems in the Mediterranean of the National Research Council of Italy (CNR- ISAFOM)
Via della Madonna Alta, 128 - 06128 Perugia (PG) Italy; *Department for Innovation in Biological, Agro-Food and Forest Systems (UNITUS-DIBAF) University of Tuscia*, Via S. Camillo de Lellis, snc - 01100 Viterbo (VT) Italy

https://www.forest-modelling-lab.com/vincenzo-saponaro

Vincenzo Saponaro has a master in Ecobiology at the University 'La Sapienza' (Rome). He worked at the Department of Agriculture, Food and Environment of the University of Pisa in a project focused mostly on advancing the concept of hyperspectral phenotyping of plant stress, across a range of plant species and over a

variety of stressors. Currently is a Ph.D. student in Forest Ecology at the University of Tuscia (Viterbo) and at the CNR-ISAFOM of Perugia to study the interaction between primary productivity exacerbated by climate change across Europe. He is fascinated by science and its power, he fights for Nature and Human Rights.

Maria Rosaria Orrico

mariarosaria.orrico@cnr.it

Institute for Agriculture and Forestry Systems in the Mediterranean of the National Research Council of Italy (CNR- ISAFOM)
Via Cavour, 17 - 87036 Rende (CS) Italy

Maria Rosaria Orrico is a technician at the National Research Council of Italy (CNR) – Institute for Agriculture and Forestry System in the Mediterranean (CNR-ISAFOM). During her tenure, the Director confers her the responsibility of both the secretariat management and the protocol service of the Institute. During the organisation of scientific-informative events and conferences, she manages the logistic aspects of locations, invitation and registration of participants and the production of graphic works (flyer, brochure, poster) for the dissemination of results of the research in which the Institute is involved.

Elisa Grieco

elisa.grieco@cnr.it

Institute for Agriculture and Forestry Systems in the Mediterranean of the National Research Council of Italy (CNR- ISAFOM)
Via della Madonna Alta, 128 - 06128 Perugia (PG) Italy

https://www.forest-modelling-lab.com/elisa-grieco

Elisa Grieco is a technologist at the National Research Council of Italy (CNR) - Institute for Agriculture and Forestry Systems in the Mediterranean (CNR-ISAFOM). She works on administrative and scientific management of European projects and supports for research, communication and dissemination of project results including planning of project activities through coordination actions of working groups. Previously, she worked at the Institute of BioEconomy (CNR-IBE) on strengthening communication to support research and technology transfer in agriculture and rural development in Senegal. She has a Ph.D. in Forest Ecology and a degree in Forest and Environmental Science attained at the University of Tuscia (Viterbo). She worked on supporting EU-Africa cooperation on research infrastructure for food security and GHG observations, she was part of the coordination office of European projects. Her professional journey included deforestation assessment in tropical forests. She worked on projects for the installation of Eddy Covariance Flux Tower in the Ankasa Conservation Area (Ghana) where she also analysed carbon stock dynamics after deforestation and the impact of land use change in the region. Her expertise focuses on sustainable development, food security, land use change, forestry, and climate change adaptation and mitigation.

CONTENTS

Figures

PREFACE

The concept of Anthropocene, although still under scrutiny by the global scientific community, has been widely accepted as representing a unique, time interval in Earth's history that reflects an abrupt and largely irreversible departure of the Earth System away from the relatively stable environmental conditions of about the last 10,000 years, the Holocene, into a new and still-evolving state where the whole biosphere is, in some way, under the influence of mankind. Human society must therefore assume responsibility for the stewardship of the Earth system, guided by the principles and concepts of the science of sustainability, since scientific evidence shows that even the most remote and natural places of our planet are influenced, even dominated, directly or indirectly, by the impact of our various economic activities. If there are no ecosystems that can be said to be outside of our influences, we must ask ourselves the question of what their impacts are and what actions must be undertaken to mitigate their effects and encourage, to varying degrees, their adaptation and resilience.

Forest ecosystems are among the most important green infrastructures at the European and global scale; they are key elements to preserve biodiversity and to achieve carbon removal and climate mitigation targets at continental and global scale, to attain carbon neutrality by 2050. However, it is crucial to combine forest-based mitigation with adaptation as climate change is already heavily impacting through forest disturbances on carbon sequestration in forests and their products.

The book '*Monitoring and Predicting Forest Growth and Dynamics*' on the theoretical background underlying the '*Three Dimensional — Coupled Model Carbon Cycle — Forest Ecosystem Module*' (3D-CMCC-FEM), by Alessio Collalti and his colleagues, is a highly needed instrument to provide forest ecologists, silviculturalists and forest planners with innovative and state-of-the-art technologies and tools to assess and understand how climate change may affect forest ecosystems, forestry activities, and forest production. In fact, informed actions on strategic forest policy and planning need to be based on robust data reflecting an urgent need for a more transparent, harmonised, and robust monitoring framework.

The work by Collalti et al. adds to the vast production of modelling tools developed even since the years 70's and 80's by forest ecologists and silviculturalists from all over the world, but is characterized for a complete and detailed analysis, at a range of spatial scales, of tree and forest growth, incorporating important drivers and processes as radiation interception, carbon dynamics, nutrient uptake and cycling and water relations. Other significant components of this multifaceted numerical tool deal with such important, but still poorly simulated aspects of forest dynamics, as natural regeneration and mortality, structural diversity, and disturbances, including man-made silvicultural regimes and operations.

The increasing trend in the frequency of environmental disturbances (fires, wind, parasites) and mega-disturbances (combined heat waves and drought) are making the stability of forest ecosystems, especially temperate and boreal forests, increasingly critical. Apart from the growing need for wood as a renewable

and low-carbon biomaterial, for the world bio-economy, a strong motivation in favour of active forest management derives precisely from the opportunities provided by silviculture to promote the adaptation and resilience of forest ecosystems in comparisons of environmental changes at a global level.

Modelling tools, as the '*Three Dimensional — Coupled Model Carbon Cycle — Forest Ecosystem Module*' (3D-CMCC-FEM), together with silvicultural experiments, flux measurements and remote sensing, are fundamental to understand the role of forest management options (i.e. even-aged vs uneven-aged forest structures, thinning, non-uniform cuts and spatial heterogeneity), combining the function of mitigation and allocation of carbon in the ecosystem with the recognition of other fundamental processes, such as structural and genetic diversification, to ensure long-term ecosystem adaptation in the context of environmental change. Furthermore, the study of the effects of silvicultural management is even more important in the Mediterranean environment, considered particularly vulnerable to the impact of climate change.

Forest management is currently the subject of a heated scientific and political debate in relation to the objectives of carbon accumulation and resilience to climate change. Trees absorb carbon dioxide from the atmosphere, but at the same time, wood can replace fossil fuels and other carbon-intensive materials such as concrete and steel, with great benefits for climate mitigation and in accordance with various international Conventions on environmental issues. However, while much has been learned about the carbon cycle in forests, there are still too many gaps in our knowledge. The 3D-CMCC-FEM by Alessio Collalti and his team is a remarkable contribution to help scientists and forest managers, in the years to come, to better understand and to identify scenarios and options on the functioning and management of forest ecosystems oriented towards climate-adaptive forestry, the storage of C in longer-lived wood products, and the conservation of forests with greater ecological value, to eventually increase the contribution of the forestry sector to the mitigation of total carbon emissions in Europe, and worldwide.

Prof. Giuseppe Scarascia-Mugnozza

University of Tuscia (Viterbo) & European Forest Institute (Rome)

Via Manziana 30, 00189 Rome, Italy

The book '*Monitoring and Predicting Forest Growth and Dynamics*' describes the theoretical background underlying the '*Three Dimensional — Coupled Model Carbon Cycle — Forest Ecosystem Module*' (3D-CMCC-FEM), developed by Alessio Collalti and his team at the Forest Modelling Laboratory of the National Research Council of Italy. The model is, in our view, a remarkable piece of work. It incorporates virtually all current, and relevant historical knowledge, about tree physiology and the interactions between physiological processes and environmental conditions. Their book describes the history, development, and refinement of 3D-CMCC-FEM which, it could be said, is representative of the general evolution of ecosystem models. These have developed from those that deal with forest canopies as single leaves ('big leaf' models) to those with multiple foliage layers, with climatic inputs ranging from monthly data to daily time-steps, and spatial resolutions reduced from a square kilometre down to 100 square meters. 3D-CMCC-FEM produces detailed predictions of almost every aspect of tree and forest growth, incorporating detailed calculations of radiation interception at various levels with sub-routines for (among other processes) carbon dynamics, nutrient uptake and cycling and water relations. It uses daily weather data as inputs and can provide multi-variable outputs for daily or monthly time steps.

As such things must, 3D-CMCC-FEM builds on the base provided by earlier work of this kind: in this respect, our much simpler 3-PG model, written 25 years ago, which remains a widely used operational and research tool, was an important part of the foundation, but there were of course, many others. They are reviewed and acknowledged in the section on 'Model History', which provides a good and comprehensive introduction to the ideas behind the model, and review of the works that influenced it. It is interesting to note that the evolution of 3D-CMCC-FEM from 3-PG, which uses about 100 lines of code, has involved writing 30,000 lines of code, which might give pause for thought with regard to bugs and errors. The code for 3D-CMCC-FEM is free (it can be downloaded from GitHub, a repository for codes), anyone can download, use, and implement it, provided that they cite the authors and provided it is not used for commercial purposes. Making the code freeware, albeit under some understandable constraints, is important: without that 3D-CMCC-FEM would not become widely used, however good it is. The authors have made the code available to thousands of collaborators and the model has been, and is being, widely and thoroughly tested. This approach provides some insurance in relation to the matter of errors and de-bugging: with hundreds possibly thousands of scientists using and testing the model, most problems will be identified and solved.

An obvious drawback to this kind of model may be the high demand for initialisation data, and the detailed data needed to test and parameterize the various sub-models and sub-routines. However, the widespread collaborative testing that is being done will ensure that many of the data required will be obtained. Furthermore, the global network of eddy-flux towers, where carbon and water vapor exchange are monitored continuously, provides detailed data that can be used as inputs to 3D-CMCC-FEM and to test its outputs.

In recent years the frequency of global coverage by satellites has increased from a few days per month to almost daily, while spatial resolution has improved from square kilometres down to 100 square meters, or

less. Furthermore, the spectro-resolution of satellite-borne sensors has increased to the extent that changes in biodiversity can often be discerned. It has therefore become increasingly feasible to examine the consequences of planned and unplanned disturbances at a range of spatial resolutions. Combining satellite coverage with airborne LiDAR measurements allows identification, analysis and validation of detailed structural changes in forests at spatial scales across large regions where, in the past, only major disturbances could be recognised. 3D-CMCC-FEM therefore provides very powerful tools for assessing the consequences of planned and unplanned forest disturbances, and the impacts of adverse conditions, at a range of spatial resolutions. The assessments can include impacts on wood production as well as evaluations of the roles of forests as ecosystems in the global carbon balance and in hydrology. It follows that, in this era of climate change, 3D-CMCC-FEM provides an excellent tool for assessing the effects of predicted changes in climate, whether they be in temperature regimes, atmospheric CO_2 concentrations or water regimes. Used in association with powerful modern remote sensing and LiDAR measurements, the prospects are good for accurate, tested analytical predictions of climatic impacts as well as evaluations of the effects of management of forests for wood production and assessments of their roles in global carbon balance, hydrology and as ecosystems.

3D-CMCC-FEM is now freely available to download. This means that the model can be widely tested and further improved by scientists and practitioners around the world. All will have the opportunity to test the model in many ways, including the extent that monthly time-steps, with much-reduced data requirements, provide suitable information for foresters and environmentalists to make many practical decisions. We congratulate the authors on this contribution and look forward to their model's widespread usage.

Prof. Emeritus Richard (Dick) H. Waring

Marcus Wallenberg Prize 2020 in Forestry Winner

2911 NW 13th Place, Corvallis, Oregon, U.S.A.

Prof. Emeritus Joseph J. (Joe) Landsberg

Marcus Wallenberg Prize 2020 in Forestry Winner

Dudley Street, Ivanhoe, Victoria, Australia

Models should be useful. Developing a useful model of nature requires vision, choices, perseverance, and communication. Vision should answer the questions 'Useful to whom? And for what?'. A clear vision guides the hard choices around what facets of the real world to include and exclude, what to allow to evolve dynamically and what to fix in place, what to connect and what to isolate.

Clear vision and strategic choices and compromise are rarely achieved in a straight-line path. Building a model that can serve as a trusted and robust scientific instrument requires an iterative approach and a willingness to revisit and revise, to evaluate and adapt, and to persevere in the face of inevitable false starts and dead ends. Communicating vision and choices is the difficult 'last mile' that can bring a potentially useful model to life as a tool that actually gets used to help us understand nature, to anticipate the dynamics of the real world, and to explore our own influence on possible futures.

Collalti and co-authors rise to all these challenges in their current work on '*Monitoring and Predicting Forest Growth and Dynamics*'.

Numerical models of forest processes have a decades-long history of development and application, and here the authors give us both a clear view of that history and a compelling vision for how their own model is positioned in the current landscape to serve important and previously unmet needs. They build up a rational picture of the current model structure and function based on decisions made through 13 years of iterative model development and evaluation. Just as importantly, they show us what the current model lacks, what new capabilities are currently in development, and where its fitness for its intended purpose can be extended and improved in future versions.

Collalti et al. tell us that their model of forest growth and dynamics (3D-CMCC-FEM) is intended to represent the connected system of trees, litter, and soil and the accumulated quantities and fluxes of energy, water, carbon, and nutrients within and through that system. The model is primarily a research tool and is updated over time to include the latest process understanding. Diameter at Breast Height (DBH) is a central organizing concept, making it clear that the model is designed to be informed by and evaluated against the fundamental observable quantity of a forest at the stand scale. Consistent with a stand-level conceptualization of forest ecosystem processes, individual trees are not represented explicitly. Instead, they are aggregated into classes based on similarity, with the model tracking characteristics of the average individual tree and the number of such individuals in each class. These choices make it clear that the model is intended to bring state-of-the-art science to the service of a working forester or land manager, informing real-world decisions at the scales where assessment is carried out and actions are implemented.

The unique flexibility and utility of 3D-CMCC-FEM starts with its grounding in diameter a breast height and grows out from there through a nested hierarchical organization that captures observable variance in species, stem diameter, tree height, and age. By clustering stand-level variance represented by many individuals into discrete categories for height, stem diameter, and age for different species, this model structure allows prediction of stand dynamics as influenced by competition for light, space (crown area), and water.

This is done with a minimal computational cost compared to models simulating stand structure and function at the scale of individual trees. Species-level details of plant physiology studied at the scale of leaves and individual trees are applied within this structure to bring sensitivity to driving factors such as temperature, moisture availability, and atmospheric CO_2 concentration to predictions of evolving growth rates and stand structure, augmenting the stand-level measurements accessible to most forest managers. This hierarchical system makes it possible to simulate a wide range of management practices such as thinning, variable rotation lengths, mixed species stands, and fertilization, all under multiple potential future climate scenarios.

Every aspect of the model structure and function described here is supported by empirical study, usually with multiple published results from the 3D-CMCC-FEM team and their collaborators to underpin each major model component or process. The team is as capable in the field as they are at the keyboard, which brings increased value to both the empirical studies and to the modelling results.

The development also borrows strategically from approaches used successfully in other models, for example in the areas of crown area dynamics, temperature acclimation, and litter decomposition. Model uncertainty is presented in a realistic light. Key figures show the expected range of variability in simulated forest structure and function compared to observations across a broad range of sites and species. Given the fundamental basis of the model in stem diameter measurements, the figures in Chapter 6 (Forest Dendrometric and Structural Attributes) are especially helpful.

The model is relatively unbiased and it captures a majority of the observed variance in many stand attributes, but the real world has significant sources of variance the model fails to capture. By seeing these metrics the practitioner can make informed decisions about how to use the simulation results. The authors clearly address the areas where further development is underway, or planned, or needed. For example, while nitrogen pools and fluxes are included in the tree, litter, and soil components there is not yet a representation of limitations to microbial processes or plant growth in relation to mineral nutrient supply.

Similarly, the dynamics of cohort merging under long sequences of disturbance and regeneration is identified as a topic for future development. Requirements for stand initialization are an important limitation of the current model structure, and this is also explicitly addressed at multiple points in the description of model processes and in the exploration of model uncertainty. Initial conditions for stand structure including species, density, diameter at breast height, height, and age are specified by the user.

Species-specific parameters defining plant physiological relationships and allometry are also prescribed. Even with an accurate description of stand conditions and environmental factors and forcing, any parametric or structural biases or misrepresentations within the model will cause anomalies in the modelled fluxes and state variables in the early stages of each simulation. The authors see and document this behaviour in several places. Other work has shown that model spin-up procedures are required to avoid these anomalies, and Collalti and co-authors are clear in stating that such procedures are not yet in place for 3D-CMCC-FEM. This

is likely to be an important area for future development and could help to make an already very capable and impressive model even more useful for its intended applications.

Dr. Peter E. Thornton

Corporate Fellow, Environmental Sciences Division

Director, Climate Change Science Institute

Oak Ridge National Laboratory

Oak Ridge, Tennessee, USA

TABLE OF SYMBOLS

The following is a list of major symbols used in this book. Each symbol is defined with a short description and its unit. When a variable has, and/or is computed by, more than one temporal scale (e.g. GPP) we use a generic definition of 'time' considering that it can be expressed (and computed by) more than one temporal scale (e.g. day^{-1}, $month^{-1}$, and $year^{-1}$). This table is conceived to enable readers to interpret equations, formulas, and theoretical frameworks. For a complete list of symbols or variables, see Collalti et al. (2023).

Symbol	***Description***	***Units***
APAR	Absorbed photosynthetic active radiation	$molPAR^{-2}\ day^{-1}$
A_r	Temperature correction factor for R_m acclimation	—
ASW	Available soil water	$mm\ m^{-2}$
ASW_{FC}	Available soil water at field capacity	$mm\ m^{-2}$
a_S	Sub-optimal carbon allocation fraction to stem	—
a_L	Sub-optimal carbon allocation fraction to leaves	—
a_R	Sub-optimal carbon allocation fraction to roots	—
BA	Basal area	$m^2\ ha^{-1}$
bb	Exponent for decomposition	—
BPE	Biomass production efficiency	—
CAI	Current annual increment	$m^3\ ha^{-1}\ year^{-1}$
CC	Canopy cover projection	$m^2\ cell\ size^{-1}$
$Ccond_{s\,x}$	Species-specific parameter defining the closure degree of stomata with VPD	mbar
C_p	Specific heat of the air	$W\ m^{-2}$
CRA_x	Species-specific parameter for the Chapman-Richards equation	—
CRB_x	Species-specific parameter for the Chapman-Richards equation	—
CRC_x	Species-specific parameter for the Chapman-Richards equation	—
CUE	Carbon use efficiency	—
DBH	Diameter at breast height	cm
ET	Evapotranspiration	$mm\ time^{-1}$
fx	Multipliers or scaling factors (generic)	—
gC	Canopy conductance	$m\ sec^{-1}$
GDD	Species-specific parameter for growing degree day for vegetation start	°C
$GDD_{seed\,x}$	Species-specific parameter for growing degree day for germination	°C
$gl_{bl\,x}$	Species-specific parameter for boundary layer conductance	$m\ sec^{-1}$
$gl_{C\,x}$	Species-specific parameter for cuticular conductance	$m\ sec^{-1}$
GPP	Gross primary production	$gC\ m^{-2}\ time^{-1}$
g_s	Stomatal conductance	$m\ sec^{-1}$
$g_{s\,max\,x}$	Species-specific parameter for maximum stomatal conductance	$m\ sec^{-1}$
g_sWUE	Stomatal water use efficiency	$gC\ m^{-2}\ year^{-1}$ or $KgH_2O\ year^{-1}$
H_{fus}	Latent heat of fusion	$kJ\ kg^{-1}$

H_{sub}	Latent heat of sublimation	kJ kg^{-1}
I_o	Incoming shortwave radiation	W m^{-2} or MJ m^{-2} day^{-1}
iWUE	Intrinsic water use efficiency	gC m^{-2} $time^{-1}$ or KgH_2O $time^{-1}$
J_{cmax}	Maximum rate of electron transport at current temperature	µmol m^{-2} s^{-1}
J_{cmax25}	Maximum rate of electron transport at 25 °C	µmol m^{-2} s^{-1}
k_{l_s}	Decomposition rate for litter (soil)	$year^{-1}$
k	Species-specific light extinction coefficient	—
$K_m^{CO_2}$	Michaelis-Menten Rubisco affinity coefficients for CO_2	µmol mol^{-1} CO_2
K_O	Michaelis-Menten inhibition coefficient for O_2	µmol mol^{-1} O_2
LAI	Leaf area index	m^2 m^{-2}
M_{age}	Age mortality factor	—
MAI	Mean annual increment	KgC m^{-2} or MgC cell $size^{-1}$
M_b	Background mortality factor	—
$Nage_x$	Species-specific parameter controlling the power of relative age in f_{age} in age modifier	—
NEE	Net ecosystem exchange	gC m^{-2} $time^{-1}$
NEP	Net ecosystem production	gC m^{-2} $time^{-1}$
NPP	Net primary production	gC m^{-2} $time^{-1}$
NPP_{woody}	NPP for woody pools	gC m^{-2} $time^{-1}$
P	Air pressure	Pa
PAR_0	Incoming photosynthetic active radiation	molPAR^{-2} day^{-1}
PAR_{refl}	Reflected photosynthetic active radiation	molPAR^{-2} day^{-1}
R_a	Autotrophic respiration	gC m^{-2} $time^{-1}$
$Rage_x$	Species-specific parameter controlling the Relative age to give f_{age} = 0.5 in age modifier	—
rbl	Boundary layer resistance	m sec^{-1}
R_{eco}	Ecosystem respiration	gC m^{-2} $time^{-1}$
R_g	Growth (or synthesis) respiration	gC m^{-2} $time^{-1}$
R_{gas}	Gas law constant	m^3 Pa $molK^{-1}$
R_h	Heterotrophic respiration	gC m^{-2} $time^{-1}$
rh	Resistance to sensible heat flux	m sec^{-1}
rhr	Combined resistance to convective and radiative heat transfer	m sec^{-1}
R_m	Maintenance respiration	gC m^{-2} $time^{-1}$
R_n	Net radiant energy flux	W m^{-2}
rv	Resistance to water vapour flux	m sec^{-1}
$SAP_{A\,x}$	Species-specific parameter reflecting constant in sapwood area vs. DBH relationship	—
$SAP_{B\,x}$	Species-specific parameter reflecting power in sapwood area vs. DBH relationship	—
SLA_x	Species-specific leaf area	m^2 KgC^{-1}

$Stem_{const}$	Species-specific parameter reflecting constant in stem mass vs. DBH relationship	—
$Stem_{power}$	Species-specific parameter reflecting power in stem mass vs. DBH relationship	—
T_{10days}	10-day running weighted average temperature	°C
$T_{10days\ daytime}$	10-day running weighted average daytime temperature	°C
$T_{10days\ nighttime}$	10-day running weighted average night-time temperature	°C
$T_{10days\ avg}$	10-day running weighted average mean temperature	°C
$T_{10days\ soil}$	10-day running weighted average soil temperature	°C
$T_{avgseed\ x}$	Species-specific parameter for maximum temperature for seedlings survival and development	°C
T_{base}	Base temperature	°C
T_b	Base temperature for decomposition	°C
t_{coeff}	Snowmelt coefficient	Kg m^{-2} $°C^{-1}$ day^{-1}
tCWS	Total C-woody stocks	MgC ha^{-1}
T_{day}, T_{night}, T_{avg}	Daytime, night-time and mean daily temperature	°C
T_{max},T_{min}	Maximum and minimum air temperature	°C
$T_{max\ x}$,$T_{min\ x}$	Species-specific parameter for daily maximum and minimum air temperature for temperature modifier	°C
$T_{opt\ x}$	Species-specific parameter for optimum air temperature for temperature modifier	°C
T_{soil}	Daily soil temperature	°C
$T_{start\ x}$	Species-specific parameter for thermic-sum at which vegetative period starts	°C
V_{cmax}	Maximum Rubisco carboxylation rate at current temperature	µmol m^{-2} s^{-1}
V_{cmax25}	Maximum Rubisco carboxylation rate at 25 °C	µmol m^{-2} s^{-1}
VPD	Vapour pressure deficit	hPa
VWC	Volumetric water content	%
VWC_{FC}	Volumetric water content at field capacity	%
VWC_{sat}	Volumetric water content at saturation	%
WUE	Water use efficiency	gC m^{-2} $time^{-1}$ or KgH_2O $time^{-1}$
Y	Respiration to photosynthesis fixed fraction	—
$\alpha_{DBHDC\ x}$	Species-specific crown competition allometric parameter	—
α_I	Fraction of decomposed carbon flux entering the litter	—
α_S	Fraction of decomposed carbon flux entering the soil	
$\alpha_{max\ x}$	Species-specific parameter for potential maximum quantum canopy efficiency	molC $molPAR^{-1}$
α_{seed}	NPP fixed fraction for C-fruit allocation	%
$\beta_{DBHDC\ x}$	Species-specific crown competition allometric exponent parameter	—
$\beta_{seed\ x}$	Species-specific parameter controlling the percentage of empty seeds	—
$\gamma_{seed\ x}$	Species-specific parameter controlling germination capacity	—
γ	Psychrometric constant	kPa $°C^{-1}$

Δe	Slope of the saturation vapour pressure-temperature relationship	Pa °C^{-1}
$\varepsilon_{L\,x}$	Species-specific parameter controlling maximum allocation to leaf in optimal conditions	—
$\varepsilon_{R\,x}$	Species-specific parameter controlling maximum allocation to root in optimal conditions	—
$\varepsilon_{S\,x}$	Species-specific parameter controlling maximum allocation to stem in optimal conditions	—
ε_{snow}	Absorptivity of snow	—
$\varepsilon_{max\,x}$	Species-specific parameter for potential maximum quantum canopy efficiency	gC molPAR^{-1}
ρ_{air}	Mean air density at constant pressure	kg m^{-3}
ρ_x	Species-specific parameter for albedo	—
ρ_{snow}	Snow albedo	—
ρ_{soil}	Soil albedo	—
τ_{CO2O2}	CO_2:O_2 specificity ratio	—
$\tau_{leaf\_fineroot}$	Leaf and fine root turnover rate	year^{-1}
$\tau_{sapwood}$	Sapwood turnover rate	year^{-1}
$\tau_{sapwood\_juvenile}$	Juvenile sapwood turnover rate	year^{-1}
$\tau_{sapwood\_mature}$	Mature sapwood turnover rate	year^{-1}
$\tau_{livewood}$	Livewood turnover rate	year^{-1}
$\tau_{livewood\_juvenile}$	Juvenile livewood turnover rate	year^{-1}
$\tau_{livewood\_mature}$	Mature livewood turnover rate	year^{-1}
φ_x	Species-specific parameter for stem form factor	—
ψ	Soil water matric potential	MPa
$\psi_{open\,x}$	Species-specific parameter controlling leaf matric potential of stomatal start closure	MPa
ψ_{sat}	Soil water matric potential at saturation	MPa
$\psi_{close\,x}$	Species-specific parameter controlling leaf matric potential of stomatal total closure	MPa
ω_x	Species-specific parameter controlling the sensitivity of allocation to changes in soil water availability and light	—

CODE AVAILABILITY

The '*Three Dimensional — Coupled Model Carbon Cycle*' (3D-CMCC) with its '*Forest Ecosystem Module*' (FEM), hereafter '3D-CMCC-FEM', serves as a numerical tool primarily intended for research purposes. Maintained by the Forest Modelling Laboratory of the Institute for Agricultural and Forestry Systems in the Mediterranean at the National Research Council of Italy, this model offers benchmark code versions for public access. These versions are regularly updated to integrate the latest findings from cutting-edge research. The code and accompanying executables provided herein represent the most current benchmark iteration. The 3D-CMCC-FEM code, in all its versions, is subject to copyright. While freely available as open-source software, its usage is restricted to non-commercial applications. The model remains in its essence a research tool. Developed entirely from open-source components, its design encourages user contributions and ease of utilisation. However, its distribution comes with no warranties, including implied warranties of merchantability or fitness for specific purposes. The 3D-CMCC-FEM code is licensed under the GNU General Public License (GPL), accessible at https://github.com/Forest-Modelling-Lab/3D-CMCC-FEM. For comprehensive details, please refer to the GNU General Public License. If a copy of the license was not provided with the program, it can be obtained at http://www.gnu.org/licenses/gpl.html.

The development and maintenance of 3D-CMCC-FEM overseen by the Forest Modelling Laboratory at the National Research Council of Italy (https://www.forest-modelling-lab.com/), specifically the Institute for Agricultural and Forestry Systems in the Mediterranean (CNR-ISAFOM) located in Perugia. All source code and documents are protected under copyright by CNR-ISAFOM and the Forest Modelling Laboratory.

If you have replicated and/or modified the 3D-CMCC-FEM code, whether in its entirety or portions thereof, refrain from publishing any data under the name 3D-CMCC-FEM or its variants without prior coordination with the listed developers. Alternatively, provide sufficient details about your modifications to enable replication.

The 3D-CMCC-FEM has been primarily developed by Alessio Collalti and subsequently maintained and updated by Daniela Dalmonech, who are both part of the Forest Modelling Laboratory at the National Research Council of Italy (CNR), Institute for Agricultural and Forestry Systems in the Mediterranean (ISAFOM), Via della Madonna Alta, 128, 06128 — Perugia (PG), Italy. The Forest Modelling Laboratory, the Institute for Agricultural and Forestry Systems in the Mediterranean, and the CNR hold no liability for the use of the 3D-CMCC-FEM in its provided state or any modifications made by third parties thereafter. The Forest Modelling Laboratory, the Institute for Agricultural and Forestry Systems in the Mediterranean, and the CNR explicitly disclaim responsibility for any losses, damages, or costs incurred by individuals relying on this software. Users are considered to have accepted these terms of use by utilising this software. Removing this statement would contravene CNR's original intent in releasing the 3D-CMCC-FEM.

Version 5.6 ('v.5.6') of the 3D-CMCC-FEM code, encompassing Light Use Efficiency and the fully BioGeoChemical version, is open-source. The code can be freely accessed and downloaded from the GitHub Repository at https://github.com/Forest-Modelling-Lab/3D-CMCC-FEM.

This document serves as the foundation for version 5.6 ('v.5.6') of the Forest Ecosystem Module (FEM), an evolving research tool. Therefore, we cannot guarantee that the code and the assumptions behind the code will remain unchanged because the model is constantly updated to incorporate scientific advances and new emerging or old theories (e.g. the non-photosynthetic centric representation of growth, Körner 2013). Some figures in the text come from published scientific articles that refer to model versions no longer maintained but that, in any case, represent part of the history of the model. Presented here are the general theoretical principles and equations, currently used in versions 5.5 and 5.6, primarily utilised as a compendium to interpret, and sometimes to decipher, the 3D-CMCC-FEM model's responses, at least in the autotrophic sphere, and represent the state-of-the-science as of 2024. Similarly, this guide helped us to recap and summarise where we arrived with the model development, its limitations and future aims for its further improvements. While this guide does not include all equations within the model, it contains the essential equations, logic, and assumptions underpinning the 3D-CMCC-FEM model. Some equations described here are, indeed, approximations of those more complex ones present in the model code. However, in this guide, all processes are described and discussed as implemented into the model, and the name of the source code file where the processes are implemented into the model is also provided (but this may change over time). Other equations (or the more complex forms) not discussed herein can be found solely in the model's source code or related literature. In instances where well-known approaches, such as the Farquhar – von Caemmerer – Berry model for photosynthesis (Farquhar et al. 1980) or the Penman-Monteith model for transpiration, are employed in the 3D-CMCC-FEM, readers are redirected to the initial model descriptions, with modifications to the original formulation, if any, outlined. For an in-depth description of the physiological processes governing forest growth and development, we direct the reader to excellent textbooks (for example Landsberg and Sands 2011; Bonan 2019; Mäkelä and Valentine 2020) and scientific literature. Additional information, as well as technical descriptions for model runs, can be found in the 3D-CMCC-FEM User's Guide (Collalti et al. 2023). This guide is not intended to give guidance on troubleshooting problems. Please read the User's Guide first (Collalti et al. 2023) and then contact us (forest.modelling.lab@isafom.cnr.it) in case of persisting problems or to report potential emerging code bugs.

1. MODEL DESCRIPTION

The 3D-CMCC-FEM is a dynamic eco-physiological, biogeochemical, biophysical process-based model that simulates the carbon (C), nitrogen (N), energy, and water (H_2O) fluxes and the C- and N-stocks, and the growth dynamics occurring both in homogeneous as in the heterogeneous forests. The model considers different plant species (or Plant Functional Types, PFTs), for different ages, tree diameters, and height classes. Indeed, the 3D-CMCC-FEM model is specifically designed to represent forest stands, from simple ones to those with complex structures, involving several cohorts competing for light and other resources in a prognostic way (i.e. it is not constrained by diagnostic observations over time but rather builds from a series of 'first principles' given the initial conditions of a system). The 3D-CMCC-FEM is conceptually similar to other forest models (e.g. 3-PG, Landsberg and Waring 1997; 4C, Lasch-Born et al. 2020; HETEROFOR; de Wergifosse et al. 2022), biogeochemical models (e.g. BIOME-BGC; Thornton 2002), DGVMs (Dynamic Global Vegetation Models; e.g. LPJ, Sitch et al. 2003) and also to the cohort-based ecosystem demography models (e.g. ED, Moorcroft et al. 2001; CLM-ED; Fisher et al. 2015). The 3D-CMCC-FEM model is structured around three defined sub-modules (or main routines) which sort the main processes acting at the tree level (*tree_model.c* routine), litter level (*litter_model.c* routine), and soil level (*soil_model.c* routine) in several different subroutines; the last sub-model can run potentially alone simulating the condition of bare soil. All sub-models exchange each other information with the below one on the same day (e.g. the radiation available for the soil after accounting for the leaf absorption) or the day after (e.g. the available water content for leaf transpiration). The 3D-CMCC-FEM is structured to simulate key physiological processes (e.g. photosynthesis and trees' respiration) and hydrological mechanisms (e.g. leaf transpiration, rainfall, and snow interception) on a daily scale and at different hierarchical organisation (e.g. from stomata to stand scale level). It also addresses processes such as mortality and self-pruning at daily and annual scales, tailored to the species-specific level (Collalti et al. 2019). The 3D-CMCC-FEM simulates autotrophic C-fluxes, accounting for gross and net primary productivity (GPP and NPP, respectively), C-partitioning and allocation across several main plant compartments (stem, branch, leaf, fruit, fine and coarse root, Non-Structural Carbon) and other sub-compartments (sapwood/heartwood biomass, live/dead biomass). Besides the carbon pools for any of these compartments and sub-compartments, the 3D-CMCC-FEM records, in the most current versions, also daily changes in the amount of nitrogen content both in the autotrophic and heterotrophic component and, thus, the heterotrophic C-fluxes in the litter and soil (e.g. Heterotrophic Respiration) as at the ecosystem level (e.g. Net Ecosystem Exchange and Ecosystem Respiration) Additionally, the 3D-CMCC-FEM can assess water fluxes in terms of leaf and canopy transpiration, leaf, canopy, and soil evaporation, and the overall forest water balance including snow dynamic. The 3D-CMCC-

FEM model also considers management practices (or other non-anthropogenic disturbances), such as thinning and harvesting, as well as irrigation and pruning, to predict their effects, among other things, on forest growth and carbon sequestration capacity and carbon stocks (**Figure *1***).

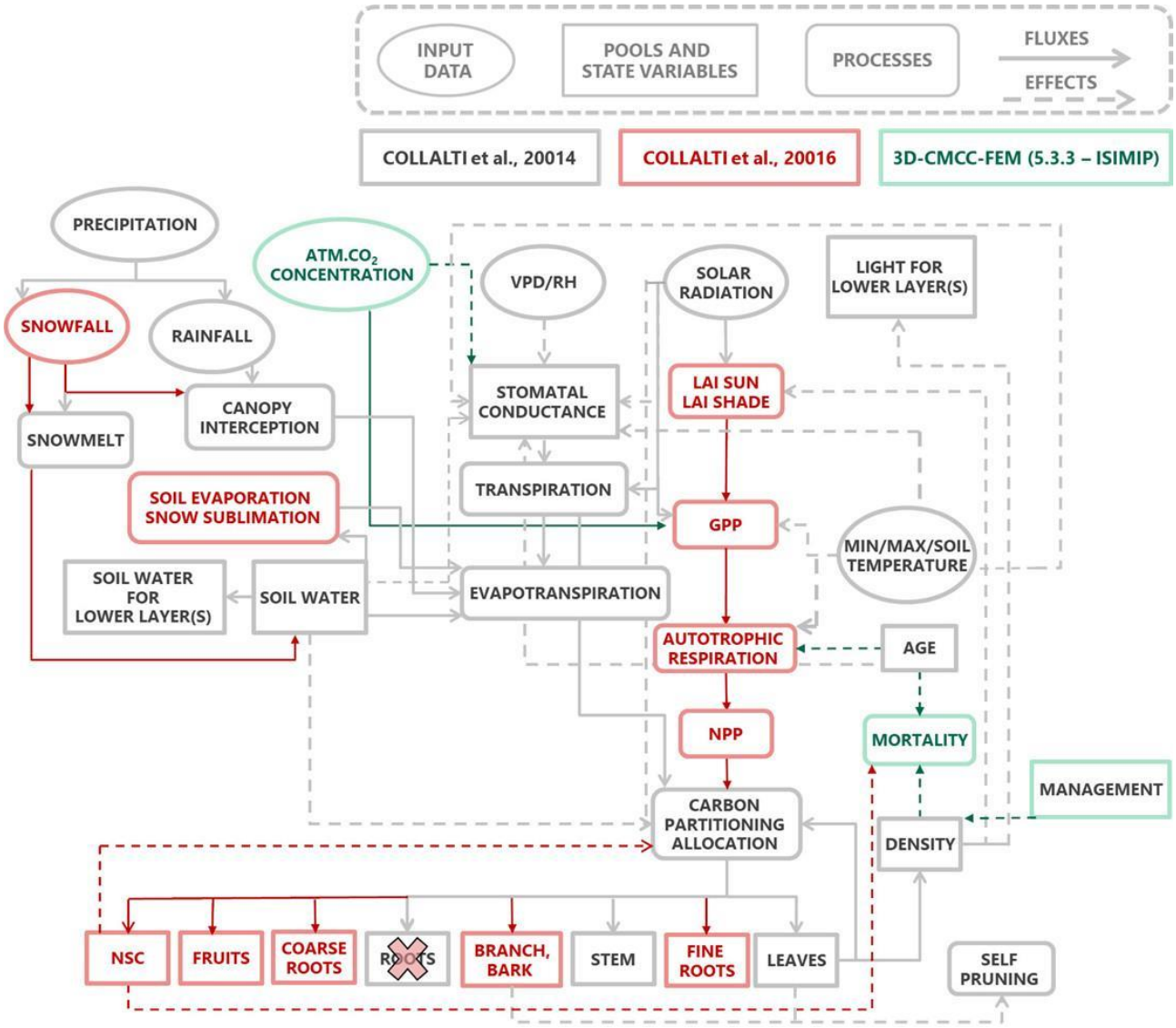

Figure 1 Flowchart of 3D-CMCC-FEM (redrawn from *Collalti et al. 2014*, then modified based on *Collalti et al. 2016*, *2018*).

1.1 Model History

The 3D-CMCC-FEM has been primarily implemented by Alessio Collalti, formerly at the Tuscia University (UNITUS), Department for Innovation in Biological, Agro-food and Forest systems (UNITUS-DIBAF) as Ph.D.

Thesis in 2011 (Collalti 2011); and subsequently at both the Foundation Euro-Mediterranean Centre on Climate Change (CMCC) Impacts on Agriculture, Forests and Ecosystem Services Division (IAFENT-CMCC) and at the Forest Modelling Laboratory at the National Research Council (CNR), Institute for Agricultural and Forestry Systems in the Mediterranean (CNR-ISAFOM). The last remains the only developer and owner of all model versions since 2018. The first lines of 3D-CMCC-FEM model code were written in 2008 at the University of Tuscia of Viterbo, for the Ph.D. Thesis of Alessio Collalti, which was originally called '3D-VT'. That module was designed as a single light interception and carbon allocation module (Collalti et al. 2010), built to be coupled with other models (such as 3-PG, '*Physiological Principles Predicting Growth*' model by Landsberg and Waring 1997) to simulate mixed forests and not just plantations. However, the 3-PG model code architecture showed from the very beginning to be not suitable for incorporating the '3D-VT' algorithms developed as object-oriented modules to be resolved iteratively among different layers, cohorts, and species to simulate mixed forests. Together with Alessio Ribeca, Alessio Collalti, using concepts and algorithms from also the 3-PG model, designed and wrote a brand new code to handle the challenge. Thus was born the '*Three Dimensional — Coupled Model Carbon Cycle — Forest Ecosystem Model*' (3D-CMCC-FEM) at the University of Tuscia and subsequently at the 'Euro-Mediterranean Centre for Climate Change'. At that institution, the 3D-CMCC-FEM was further developed between 2011 and 2018. During those years, several improved versions of the model were developed to provide the scientific pillars of today's model formulation. In the early versions of 2011 and 2014 (Collalti 2011; Collalti et al. 2012, 2014; Vacchiano et al. 2012), only carbon and water cycles were simulated, at monthly time steps, representing fluxes of carbon and water, carbon allocation was simulated between three main compartments (stem, leaf and root) subsequently increased to six (and four sub-compartments), while plant respiration was considered a fixed fraction of GPP (Waring et al. 1998; Collalti and Prentice 2019; Landsberg et al. 2020). This first model version was tested and validated in 2010 for some environmental variables and stand attributes in a Turkey Oak (*Quercus cerris* L.) forest at 'La Torre di Feudozzo' (Italy), in collaboration with the National Research Council of Italy (CNR). The results were published in 2014 (Collalti et al. 2014). Parallel to a prognostic version of the model, a 'satellite-derived' version was developed to provide direct estimates of the Leaf Area Index (LAI) via the Normalised Difference Vegetation Index (NDVI) (Natali et al. 2012; Collalti et al. 2013). Due to the model's inherently prognostic nature for studies under climate change scenarios, this version is no longer maintained. The 'v.5.1' version of 2016 (Collalti et al. 2016) was updated several times to include N-dynamics, Non-Structural Carbon (NSC; Merganičová et al. 2019; D'Andrea et al. 2020, 2021) and the ability to run simulations at a daily time scale. The idea to move from simulations at monthly scales to daily scales was related to the increasing (as it currently is) climate extreme events because of climate change, events that would have been 'averaged' through the month with monthly model runs. More

importantly, this version included a significant refinement: autotrophic respiration was calculated mechanistically by components similar to that in BIOME-BGC (Thornton 1998; Thornton et al. 2002). With the increasing global warming rate we believed that considering two, although interlinked, processes such as photosynthesis and plants' respiration, as reacting in a similar manner (i.e. maintaining stoichiometrically fixed at the same rate of change) as anachronistic and we drifted for a more realistic, yet complex, representation of autotrophic respiration. These refinements to the code represent the most advanced version of the model. The 'v.5.1' was validated against Eddy Covariance measurements at ten Fluxnet-forest sites across Europe spanning from Mediterranean to temperate (oceanic and continental) and boreal climate. In 2017, Carlo Trotta (a former collaborator) developed a specific version of the model called 'v.3D-CMCC-Olive', a module of the model specifically parameterized through Bayesian calibration for European Olive trees (*Olea europaea* L., and the different *subsp*. and cultivars) which also included the possibility for pruning and irrigation. These are retained in the subsequent versions (Trotta et al. 2018, 2019). In 2017, Sergio Marconi implemented on the 'v.5.1' (called 3D-CMCC-PSM, '3D-CMCC-Phenology and Soil Model') with some new formulations for phenology and NSC utilisation during the bud-break period for deciduous and leaf turnover for the evergreen species, and soil C-dynamic by partially coupling the 3D-CMCC-FEM with the DNDC model (Marconi et al. 2013, 2014, 2017). This new version was validated against eddy covariance measurements (Pastorello et al. 2020) across six different forest sites of the Fluxnet network in Europe. In the 'v.5.3.3-ISIMIP' of 2018 (Collalti et al. 2018), the effect of rising atmospheric CO_2 concentration and the effect acclimation to increasing temperature on maintenance respiration, following Smith and Dukes (2012), by including the chance to simulate forest management, opened the possibility to use the 3D-CMCC-FEM model over long-simulation runs both under climate change scenarios as under different silvicultural schemes. In the 'v.5.4-BGC' (Collalti et al. 2019), the Farquhar von Caemmerer and Berry biogeochemical model version (FvCB, Farquhar et al. 1980) was implemented and it parallels the Light Use Efficiency empirical model (LUE, Monteith 1977). Indeed, in the 'v.5.4-BGC' (Collalti et al. 2019, 2020a; Engel et al. 2021) and subsequently, to simulate plant photosynthesis, the Light Use Efficiency (LUE) module can be switched with the FvCB module depending on the user's needs. The 'v.5.4-BGC', which remains very close to the more recent versions of the model, has been tested for its sensitivity with over 55 species-specific parameters and under climate change scenarios over 100 years run testing model sensitivity for parameters to the different phases of forest development. With the 'v.5.4-BGC' version Collalti et al. (2020a) tackled two well-known ecological theories for plant respiration: one which links respiration to photosynthesis (the Waring et al.'s hypothesis of respiration as a fixed fraction of photosynthesis); and the 'metabolic scaling' hypothesis that links respiration to the (overall) biomass (Reich et al. 2006). Recently, the most to-date advanced (and minor bugs fixed) model versions ('v.5.5-ISIMIP' and 'v.5.6') have been

included in a broad model intercomparison project across Europe (i.e. ISIMIP, Inter-Sectoral Impact Model Intercomparison Project; Reyer et al. 2020; Mahnken et al. 2022a, 2022b, 2023). It exhibited extremely good performances, compared to other models, both in terms of accuracy, realism, and general applicability. Dalmonech et al. (2022) with the 'v.5.5' and Testolin et al. (2023) with the 'v.5.6' tested both versions under climate change scenarios and their uncombined and combined effects under a portfolio of diverse management schemes in Europe as well as in southern Italy. The new 'v.5.6' implements a new formulation (and relative parameterization) for sapwood and livewood dynamics and new forest management schemes. In 2024, Vangi et al. (2024a, 2024b) provided an in-depth analysis of the effects of stand age under climate change scenarios on forest sensitivity, stability, and resilience if the forest stands described in Dalmonech et al. (2022) would have been, conversely, led to the develop undisturbed with no management interventions. Morichetti et al. (2024) also analysed the effects of climate change on the sink/source capacity for the mean seasonal carbon cycle under the locally bias-corrected (ISIMIP 2bLBC experiments) climate scenarios. Recently, the 3D-CMCC-FEM has been applied on large scale using National Forest Inventory (NFI) at the regional level in Italy by Daniela Dalmonech (Dalmonech et al. 2024) and validated against a suite of Remote Sensing-based products at species level (**Figure 2**), and at overall national level by Elia Vangi (Vangi et al. *in prep.*) and against remotely sensed products and INFI data. In addition, a R-package for running the 3D-CMCC-FEM ("R3DFEM") has been recently developed for simulations under R-Studio environment (https://github.com/Forest-Modelling-Lab/R3DFEM; Vangi et al. 2024c). The 3D-CMCC-FEM model outputs are also part, together with simulations from other fifteen European forest models, of the first (and to date unique) harmonised database of European forest simulations under climate change (Grünig et al. 2024). Overall, in the ten years since its first publication, the 3D-CMCC-FEM model has been run for about 7000 different forest stands and was validated for many of these sites (see **Figure 3**). A fully updated list of references can be found in the README file at: https://github.com/Forest-Modelling-Lab/3D-CMCC-FEM

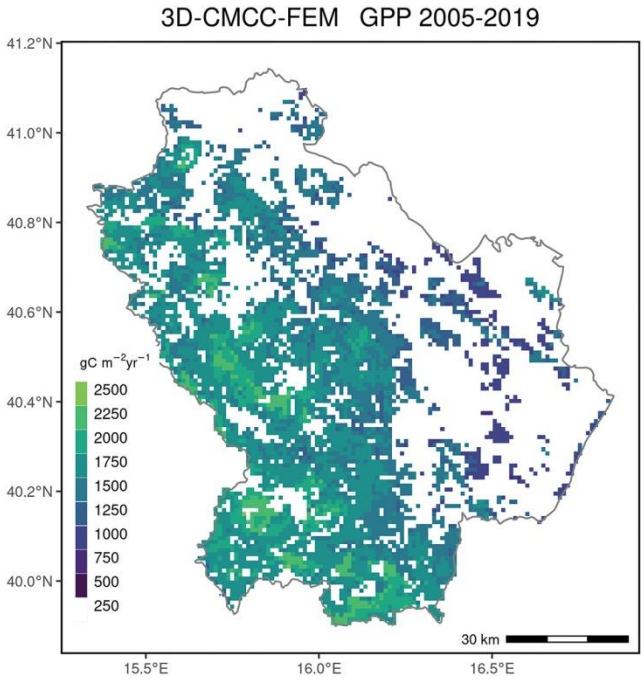

Figure 2 3D-CMCC-FEM simulation of Gross Primary Productivity (GPP, gC m^{-2} $year^{-1}$) at a regional level at a resolution of 1 x 1 km (figure from Dalmonech et al. 2024).

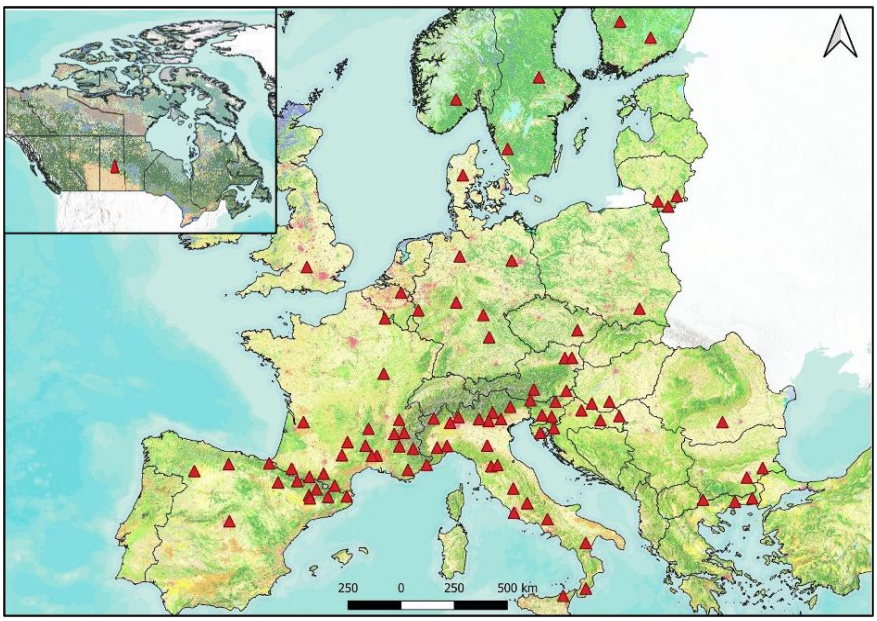

Figure 3 3D-CMCC-FEM has been widely applied to different species across Europe and Canada.

1.2 HIERARCHICAL STRUCTURE

The 3D-CMCC-FEM adopts a hierarchically structured approach centred on a primary homogeneous matrix partitioned into cells of varying dimensions, ranging from 10m x 10m to 1km x 1km, depending on the level

of resolution, such as species or plant functional type, with customizable settings for users. This design facilitates the modelling of intricate forest ecosystems, encompassing diverse types such as uneven-aged, multi-layered, and mixed-species forests (refer to Paragraph 1.4 Model Initialization: the Forest Structure and the Pools). The architecture of the code (more than 30,000 lines code) permits the categorization of trees into representative classes, each characterised by specific attributes such as carbon pools, leaf area index, and tree height, based on age, species, and forest structural traits (Collalti 2011; Collalti et al. 2014; Engel et al. 2021; Mahnken et al. 2022a). It is worth noting that all variables are normalised per square metre, hectare, or cell size, depending on the variable type. Simulations are conducted for each cell across various tree height classes, further subdivided based on diameter at breast height (DBH), age, and species. In essence, the code architecture allows for the aggregation of trees into representative classes distinguished by species-specific and structural characteristics, identified by model-assigned indexes, namely species (x index), tree diameter at breast height class (y index), height/layer class (z index), and age cohort (k index). Each nested class is characterised by its species-related parameterisation and variables, including biomass pools, crown area, light attenuation, and mortality. In addition to species-level classification, the model offers the flexibility to define tree phenology by selecting between two distinct phenotypes: evergreen or deciduous. A dedicated sub-module for forest management enables the simulation of forest development under various silvicultural practices (refer to paragraph 7). Critical variables such as Gross and Net Primary Production (GPP and NPP), Leaf Area Index (LAI), Available Soil Water (ASW), and Evapotranspiration (ET), among others, are computed on daily, monthly, and annual scales, considering soil characteristics and pools for each cell. Cumulative values are ultimately determined, summing up across x, y, k, and z classes, at both cell and matrix levels.

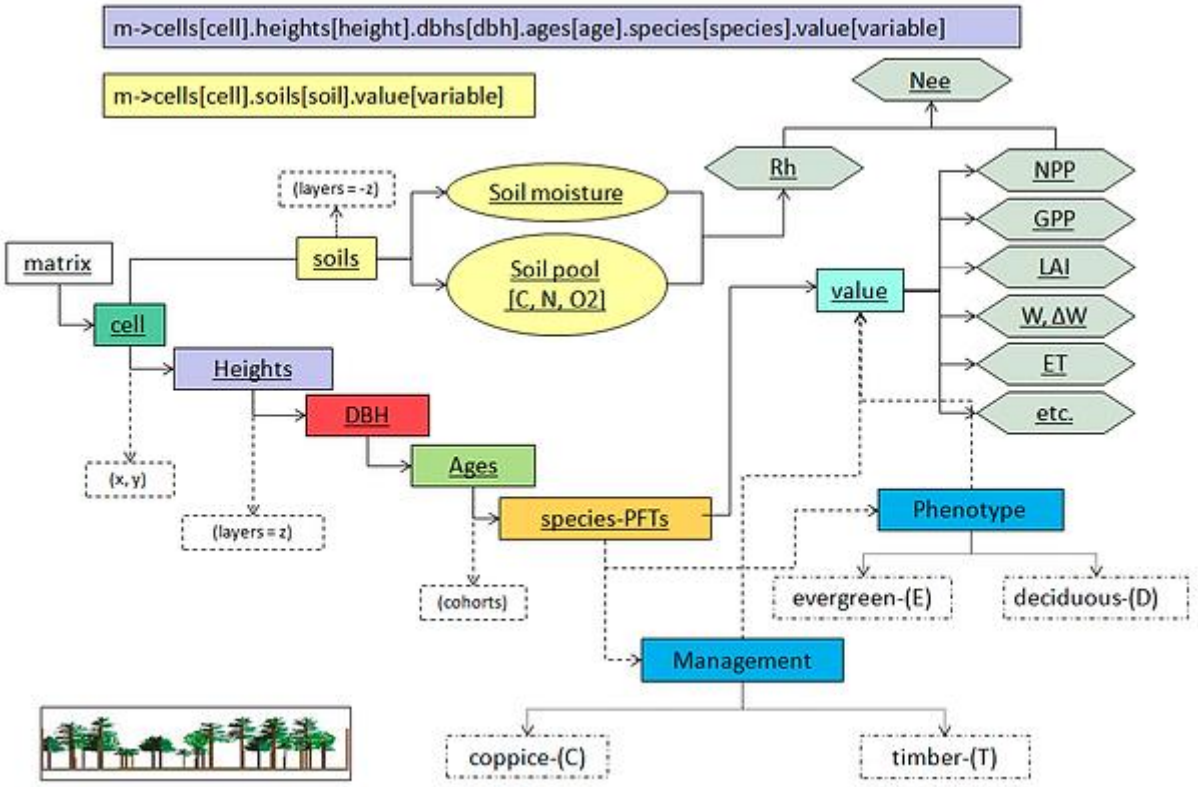

Figure 4 Flowchart of the 3D-CMCC-FEM C-programming logical structure

1.3 INPUT AND OUTPUT DATA

Specific input data are required to run the 3D-CMCC-FEM:

- State variables. Initial stand conditions representing the stand at the beginning of the simulation: species name, age, tree height, average DBH, and number of trees based on size cell (see paragraph 6). The model simulates actual vegetation (and not the potential one), thus, any spin-up run or initialization starting from bare soil conditions is not considered. Initial stand data must be provided by the user and need to be organised a bit before being used properly by the model. For more, even technical, details, see the paragraph 1.4 Model Initialization: the Forest Structure and the Pools' and Collalti et al. (2023). Note: these data are necessary only at the beginning of the simulation to represent initial stand conditions.
- State variables. Soil (e.g. soil depth, sand, clay, and silt percentages) and topographic information (e.g. elevation). All these data are mandatory.
- Parameters. Species-specific parameters are primarily rooted in their eco-physiological and allometric characteristics and traits. These species-specific parameters are typically derived from a

combination of forest inventories and literature search (see Collalti et al. 2019, for species-specific sensitivity analysis on model parameters and discussion around their constancy) and are considered to not vary over time. All these parameters are mandatory.

- Drivers. Meteorological forcing data which are: daily maximum (T_{max}, °C) and minimum air temperature (T_{min}, °C), vapour pressure deficit (VPD in hPa; or relative humidity, RH, in %), downwelling shortwave radiation at the surface I_0 (MJ m^{-2} day^{-1}) and precipitation amount (mm day^{-1}). All these data are mandatory. In addition, the model uses the daily mean temperature (T_{avg}, °C) and soil temperature (T_{soil}, °C) when available or are self-computed by the model if missing in the meteorological data file. Additionally, the model incorporates other meteorological variables (such as air pressure, air density, T_{day}, T_{night}), but these are internally computed as they are derived from the mandatory variables mentioned earlier (Collalti et al. 2016).
- Drivers. Annual atmospheric CO_2 concentration (µmol mol^{-1}) is a required field, while nitrogen deposition is optional (Collalti et al. 2018).

A fifth additional file (the setting file), which is not in the input file, controls 3D-CMCC-FEM simulations set up by allowing the user to customise different simulation runs, e.g. by using the 'BioGeoChemical' version, thus, adopting the Farquhar – von Caemmerer – Berry photosynthesis model, or by specifying the starting year for forest management. In the settings file, the user decides if and how to simulate management, which includes thinning and clear-felling, and to parameterize the replanting type after the harvesting. Replanting type includes the possibility to replant using a different tree species of varying age, by setting the DBH and other variables (see paragraph 7).

Conversely, physical constants (e.g. Stefan-Boltzmann constant), are part of the model code (*constants.h*) and cannot be modified by the user (for model implementation, see the User's Guide, Collalti et al. 2023).

The primary output data of the 3D-CMCC-FEM (either at daily, monthly, or annual scales) are: Gross Primary Productivity (GPP), Net Primary Productivity (NPP), and other state variables such as Evapotranspiration (ET), Leaf Area Index (LAI) and rainfall interception and C- and N-stocks, e.g. stem biomass, fruit production, above- and below-ground biomass, volume, but there are many others representing the overall C- and N-cycle, Energy and H_2O-cycle and forest stand attributes. A complete list of output variables is provided in Collalti et al. (2023).

Results are obtained either at the class level (species, diameter, tree height, or age class level), at layer level (as the sum of all tree height classes in the same layer), and at grid level (i.e. cell or ecosystem level, as the sum of all classes). The 3D-CMCC-FEM model provides information to support decision-making in forest

management planning, such as mean annual volume increment (MAI), current volume increment (CAI), C-Woody Stocks (CWS), Wood Production (WP), basal area (BA), and DBH (**Figure 5**).

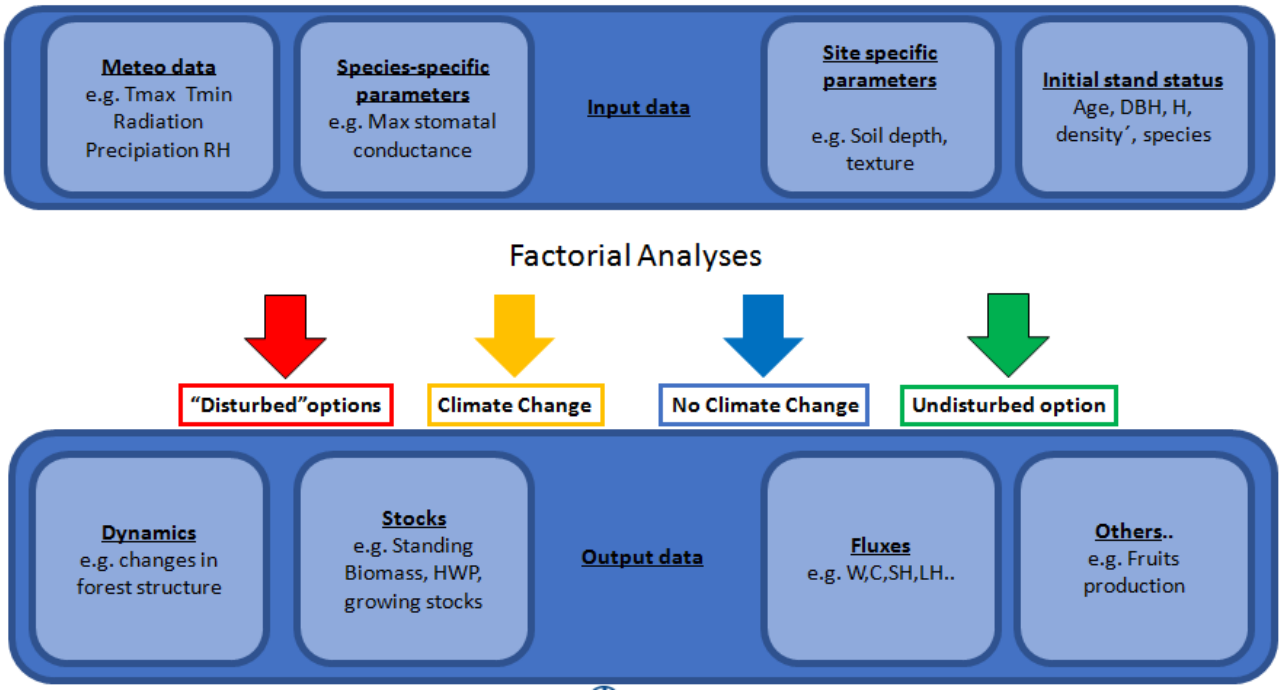

Figure 5 3D-CMCC-FEM input and output data

1.4 Model Initialization: the Forest Structure and the Pools

(routines: *structure.c* , *initialization.c*)

1.4.1. Forest Structure

The user provides the initial stand characteristics as mandatory input data (i.e. Species, Ages, DBHs, Three Height, Tree Density) from which the 3D-CMCC-FEM will generate the stand structure. 3D-CMCC-FEM is not an 'individual-based' model and uses data aggregated (but it can be used to simulate individual trees), 'entities', representing classes, such as tree height classes, DBH classes, cohorts, and species, as follows: (1) for any species in a cell the different tree height can be considered (or grouped) into a number of relative tree height classes, (2) for any tree height class in a cell the different DBH can be considered (or grouped) into a number of relative DBH classes, (3) for any DBH class in a cell the different ages can be considered (or grouped) into a number of relative ages classes (i.e. cohorts) (Collalti 2011; Collalti et al. 2014). Any of those nested species->tree height->dbh->age classes is represented by its 'average tree' which records the variables considered (e.g. *Fagus sylvatica*->20 metre height->25 cm of DBH->40 years old ->Net Primary Production)(see **Figure *6***). The user may, in a pre-processing phase, choose the level of aggregation, as

previously described, into DBH classes of e.g. 10 cm. A similar, although less accurate approach, has also been adopted in the Ecosystem Demography (ED) model (Moorcroft et al. 2001) and, more recently, in the CLM-ED and FATES model (Fisher et al. 2015).

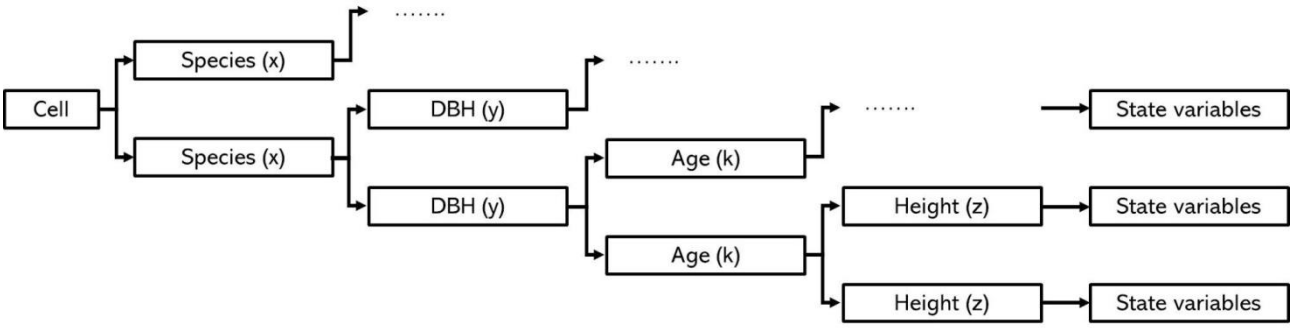

Figure 6 Model data management flowchart. For each cell of the matrix, the model can be initialized considering multiple species (x index). For each species, the model can consider multiple tree diameters at breast height (DBH) class (y index) that can be grouped into specific and multiple tree height classes (z index, but see how the model groups into specific layers), for each tree DBH class the model can consider multiple cohorts (k index). Each nested class has its state variables (figure redrawn from Collalti et al. 2014).

As an example, a user might divide to simulate a stand composed of two species (i.e. A and B), with different DBH classes (i.e. 5 and 15 cm), with different Tree Height classes (i.e. 10 and 20 m), and different ages (i.e. 8 and 16 years old) in the following way:

1)	A(x)->5(y)->10(z)->8(k)	9)	B(x)->5(y)->10(z)->8(k)
2)	A(x)->5(y)->20(z)->8(k)	10)	B(x)->5(y)->20(z)->8(k)
3)	A(x)->5(y)->10(z)->16(k)	11)	B(x)->5(y)->10(z)->16(k)
4)	A(x)->5(y)->20(z)->16(k)	12)	B(x)->5(y)->20(z)->16(k)
5)	A(x)->15(y)->10(z)->8(k)	13)	B(x)->15(y)->10(z)->8(k)
6)	A(x)->15(y)->20(z)->8(k)	14)	B(x)->15(y)->20(z)->8(k)
7)	A(x)->15(y)->10(z)->16(k)	15)	B(x)->15(y)->10(z)->16(k)
8)	A(x)->15(y)->20(z)->16(k)	16)	B(x)->15(y)->20(z)->16(k)

This produces a combination of sixteen interacting, different classes, each with its own state variables to simulate in a model run. This complex configuration for input data is potentially doable for model runs, although this is largely time-consuming and is not recommended. Alternatively, the user, can simplify and speed up the model run by aggregating, e.g. for average DBH, tree height, and age in such a way:

1)	A(x)->10(y)->15(z)->12(k)	2)	B(x)->10(y)->15(z)->12(k)

The level of aggregation depends on the aim of the user; for example, a simulation to assess the effect of light competition should not consider aggregating tree height classes to permit consideration of differences in tree heights.

The vertical structure

During the initialization phase of the 3D-CMCC-FEM model, as well as at the beginning of each year, the vertical structure of the stand must be defined into one or in a number of different discrete layers, i.e. monolayer, bi-layer (dominant and dominated layer) or multi-layer, as shown in **Figure 7**. The vertical stacking of each tree height class and, thus, the number of layers that the model has to consider, can be set by the user by defining the maximum intervals (in metres) distinguishing between two different tree height classes. For example, if the value was in '*Tree_layer_limit*' at 3 metres, and the difference between two tree height classes were less than 3 metres, these two tree height classes would not be distinguishable by the model. In this case, these two three height classes are considered within the same layer (hereafter noted as 'z') and no competition for light is accounted for. Otherwise, if the differences between the two tree height classes exceed 3 metres, these two classes would be treated as two different distinct layers, one dominant the other in competition for light, so long as but till (and if) the differences in tree height remain above the 3 metres. This means that only a wide advantage in terms of tree height translates into a significant advantage in terms of light competition and, thus, light availability, even at the seedling stage. The number of layers is, however, iteratively and dynamically accounted for, based on current forest conditions and not fixed to a prescribed number. Ultimately, any species, DBH class, and cohorts, based on its tree height class and their relationship with the other tree height classes are assigned a canopy layer. A similar scheme of vertical discrimination is also thought for the below-ground with a number of different soil layers that can be considered in the model. However, such an option is still under development.

The horizontal structure

Horizontally, trees of each class are homogeneously distributed within the grid cell, and the canopy cover percentage of the grid cell is computed for each layer according to tree density with some allometric constraints. Forest horizontal structure is represented two-dimensionally in a similar, yet not equal, spatial arrangement of crowns as in the '*Perfect Plasticity Approximation*' (PPA; Purves et al. 2008), i.e. the plants tend to fill with their leaves all of the available canopy space, as in the GFDL Land model (Weng et al. 2015) and, with similar logic, in CLM(ED)(Fisher et al. 2015). The 3D-CMCC-FEM is a 'spatially implicit model' and does not require the spatial position of each single tree within the grid cell. The fraction of the cell covered by the canopy (CC) for each layer is also computed by considering the crown area projection of each single

tree and then scaled up to the cell level considering all trees in that layer. Crown areas are assumed, during the initialization phase, at their maximum attainable values at the '$DBHDC_{max}$' value (i.e. current DBHDC = '$DBHDC_{max}$'), a species-specific parameter controlling the maximum DBH:Crown Diameter ratio. In the initialization phase, if by considering DBHDC at its maximum value and by summing all crown areas of each single tree within a layer the overall Canopy Cover (CC) should exceed the maximum CC based on a species-specific '*Light_tol*' parameter, the model arranges and reduces iteratively its actual DBHDC up to a certain value (and not below the '$DBHDC_{min}$', i.e. the minimum DBH to DC, Crown Diameter, ratio). The '*Light_tol*' parameter, and then the CC, is based on the species shade (or light) tolerance, which varies between different species. The 3D-CMCC-FEM model, indeed, considers different potential and maximum rates of cell maximum coverage. Therefore, shade-intolerant species are parameterized to cover up to 90% of the area available (i.e. cell size), and very shade-tolerant species up to 110%, i.e. with a 10% overcrowding allowed. In the subsequent years, during the forest structure updates, any value that exceeds the maximum CC for that species in that layer leads the model to reduce the crown area up with the self-pruning function but only to a certain level (i.e. '$DBHDC_{min}$'). If the current DBHDC is already at the minimum level the model activates the self-thinning mortality (see 'Mortality' paragraph for an in-depth description) routine and reduces the tree number up to satisfy this condition. The '*DBHDC*' is a dynamic variable controlling the actual crown area and, at the same time, a measure of tree-tree competition in the 3D-CMCC-FEM model (Collalti 2011; Collalti et al. 2014). The higher the competition for space horizontally, the smaller the crown area becomes. In 3D-CMCC-FEM, crowns are overall represented as cylinders. Despite its remarkably simple assumptions the PPA has been shown to be able to adequately reproduce even in large-scale applications of forest structure and the related processes (Purves et al. 2008; Bohlman and Pacala 2012; Fischer et al. 2016).

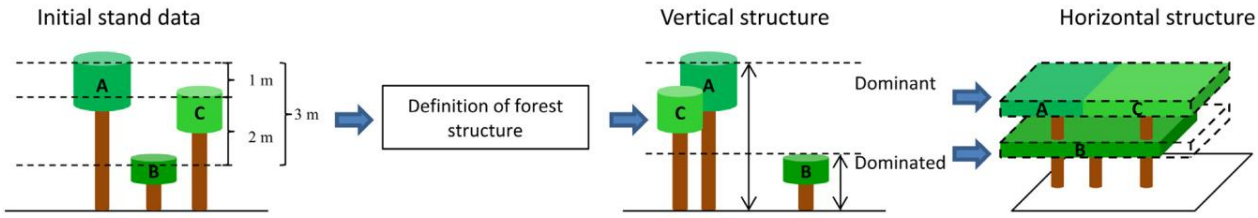

Figure 7 Model forest structure definition and the Perfect Plasticity Approximation. At the beginning of each year simulation, the model redefines the vertical (i.e. number of layers and class position into the vertical structure, *z* value) and horizontal (i.e. class canopy coverage) forest structure depending on initial cell data (first year of simulation) or changes in state variables (next years) (figure from Collalti et al. 2014).

1.4.2. Biomass Pools

As described above, 3D-CMCC-FEM requires specific stand-level inputs to run, some are mandatory, and others are optional. The optional data refers to some C-pools (i.e. stem, leaf, fine root, and coarse root dry mass). If these optional data are not provided by the user the 3D-CMCC-FEM model, starting with DBH, Tree Height, Species, and Tree Density, will initialise these missing C-pools and calculate the other state variables (both as C- and N-pools). This C- and N-pools data initialization is computed at the beginning of the simulation and updated at the beginning of each simulation year according to species-specific parameters describing the allometric relationships. For example, starting with DBH, the model computes the stem biomass through an allometric equation (see paragraph 6). With the same equation, by inverting the variables (i.e. the DBH becomes the unknown variable) (West et al. 1991) DBH is predicted at the end of the year from the stem biomass. Leaves, branches (and bark), coarse and fine roots, as well as reserves (Non-Structural Carbon, NSC) are all computed from the initial stem biomass through allometric species-specific relationships. Similarly, sapwood, heartwood, live, and deadwood biomass are also computed. The leaf carbon pool is computed for evergreen only at the beginning of the simulation (which, in the northern hemisphere, is commonly in January month). Leaf Area Index (LAI, i.e. m^2 of projected leaf per m^2 of ground area). Leaf Area Index for each class dominated by the species *x*, with diameter *y* and age *k* and *x*, *y*, and *k* belonging to the layer *z* (for simplicity in the text, this will be indicated as '*x*', '*y*', '*k*', and '*z*' where *z* will be assumed to indicate the layer), is calculated as:

$$LAI_{x,y,k \in z} = \frac{LeafC_{x,y,k \in z} \cdot SLA_x}{CC_{x,y,k \in z} \cdot Cell_{Size}} \qquad Eq.1$$

where LeafC (KgC cell size^{-1}) is the carbon in the leaf compartment, SLA is the Specific Leaf Area (m^2 KgC^{-1}, a species-specific parameter varying with tree age and for both for sun and shaded leaves), which is a measure of the thickness of a leaf and its units are area per unit mass, *CC* is the canopy cover projection (m^2 cell size^{-1}), i.e. the sum of all crowns in a specific layer, and Cell Size is the area in m^2 of the simulation grid cell. The 3D-CMCC-FEM calculates *CC* as follows:

$$CC_{x,y,k \in z} = Crown\ area_{x,y,k \in z} \cdot N_{tree_{x,,y,k \in z}} \qquad Eq.2$$

where N_{tree} is the number of trees of a determined species, with a tree height, age, DBH, and species class within a layer. The Canopy Cover of a specific layer is obtained by integrating all *CC* with the same layer as:

$$CC_z = \sum_{x,y,,x,z}^{N} \quad CC \qquad Eq.3$$

cell size is a two-dimension (in square metres) that can be set by the user in the setting file representing the side of the square representing the grid-cell. By using species-specific parameters the model also distinguishes between the leaf carbon for sun and shaded leaves, and consequently also the LAI for sunlit and shaded leaves. Photosynthetic, respiration, and transpiration processes are calculated separately for sun and shade leaf components. This separation into a 'two big-leaves' model provides more accuracy than simple one big-leaf models and that is applied in a multi-layer modelling framework as in the 3D-CMCC-FEM model.

Nitrogen pools (and including the Rubisco amount), which are the same number as in for the C-pools (except for NSC), are computed by Carbon:Nitrogen stoichiometrically fixed ratios starting from C-pools.

The model also considers some carbon and nitrogen sub-pools, which include for example, the sapwood and heartwood mass and the live and dead wood, and some aggregated carbon pools, which include for example, the above-ground biomass (as leaf, branch, and bark, stem, and fruit summed up), or below-ground biomass (as fine and coarse root summed up) or stand attributes as Tree and Stand Volume. The live respiring wood biomass is initialised at the beginning of the simulation as a fixed fraction of sapwood mass (for stem, coarse root and branch biomass) (Pietsch et al. 2005; Hölttä and Kolari 2009; Pallardy 2010).

At the beginning of each simulation year run, the 3D-CMCC-FEM model keeps track and updates the carbon and nitrogen pools and iteratively re-computes the forest structure and stand attributes for the next year(s) as described above.

1.4.3. Numerical (Temporal and Spatial) solution of processes

The 3D-CMCC-FEM, after resolving structural discretization (vertically and horizontally) and initialising biomass pools, starts by simulating daily eco-physiological processes. This process begins from the uppermost layer, prioritising the highest tree height class, the largest DBH, and the oldest age within each layer. It then iteratively descends through the subsequent lower layer, moving to the litter layer and, at the end, to the soil layer. Each canopy layer has its own C- and N-balance as well as H_20- and Radiative-balance, meaning that any incoming upward entity (e.g. radiation, precipitation) is accounted for and resolved for the upper layer first (**Figure *8***). Therefore, the net amount of radiation received by the lower layer(s) is determined by subtracting the e.g. light, intercepted, absorbed, reflected, and then transmitted from the highest one(s).

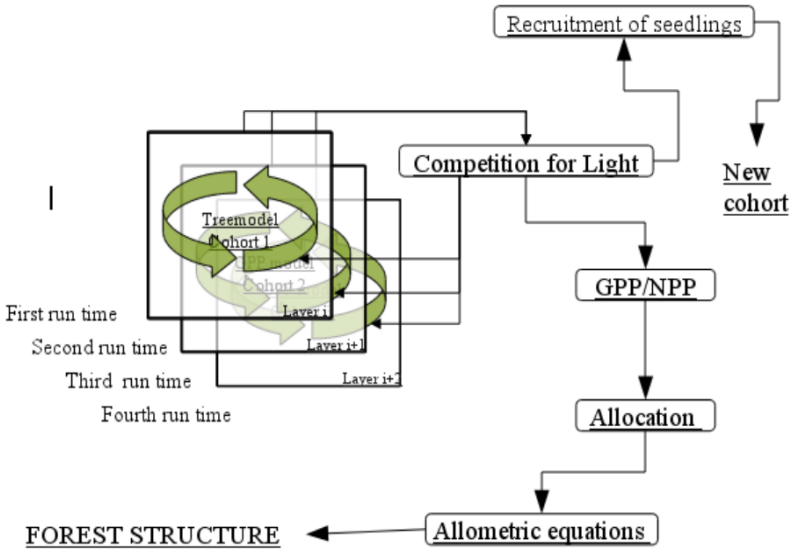

Figure 8 Proof-of-concept adopted in the 3D-CMCC-FEM for multi-layered forests in simulating the carbon cycle (figure from Collalti 2011).

1.4.4. Composite Forest Matrix (CFM)

A high proportion of the European forested area is composed of a mix of differing-aged stands and since forest C cycle processes may respond differently to climate factors at different ages (e.g. Collalti and Prentice 2019; Collalti et al. 2020b; Huber et al. 2018, 2019; Migliavacca et al. 2021), we developed a Composite Forest Matrix (CFM) approach consisting of a mixture of stands of different age, structure and associated biomass. Starting from the real stands, a prescribed number of virtual stands can be generated in order to obtain representative model outputs of a larger set of different age classes (with their associated forest attributes) that can cover an entire rotation period (≈140 years, depending on the species), similar to the approach developed by Bohn and Huth (2017). Because the 3D-CMCC-FEM model, following experimental evidence, is sensitive to the stand structure (see Collalti et al. 2019, 2020a), this procedure allows a robust assessment of the effects of management practices across the full range of applicable stand ages. A CFM framework can be created by running at each site the model from a specific year where the user can initialize the model to a specified year (e.g. to cover the entire rotation length for each species) under a contemporary climate scenario (no climate change), consisting of detrended and repeated cycles of e.g. 1996-2006 historical weather, with fixed atmospheric CO_2 concentration of 368.8 µmol mol^{-1} (or ppmv) and BAU management practices. From each of these simulations data needed to reinitialize the model at every rotation length/n_{vs} can be extracted (Figure 9)(where 'n_{vs}' represents the number of virtual stands to obtain for such analysis). Thus, in total, a number n_{vs} potential virtual stands rep-resenting different age classes (and in turn different

forest structures and their relative biomass) of the composite matrix can be selected and included in the CFM as described in Dalmonech et al. (2022) and Vangi et al. (2024a, 2024b). Such an approach somewhat draws the 3D-CMCC-FEM model results near to the Gap models (Bugmann 2001) in simulating, as a mosaic of different patches, landscape heterogeneity.

Note, this is just a pre- and post-processing and not an automated procedure within the 3D-CMCC-FEM.

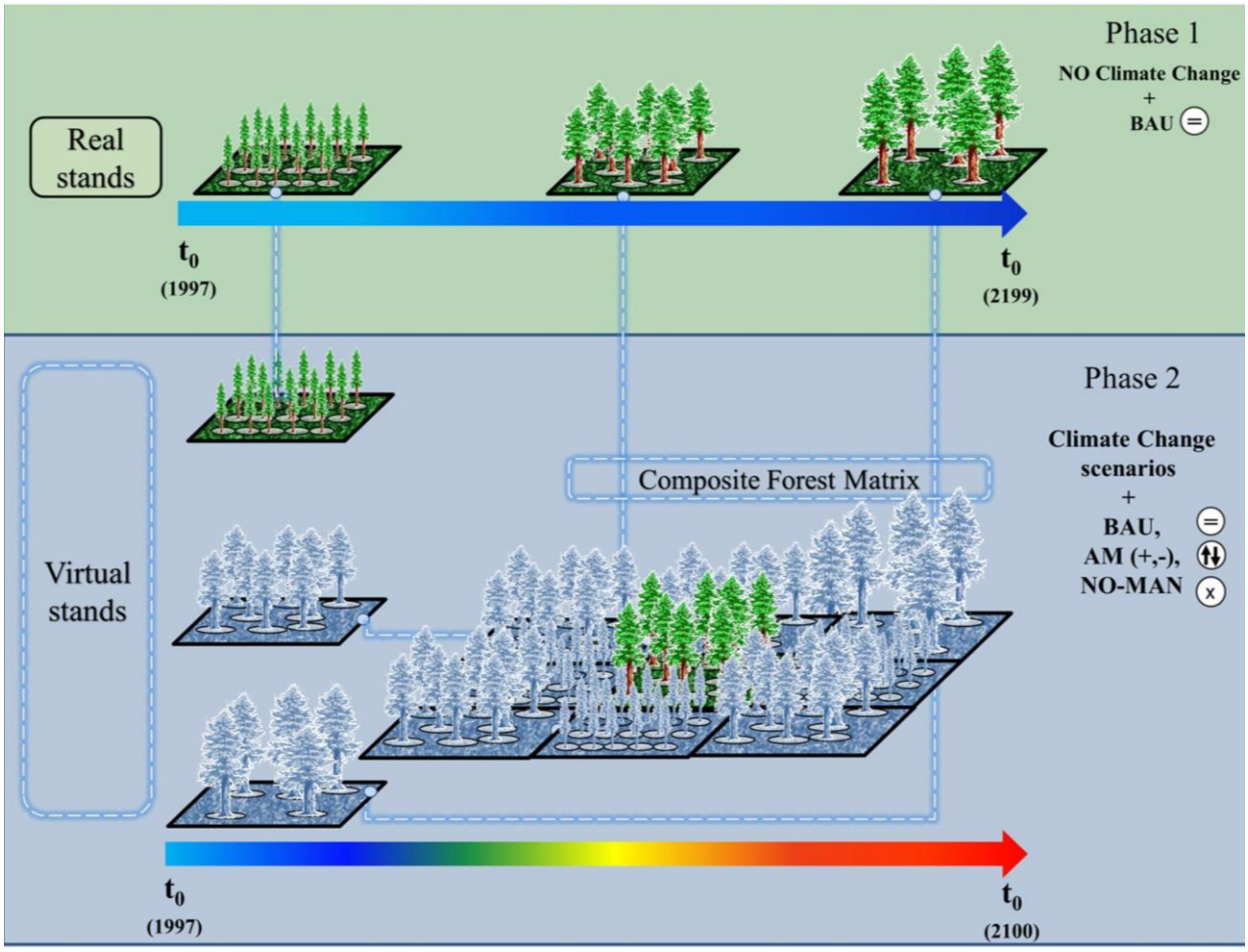

Figure 9 Conceptual scheme of the creation of the virtual stand: in Phase 1 the model is initialized with data from the actual forest stands, and then simulations are carried out for 202 years of contemporary (1996-2006) weather and atmospheric CO_2 concentration. In Phase 2, multiple stands are drawn from the simulations in Phase 1 and used to build the Composite Forest Matrix (CFM) composed of representative forest stands. The climate change (RCPs) and management scenarios (BAU, Alternative Managements, No-Management) simulations are then applied to the CFM (figure from Dalmonech et al. 2022).

2. RADIATION BUDGET

(routines: *canopy_radiation_sw_band.c*, *canopy_radiation_lw_band.c*)

Solar radiation serves as the primary driver for both the photosynthetic process and the carbon and water cycle in vegetation. The vertically resolved radiation budget and the radiative transfer module comprise light interception, and absorption (e.g. absorbed photosynthetically active radiation, APAR), which is computed through Lambert-Beer's law for sun and shaded leaves in homogeneous canopies (Thornton and Zimmerman, 2007), reflectance (i.e. the light reflected because of the species-specific albedo parameter), and transmission. The vertically structured light competition module in 3D-CMCC FEM is essentially a modified version of the Lambert-Beer law (Monteith and Unsworth 1990) approximated by the Monsi-Saeki (1953) formulation of exponential attenuation and coupled with the 'two big-leaves' approach developed for a multi-layered model (Sellers et al. 1992; Sands 1995; Medlyn et al. 2003; see **Figure *10***). The modified version permits calculating the daily amount of light available for a variable number of layers. In this way, taller trees in higher layers shade smaller trees in lower layers and have a growth advantage through the acquisition of light. Given that the 3D-CMCC-FEM model runs on a daily basis the sun position is not accounted for as it is not explicitly accounted for in the meteorological input data.

Competition for light and water represents one of the most relevant factors influencing biomass allocation. To simulate light competition, the 3D-CMCC-FEM model considers a modified version of the Lambert-Beer Law of light attenuation (Monteith and Unsworth 1990; Collalti 2011; Collalti et al. 2014), as approximated by Monsi-Saeki formulation of exponential attenuation, and coupled with the 'two-big-leaf' approach for a multi-layered model (**Figure *11***). This approach allows to scale of the physiological processes from leaf to canopy level, considering the exchanges between upper and lower layers, and between sunlit and shaded leaves, that, ultimately, account for one discrete single layer each within a single canopy. Each canopy layer (both as the overall canopy and within a single canopy) intercepts, reflects, transmits, and absorbs a fraction of the receiving light. The remaining fraction reaches the understoreys, determining different light conditions and growth rates (see also Photosynthesis and NPP paragraph).

The incoming shortwave radiation I_0 (MJ m^{-2} day^{-1}), is first converted to Photosynthetic Active Radiation (PAR_0, ≈400 to 700 nm) and then the absorbed PAR (APAR) is computed as follows:

$$APAR_{x,y,k\,\epsilon\,z} = PAR_0 \cdot (1 - e^{-k_x \cdot LAI_{x,y,k\,\epsilon\,z}}) \cdot \rho_x \cdot CC_z \qquad Eq.4$$

where *k* is the species-specific light extinction coefficient (≈0.5), a somewhat parameter describing leaf inclination and absorptivity/transmissivity capacity relative also to leaf thickness, and *ρ* is the species-specific canopy albedo (≈0.10 for evergreen and ≈0.16 for deciduous). At the layer level, this becomes the sum of all absorbed PAR by canopies at layer *z* (APARz).

The available PAR for a lower layer (i.e. the transmitted PAR) *z*—1 is then:

$$PAR_z = (PAR_0 - \sum APAR_z) = PAR_0 \cdot (e^{-k_x \cdot LAI_{x,y,k \in z}}) \cdot \rho_x \cdot (1 - CC_z) \qquad Eq.5$$

and the APAR for the layer *z*—1 becomes:

$$APAR_{z-1} = PAR_{z-1} - (1 - e^{-k_x \cdot LAI_{x,y,k \in z-1}}) \cdot \rho_x \cdot CC_{z-1} \qquad Eq.6$$

The available PAR for a lower layer (i.e. the transmitted PAR) *z*—2 is then:

$$PAR_{z-1} = (PAR_1 - \sum APAR_{z-1}) = PAR_z \cdot (e^{-k_x \cdot LAI_{x,y,k \in z}}) \cdot \rho_x \cdot (1 - CC_{z-1}) \qquad Eq.7$$

and the APAR for the layer *z*—2 becomes:

$$APAR_{z-2} = PAR_{z-2} - (1 - e^{-k_x \cdot LAI_{x,y,k \in z-1}}) \cdot \rho_x \cdot CC_{z-2} \qquad Eq.8$$

these equations for PAR, APAR, and PAR_{refl} (the reflected PAR) are iteratively solved for all the n number of layers which the forest structure should be composed of and scaling the absorbed and available light for the fraction of the layer that is covered (or not) by the canopies. The PAR reaching the soil (PAR_{soil}), for seedlings and saplings development, is the net balance between the incoming PAR_0 , the PAR not absorbed by the canopies of *n* the layer(s), and the PAR reflected because of soil albedo (ρ_{soil}). For simplicity, we avoid distinguishing here between sunlit and shaded APAR, however, the 3D-CMCC-FEM distinguishes between the

$APAR_{sun}$ and $APAR_{shade}$ for each class. Note, that initial model versions did not account for radiation reflection because of albedo which started to be accounted for only in the daily versions of the model code (Collalti et al. 2016).

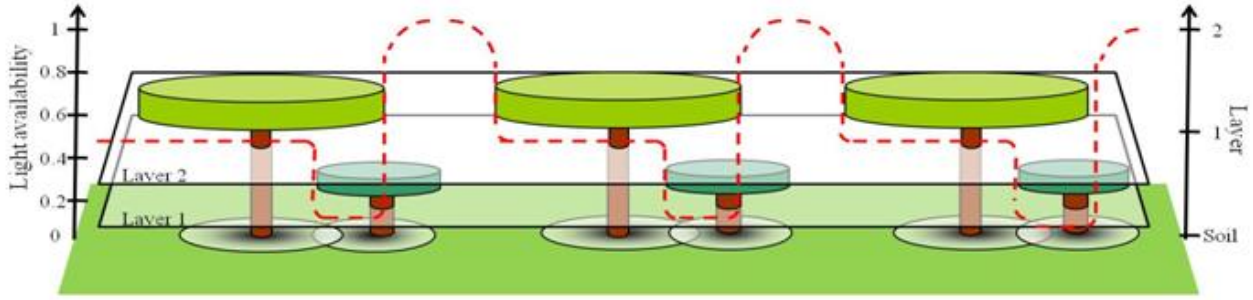

Figure 10 Conceptual representation of light availability in the 3D-CMCC-FEM through different canopy layers (figure from Collalti 2011).

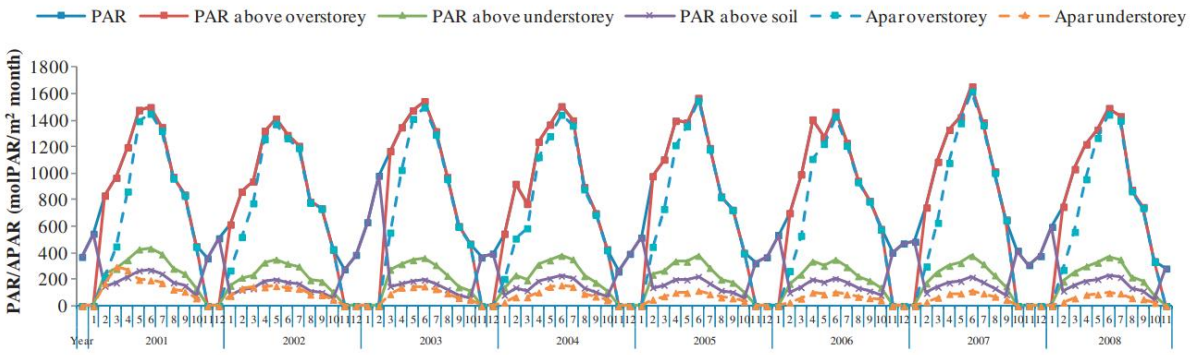

Figure 11 Monthly mean PAR (continuous line) and mean APAR (dotted line) (molPAR m^{-2} $month^{-1}$) distribution (2001–2008) through the two storeys (square point is referred to overstorey, triangle point to understorey, cross point to soil) from to the top of the canopies to the soil level in the double-layered Turkey oak (*Q. cerris* L.) forest at the Torre di Feudozzo (Italy) (figure from Collalti et al. 2014).

A similar, yet more complex, scheme is also adopted for the Net Radiation (i.e. Short- and Long-Wave net balance) (Collalti 2011).

3. CARBON AND NITROGEN BUDGET

3.1 Carbon and Nitrogen Cycles

The overall carbon budget in the 3D-CMCC-FEM is the result of processes representing incoming fluxes (i.e. photosynthesis), two main outgoing fluxes, i.e. autotrophic, R_a; and heterotrophic respiration, R_h; their sum is the ecosystem respiration, R_{eco}, and the change in C-stocks due to turnover and/or mortality and, when applied, to disturbances, e.g. thinning. The net balance at the autotrophic level is represented by the Net Primary Production (NPP; Gross Primary Production, GPP minus R_a). The net balance at the ecosystem level is the Net Ecosystem Exchange (NEE; GPP minus R_{eco})(Chapin et al. 2006). 3D-CMCC-FEM does not simulate to date any outgoing C-fluxes due to non-anthropogenic disturbances, e.g. fire. Therefore, NEE can be considered pragmatically as equal to Net Ecosystem Production (NEP = GPP — R_a — R_h — disturbances). As similarly as for fluxes (e.g. GPP, R_a, NPP, and so on) also C-stocks have their own carbon budget which is represented by 'incoming' new structural (or non-structural) biomass and the 'outgoing' dead biomass, the net balance represents the remaining biomass after these two opposite in sign fluxes. By abstraction, there are several levels of 'budget' depending on the level of representation which in 3D-CMCC-FEM are at tree- and cell-level which also include litter- and soil-level. Note, given that carbon and nitrogen are in 3D-CMCC-FEM stoichiometrically linked the same C-budget for C-stocks is specularly represented for N-stocks and it is not described here. Any budget for C, N, Energy, and H_20 is checked daily, monthly, and annually at any hierarchical level of representation for the conservation of mass and energy (see paragraph PRINCIPLE OF THE CONSERVATION OF ENERGY AND MASS8).

3.2 Photosynthesis

The carbon flux into the vegetation via the photosynthetic process, the Gross Primary Production (GPP), is computed in the 3D-CMCC-FEM model by two different, mutually independent methods: the Light Use Efficiency (LUE) empirical approach (Monteith, 1977) and the biochemical model of Farquhar, von Caemmerer and Berry (FvCB, 1980) model as adapted by de Pury and Farquhar (1997) for sunlit and shaded leaves. The use of one approach or the other depends on model user settings ('*PSN_mod'*, with 0 for the FvCB photosynthesis model and 1 for the LUE photosynthesis model).

3.2.1. Light Use Efficiency Model

(subroutine: *photosynthesis.c*)

In the empirical version (LUE version), the Gross Primary Production (GPP) for each class in the layer *z*, and dominated by a species *x* (see for example **Figure 12** and **Figure 13**), is computed as:

$$GPP_{x,y,k\in z} = (\varepsilon_{max_x} \; or \; \alpha_{max_x}) \cdot \; APAR_{x,y,k\in z} \cdot \; f_{T_x} \cdot f_N \cdot f_{CO_2} \cdot f_{phys_{x,y,k\in z}} \qquad Eq.9$$

the parameters ε_{max} and α_{max} are the species-specific prognostic potential Light Use Efficiency (in grams of carbon or moles of carbon per moles of PAR, respectively) and depend on the species x. APAR is the Absorbed Photosynthetic Active Radiation (molPAR^{-2} day^{-1}), i.e. the amount of the PAR entering the layer *z* which is absorbed by the canopy. The limiting factors (denoted as '$f_{variable}$') are dimensionless values ranging from 0 to 1 (see section 'Modifiers'). These factors serve as trigger modifiers related to several environmental factors, such as VPD, f_{VPD} air temperature, f_T, soil water content, f_ψ and site nutrient status, f_N including effects of stand age and atmospheric CO_2 concentration. Whether in the modifiers (as also for other variables) the '*x*' is not included as a subscript into the equation the species are not modelled to respond differently.

As in the 3-PG model, there's an additional 'physiological modifiers' f_{phys} that is defined as *min* (f_{vpd}, (f_ψ • f_{age}) (i.e. the minimum value between f_{VPD} and $f\psi$ • f_{age}). By means of the $f\psi$ modifier, the LUE photosynthetic process is linked to the hydrological cycle (see paragraph 4). Note, as also in the FvCB model (see below) the LUE version distinguishes for sunlit and shaded leaves no in terms of use efficiency (which does not vary between the sunlit shaded leaves in the model) but between their different LAI and, thus, light absorption. At the cell level, the 3D-CMCC-FEM sums up all the GPP coming from the different classes, i.e. *x, y, k* belonging to the layer *z* and the number of layers (N) as:

$$GPP = \sum_{Z=1}^{N} \quad GPP_{x,y,k,z} \qquad Eq.10$$

and across daily, monthly, and annual values.

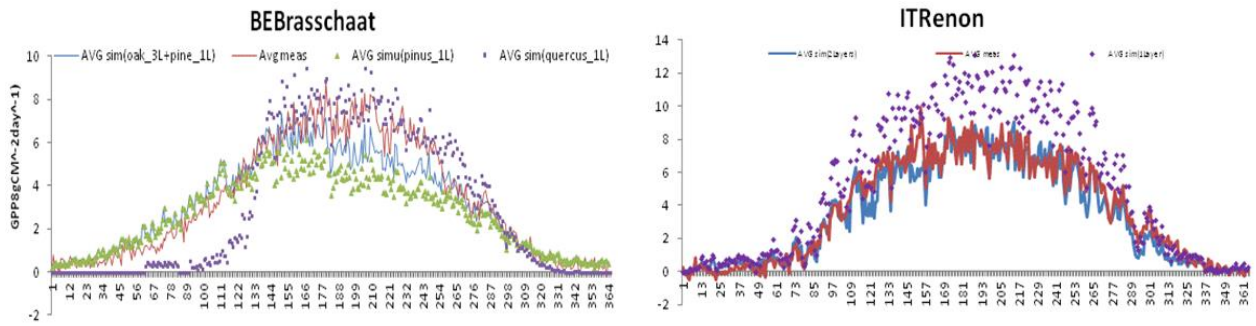

Figure 12 Daily model results for GPP (gC m^{-2} day^{-1}) with two different model configurations at Brasschaat site (Belgium, BE-Bra) and Renon site (Italy, IT-Ren). Model comparison at the Brasschaat modelled GPP by considering three canopy layers for Oaks (*Quercus robur* L.) and 1 layer for Pines (*Pinus sylvestris* L.) (blu line), by only simulating 1 layer of Pines (green line) and by only simulating 1 layer of Oaks (violet dots) versus measured GPP (red line)(left figure). Model comparison at the Renon site modelled GPP by considering two canopy layers (blu line), one single layer (violet dots) for Norway spruce (*Picea abies* (L.) H.Karst.) versus measured GPP (red line) (right figure) (Marconi et al. 2013).

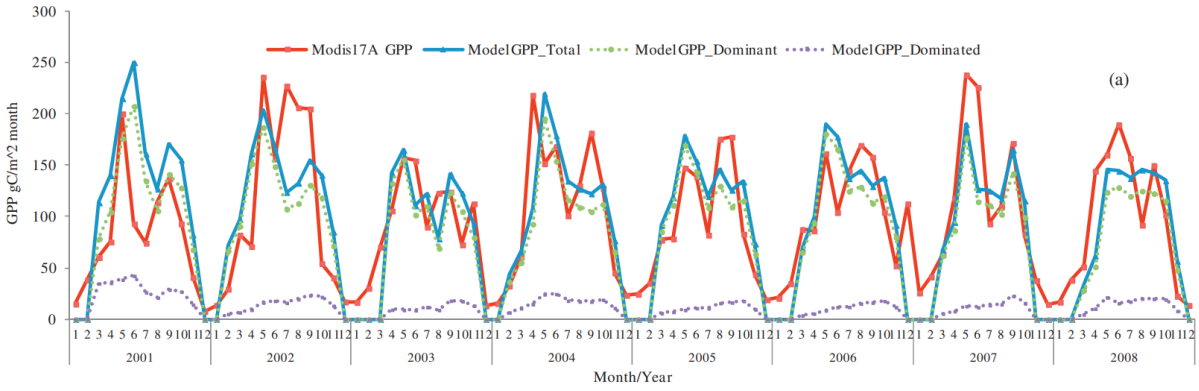

Figure 13 Comparison of MODIS monthly GPP (Modis 17A) and 3D-CMCC-FEM (v.1.0) monthly GPP (gC m^{-2} $month^{-1}$) in the double-layered Turkey oak (*Q. cerris* L.) forest at the Torre di Feudozzo (Italy) (figure from Collalti et al. 2014).

3.2.2. Biogeochemical Model

(subroutine: *photosinthesis2.c*)

In the fully biogeochemical version (BGC version), the 3D-CMCC-FEM computes the photosynthetic process at the leaf level, adopting the Farquhar et al. (1980, but see also Collatz et al. 1991) approach as modified for sun and shaded leaves by de Pury and Farquhar (1997). Hence, the effect of atmospheric CO_2 concentration is directly embedded in the photosynthesis routine. However, in the 3D-CMCC-FEM model, there is the possibility to fix atmospheric CO_2 concentration to a specific value so as to not consider the so-called 'CO_2 fertilisation 'effect'. For the temperature dependence of the Michaelis-Menten coefficient for Rubisco and the CO_2 compensation point

without mitochondrial respiration, the model adopts the parameterization described in Bernacchi et al. (2001, 2003). Temperature acclimation of leaf photosynthesis to increasing temperature is accounted for (when '*Photo_accl*' is set to 'on') following Kattge and Knorr (2007). Following the definition of Smith and Dukes (2012), acclimation is the physiological, structural, or biochemical adjustment by an individual plant in response to an environmental stimulus that is manifested as alterations in the short-term response function of a physiological process. In the de Pury and Farquhar (1997) two-leaf model (or 'sun-shade' model), the rate of photosynthesis depends on nitrogen content, which is controlled by the C:N ratio for leaves, in the sunlit and shaded leaves and Rubisco, the temperature leading enzyme kinetics, the Maintenance Respiration (R_m), and the difference between internal and external partial pressure of CO_2. The rate of photosynthesis is sensitive to the N content of leaves, the portion of N in Rubisco, and the temperature as this controls the enzyme kinetics. The amount of Rubisco depends on the user-defined fraction of leaf N in Rubisco and the user-defined C:N ratio of leaves (a species-specific parameter). Photosynthesis also depends on the amount of absorbed PAR, the calculated R_m in leaves, and the difference between the internal and external partial pressure of CO_2. As always, all steps are done separately for sun and shade leaves. The 3D-CMCC-FEM considers both the Leaf-scale maximum carboxylation rate (V_{cmax25} at 25 °C) and the maximum rate of electron transport (J_{max25} at 25 °C) and then corrected for actual leaf temperature (Medlyn et al. 1999) and soil water content (Bonan et al. 2011). Both the actual (V_{cmax}) and the maximum carboxylation rate, as well as the actual (J_{max}) and the maximum rate of RuBP regeneration are computed separately for sun and shaded leaves, as nitrogen and Rubisco vary between sun and shaded leaves, similarly as in the CLM model (Bonan et al. 2011). The net carbon uptake A (both for sun and shaded leaves) is first computed per unit of projected leaf area and then upscaled from leaf to canopy via the LAI. The final carbon flux GPP is computed by adding the maintenance respiration of the leaf pool (both as maintenance respiration for sun and shaded leaves, (see paragraph 3.8 Phenology, Partitioning and Allocation and Turnover') and accounting for cold acclimation (f_t; see below) in the coming model version:

$$GPP_{x,y,k \in z} = A_{x,y,k \in z} + Leaf\ R_{m_{x,y,k \in z}} \cdot f_t \qquad \textit{Eq.11}$$

The total GPP at stand level is the sum of GPP across species, DBH classes, cohorts, and layers. At the cell level, the 3D-CMCC-FEM sums up all the GPP coming from the different classes and number of layers (N) as:

$$GPP = \sum_{Z=1}^{N} GPP_{x,y,k,z} \qquad \textit{Eq.12}$$

and across daily, monthly, and annual values.

The 3D-CMCC-FEM capacity for simulating GPP (both in its LUE and FvCB version) has been largely tested in several sites around Europe and North Canada over the years (Collalti 2011, Collalti et al. 2014, 2016, 2018, 2020a; Marconi et al. 2017; Dalmonech et al. 2022, 2024; Mahnken et al. 2022a, Testolin et al. 2023; Vangi et al. 2024a, 2024b; Saponaro et al. 2024; Puchi et al. *in prep.*; and see **Figure *14***, **Figure *15*** and **Figure *16***)

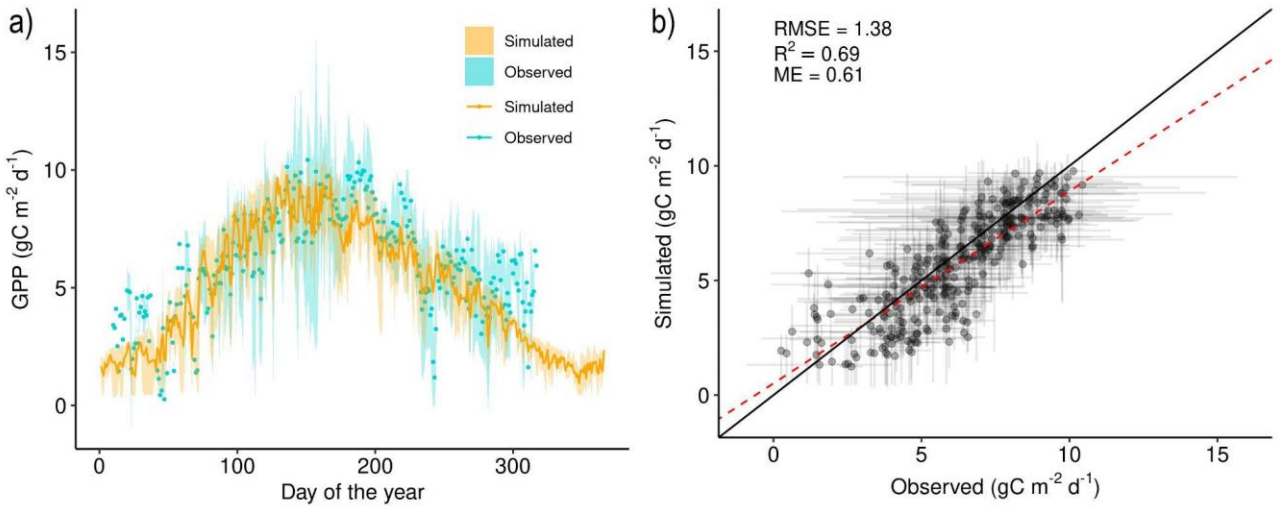

Figure 14 Evaluation of the average simulated daily GPP (gC m^{-2} day^{-1}), as the man season cycle, against the values obtained by the eddy covariance tower at the Bonis watershed in the years 2005‑2008 (a, b). The solid line represents the mean simulated value. The points represent the mean values derived by eddy covariance measurements in different years. Shaded areas (a) and error bars (b) are the intervals between the minimum and maximum values for a given day (figure from Testolin et al. 2023).

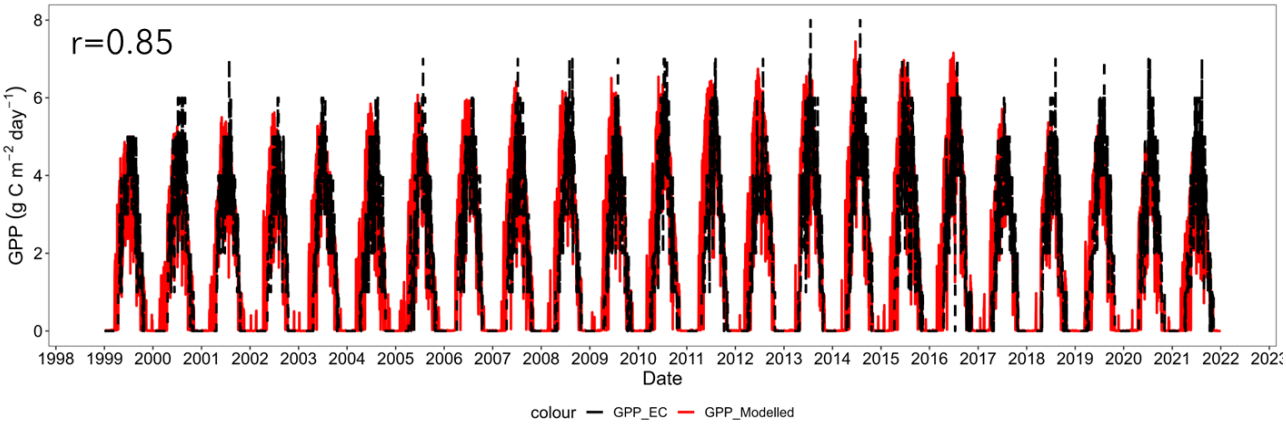

Figure 15 Comparison of daily Gross Primary Productivity (gC m^{-2} day^{-1}) between GPP from eddy covariance tower (AmeriFlux CA-OJP) and the GPP modelled using 3D-CMCC-FEM at site Prince Albert (Canada), *Pinus banksiana* Lamb. for the period 1999-2021 (Puchi et al. in prep.).

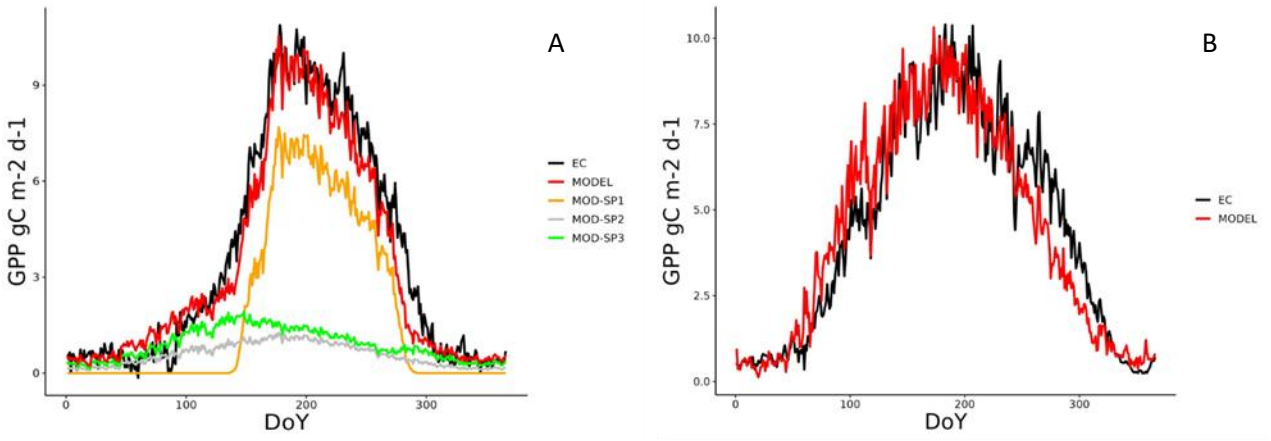

Figure 16 Daily seasonal cycle (average 2012-2020) of the gross primary productivity (GPP) in the sites of A) Torgnon, Valle d'Aosta, Italy, estimated from the measured carbon flux with the eddy-covariance methodology (EC) and modelled by the 3D-CMCC-FEM. Modelled GPP fluxes as reported as total and according to species :SP1: *Larix deciduas* Mill., SP2: *Picea abies* (L.) H.Karst, and SP3: shrubs in the understory. B) Renon, South Tirol, Italy, estimated (EC) and modelled GPP values as sum of the GPP simulated for each cohort, i.e. 5 in total**.**

The 'cold acclimation'

In recent forest modelling studies, it has been observed delay in the resumption of GPP during springtime in northern forests (Luo et al. 2023). Specifically, the modelled GPP from 3D-CMCC-FEM, compared to GPP obtained via eddy covariance, started, systematically in northern/boreal sites approximately three weeks earlier. Surprisingly, such a mismatch has been shown to hit not just the 3D-CMCC-FEM GPP results but also other models (**Figure *17***). This disparity has been elucidated by the phenomenon of 'cold acclimation' prevalent in cold environments.

Boreal ecosystems, characterized by their sensitivity to cold winters, necessitate an acclimation period for tree tissues to resume photosynthesis effectively. This acclimation process, notably observed in evergreen needle forests (Chang et al. 2021; Luo et al. 2023), is imperative for coping with the rigors of winter freezing, known as cold hardiness. The principal photoprotective mechanism employed by evergreen trees involves an increase of protective pigments to counteract ice crystal formation.

As a consequence, during the early spring season, evergreen trees require a period for metabolizing photo-pigments and for re-starting photosynthetic activity. This precautionary pause is necessary because trees cannot ensure immunity from potential cold spells that might freeze their hydraulic system. Consequently, with the onset of spring, these trees undergo a necessary phase to eliminate these pigments and initiate growth with care. This cautious approach is essential as there remains the risk of cold days that could inflict damage upon their hydraulic systems.

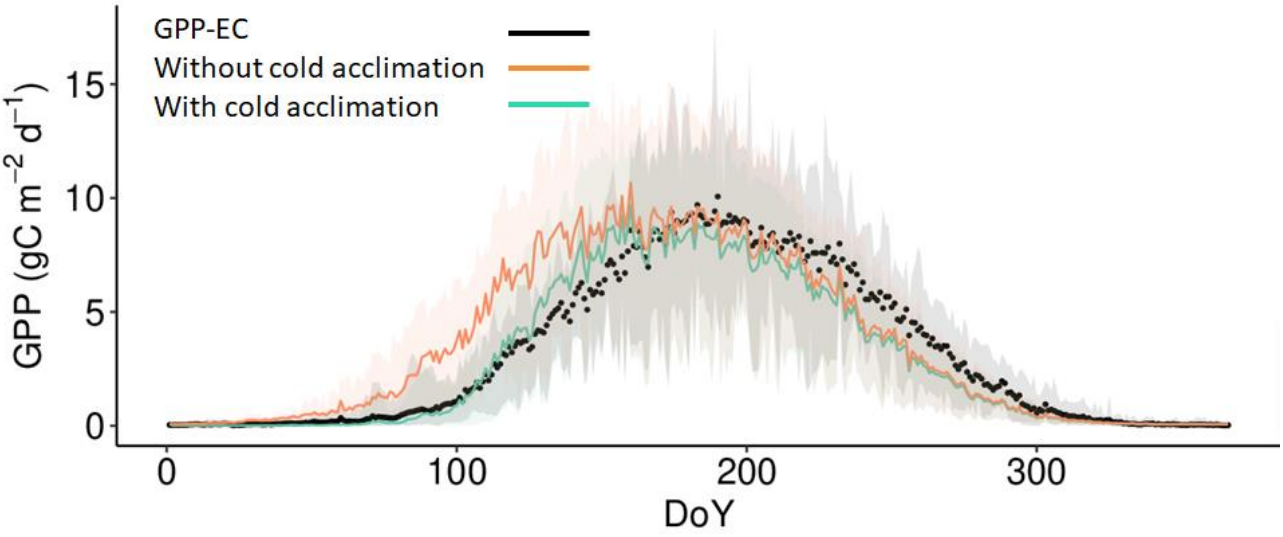

Figure 17 Comparison of the daily mean seasonal cycle of observed GPP_EC (black line), modelled GPP (gC m^{-2} day^{-1}) with cold acclimation (green line) with no cold acclimation (orange line) for the Fluxnet-site of Hyytiälä in southern Finland, an evergreen needled leaf forest, for the period 1996-2014.

In response to this delay, Mäkelä et al. (2008) suggested implementing an acclimation function to reduce this discrepancy and rectify the 'overestimation' of GPP during the early spring. The modifier (f_t) accounts for the temperature acclimation and we implemented it directly to the GPP in the model (see in the 'Multipliers' paragraph). Note that the 'cold acclimation' function does not make part of the v.5.6 and it represents a future implementation in the coming new version of the model.

3.3 Autotrophic Respiration

(subroutine: *autotrophic_respiration.c*)

Forest autotrophic respiration (R_a) plays an important role in the carbon balance of forest ecosystems. Only 30-50% of photosynthesis (GPP) is used for making leaves, wood, and root tissues, while the remaining portion returns back to the atmosphere in the form of R_a (DeLucia et al. 2007). The 3D-CMCC-FEM computes the R_a mechanistically by considering plants' respiration as the sum of maintenance respiration (R_m) of all living tissues and daily growth or synthesis respiration (R_g) — the so-called '*growth-and-maintenance-respiration paradigm*' ('GMRP'; Amthor 2000) — on a daily scale. In the 3D-CMCC-FEM, there is also the chance, coming from previous model versions, to consider (or to approximate) R_a depending only on annual photosynthesis by increasing the turnover rate parameter (i.e. the inverse of residence time or 'longevity') of live respiring biomass to 1 (see Collalti et al. 2020a, **Figure 18**) with no accumulation of live (respiring)

biomass over the years (apart from leaves and fine root in evergreen species). A different way to consider respiration as a fixed fraction of photosynthesis is by setting the parameter '*Progn_Aut_Resp*' with 'off' and the 3D-CMCC-FEM will use the Waring et al. (1998) 'fixed fraction' controlled by the '*Y*' parameter.

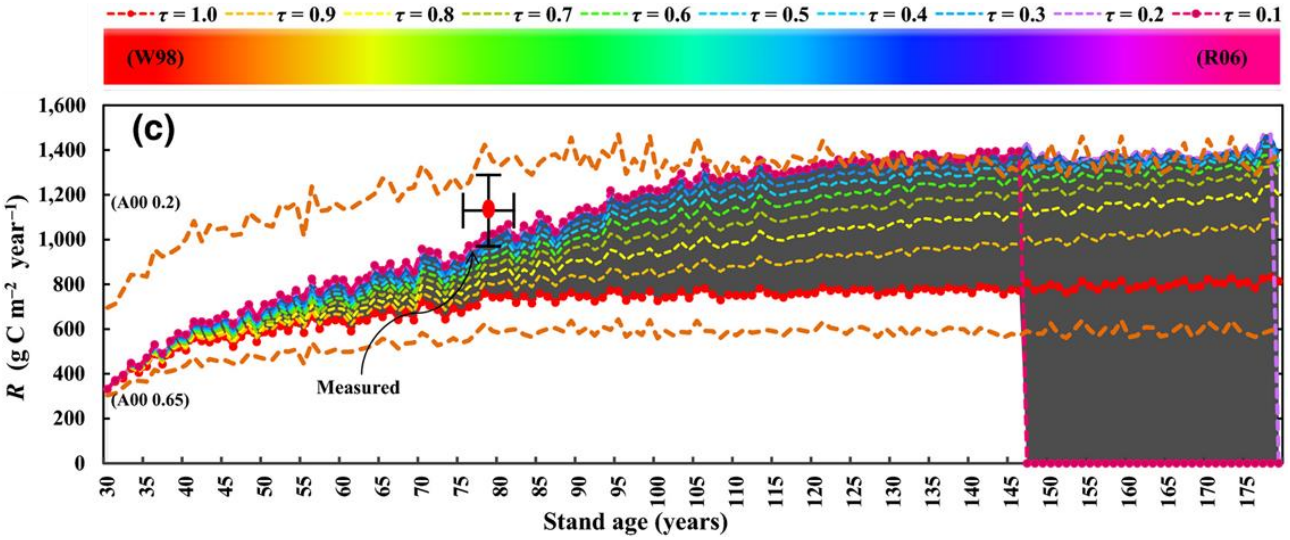

Figure 18 Model results for autotrophic respiration (R, gC m^{-2} $year^{-1}$) performed with varying τ (coloured lines). The beginning of simulations corresponds to 1950 (i.e. when the stand was 30 years old); the end corresponds to 2100 (the stand reached an age of 180 years). The dark-pointed red line can be considered as a mechanistic representation of Waring et al.'s (1998; 'W98') fixed NPP: GPP ratio (τ = 1 $year^{-1}$, i.e. all live biomass dies the year after, no live biomass accumulates over the years), while the dark-pointed pink line approximates Reich et al.'s (2006, 'R06') scaling relationship between R and biomass (τ = 0.1 $year^{-1}$; i.e. few of the previous live biomass dies the year after, most of the live biomass accumulates). Orange dotted lines represent Amthor's (2000)(A00) 'allowable' range for the NPP: GPP ratio (0.65‑0.2). The red dots give the average measured values (Wu et al. 2013) at the site for R. Vertical bars represent the standard deviation with horizontal bars representing the period 2006–2010 (stand age ≈85–90 years). The shaded area represents the overall uncertainty of model results (figure from Collalti et al. 2020a). In this case, R stands for R_a.

Maintenance respiration is the basal rate of metabolism and includes the energy expended on ion uptake and transfer within plants and the repair of injured tissue (Waring and Running 2007). R_m is computed daily (but partitioned into daytime and night-time respiration for leaves) in the 3D-CMCC-FEM as a function of both Mass and Temperature. Leaf maintenance respiration is computed using daytime temperature and night-time air temperature. Root (both for fine and coarse) maintenance respiration is computed daily using the soil temperature. Other pools (i.e. stem and branch) use average air temperature, instead. The temperature effect is simulated through the standard Arrhenius relationship but, in the most recent versions of the model, modified to consider short- and long-term acclimation responses (i.e. '*Type I*' and '*Type II*' acclimation). The original formulation in 'v.5.1' adopted the classical temperature-dependent Q10 function with Q_{10} ≈2, i.e. the rate of biochemical reactions doubles for every 10 °C increase in temperature. However, there is a compelling

body of evidence that respiratory Q_{10} is not likely to be constant but rather depends on both the shape of the temperature-response curve and the range of temperatures used in its empirical determination and that plants can adjust respiration rate in response to a change in temperature. Conversely, the formulations, in the most recent version of the 3D-CMCC-FEM, consider an acclimation, both on short- and long-term, on maintenance respiration and comprises the Q_{10} modification that more closely (and realistically) matches both the instantaneous and the longer-time responses of maintenance respiration (Tjoelker et al. 2001; Atkin and Tjoelker 2003; Atkin et al. 2005, 2008; Smith and Dukes 2012). This modification, called '*Type-I*' acclimation (or 'short-term acclimation'), is expressed as:

$$Q_{10} = 3.22 - 0.046 \cdot T_{pool} \qquad Eq.13$$

where T_{pool} is the temperature acting to a specific pool (e.g. T_{soil} for roots), and it varies between different pools (for comparison with the classical $Q_{10} = 2$ see Figure 19a). The instantaneous respiration rate at a given temperature (R_T) then becomes:

$$R_{T_{pool}} = R_{Ref} \cdot Q_{10}^{\left(\frac{T_{pool}-T_{Ref}}{10}\right)} \qquad Eq.14$$

where R_{ref} is the basal respiration rate (0.218 gC gN^{-1} day^{-1}; Ryan 1991; Thornton et al. 2007), N is the nitrogen content in the live structural tissues (leaves, fine roots, and livewood, in gN m^{-2}; Cox 2001), T_{Ref} is the reference temperature (20 °C; Thornton et al. 2007; Reich et al. 2016) and T_{pool} the temperature for each pool. For every single pool, the 3D-CMCC-FEM compute, as in Cox (2001), based on Temperature effects and Mass (i.e. the tissue nitrogen content for each live pool, N in gN m^{-2}) the maintenance respiration as:

$$R_{m_{x,y,k\,\epsilon\,z}} = R_{T_{pool}} \cdot N_{x,y,k\,\epsilon\,z} \qquad Eq.15$$

such a formulation leads to a decrease in respiration to an increase in T_{pool} at a peak temperature of ≈ 35 °C reflecting a rather instantaneous response or respiration to temperature reflecting a biochemical adjustment to this temperature increase (Atkin and Tjoelker 2003; **Figure 19**).

The '*Type II*' acclimation (or long-term acclimation') represents the likely result of biogeochemical plant adjustments and/or biogeochemical feedbacks in the long-term response of respiration rates to temperature ($R_{m\ accl}$, gC m^{-2} day^{-1}; Atkin and Tjoelker 2003; Atkin et al. 2005, 2008) that leads to a decrease in the temperature-mediated basal rate response curve with increasing temperature as described by Smith and Dukes (2012), through:

$$R_{m\ accl} = 10^{A_r \cdot (t_{10days-pool} - T_{ref})} \qquad Eq.16$$

where A_r represents a constant temperature correction factor for acclimation (0.00794; Atkin et al. 2008; Smith and Dukes 2012) and T_{10days} is the 10-day running weighted average of the previous days (daytime, nighttime, average, or soil temperature, depending on the pool considered) temperature (**Figure *19*b**). Thus, R_m, as modified with *Type-I* and *Type-II* acclimation control and accounting for mass, becomes:

$$R_{m_{x,y,k\,\epsilon\,z}} = R_{T_{pool}} \cdot N_{x,y,k\,\epsilon\,z} \cdot R_{m\ accl} \qquad Eq.17$$

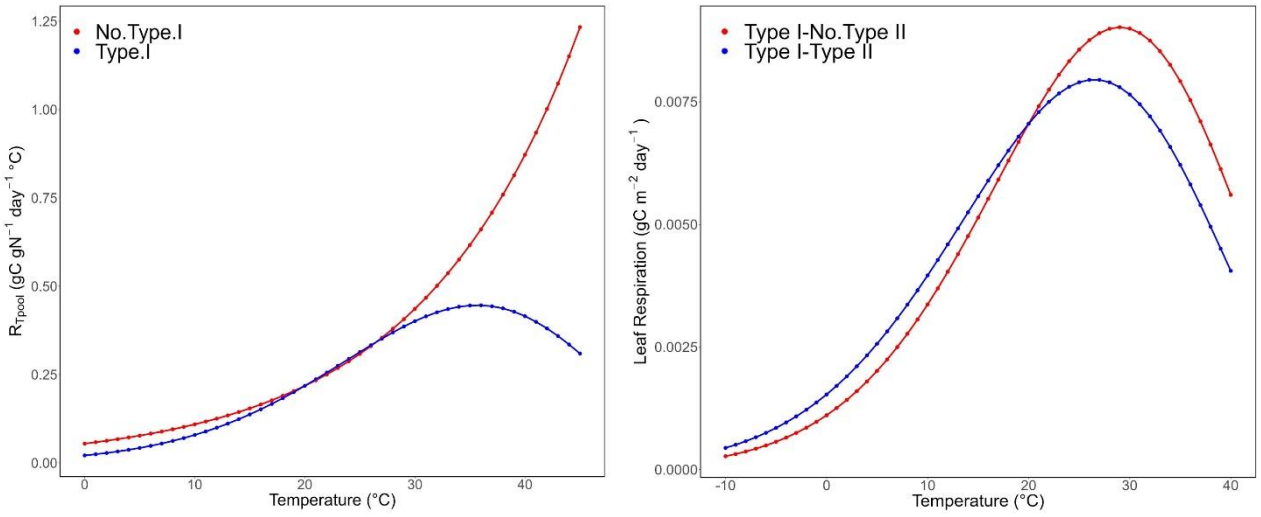

Figure 19 (Left panel) Type-I or short-term acclimation. Comparison of Q_{10} respiration rate function at varying temperature with no modification 'No Type I' (fixed Q_{10}, with Q_{10} = 2.0; red line) versus modified 'Type I' (variable Q_{10} with Q_{10} = 3.22–0.046T_{pool}, blue line) with R_{Ref} = 0.218 gC gN^{-1} day^{-1} (Ryan 1991, Thornton et al. 2007) with T_{ref} = 20 °C. (Right panel) Type-II or long-term acclimation. Comparison of daily leaf temperature respiration responses including only 'Type I' (red line) and 'Type-I' + 'Type-II' (blue line) at varying temperatures with Leaf nitrogen = 4.407 gN m^{-2}. Temperature is the T_{day} 10-day average temperature (redrawn from Collalti et al. 2018).

Acclimation of maintenance respiration (and its effects on the overall C-budget) can be switched off in 3D-CMCC-FEM by setting 'on' or 'off' in the setting file. Maintenance respiration is computed in 3D-CMCC-FEM for leaves (both as sunlit and shaded leaves) for both day and night (using T_{day} and T_{night}) because of the respiration in the FvCB photosynthesis model. Conversely, the model considers the stem and branch pool T_{avg}, and for coarse and fine root it considers T_{soil}. Therefore, the overall final maintenance respiration is the sum of each single maintenance respiration in each respiring biomass pool. Given that trees accumulate a large amount of conducting and storage tissues in biomass as they age (i.e. growth), even including the turnover of these pools, the initial increase and the subsequent observed decrease in relative NPP is often associated (but this is a much-debated topic) with age has often been assumed to reflect increasing maintenance costs, because with ageing the biomass tends to accumulate (e.g. Ryan et al. 1997; Mäkelä and Valentine 2001; Collalti et al. 2020a, 2020b). In 3D-CMCC-FEM for both stem, branch, and coarse root only the live component is considered and not all the woody biomass while for leaves and fine root, all biomass is considered (Collalti et al. 2016).

Growth (or synthesis) respiration (R_g), that is the cost for constructing and synthesise new tissues, is considered in the 3D-CMCC-FEM to vary with tree age from 0.30 to 0.25 (30% to 25%) of the new daily carbon allocated to each pool (excluding Non-Structural Carbohydrates) (Larcher 2003). This percentage does not depend on abiotic factors, as there is little evidence that the specific costs of tissue biosynthesis are e.g. temperature dependent or CO_2 dependent (Hamilton et al. 2001).

The total R_a (as the sum of R_m + R_g) at stand/grid-cell level is the sum of R_a across species, DBH classes, cohorts, and layers as follows:

$$R_a = \sum_{z=1}^{N} R_{a_{x,y,k}} = \sum_{z=1}^{N} R_{m_{x,y,k}} + \sum_{z=1}^{N} R_{g_{x,y,k}} \qquad Eq.18$$

and it is integrated across daily, monthly, and annual values.

3.4 Net Primary Productivity

(subroutine: *C-assimilation.c*)

The Net Primary Production (NPP) is calculated daily in 3D-CMCC-FEM in two steps. Firstly, the allocable NPP (NPPalloc) is computed by subtracting the Maintenance Respiration (R_m) from the Gross Primary Production (GPP) as follows:

$$NPPalloc_{x,y,k \in z} = GPP_{x,y,k \in z} - R_{m_{x,y,k \in z}} \quad \textit{Eq.19}$$

This fraction of NPP is allocated to the different plant pools according to phenological phase and allocation rules as described in the paragraph 3.8 Phenology, Partitioning and Allocation and Turnover. When R_m exceeds GPP, NPP is negative and respiration is fuelled by NSCs (as it happens also during the dormant season for deciduous).

After the partitioning of the allocable NPP, the effective plant NPP is computed by subtracting the Growth Respiration (R_g) as follows:

$$NPP_{x,y,k \in z} = NPPalloc_{x,y,k \in z} - R_{g_{x,y,k \in z}} \quad \textit{Eq.20}$$

This is computed for each plant C-pool, other than the NSC-pool, and each class. At the cell level, the 3D-CMCC-FEM sums up all the NPP coming from the different classes and number of layers (N) as:

$$NPP = \sum_{z=1}^{N} NPP_{x,y,k} \quad \textit{Eq.21}$$

and across daily, monthly, and annual values. The 3D-CMCC-FEM capacity for simulating NPP (both accounting for R_a empirically or mechanistically) has been tested in several sites around Europe over the years (Collalti 2011; Collalti et al. 2014, 2018, 2020a; Engel et al. 2021; Dalmonech et al. 2022; Vangi et al. 2024a, 2024b; and see **Figure *20***)

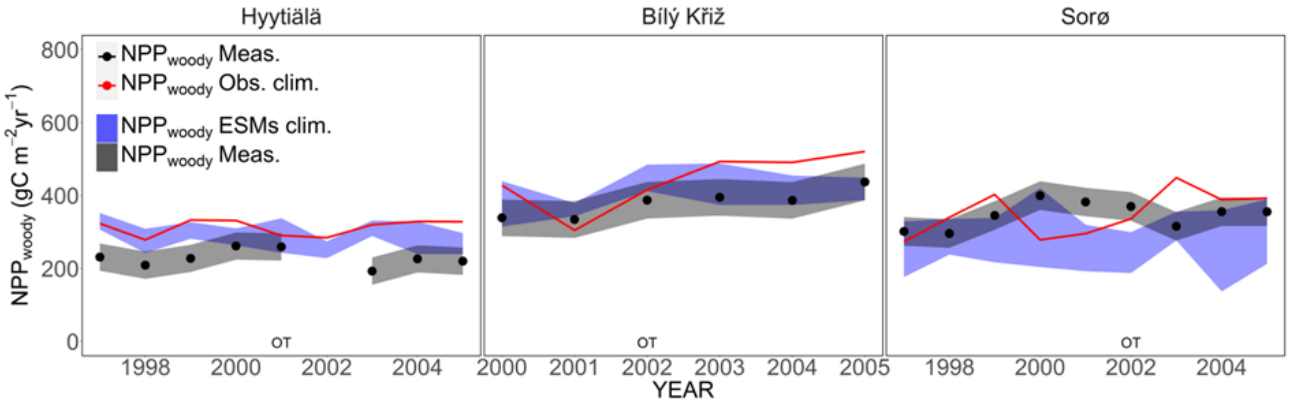

Figure 20 Comparison of the predicted annual NPP_{woody} (the annual NPP allocated to woody pools, gC m^{-2} day^{-1}) with site observations at three modelling stands. The blue shaded area represents the maximum and minimum bounds NPP_{woody} values among the five Earth System Models (ESMs) forcing meteorological data; the red line represents the average NPP_{woody} values when the model is forced by observed climate. Black dots represent the measured NPP_{woody} values (i.e. NPP_{woody} Meas.), and the grey shaded area represents the relative uncertainty bounds. At the Hyytiälä site, NPP_{woody} observed data for the year 2002 was missing. OT = observed thinning at the site; ESM = model forced with Earth System Models climate (figure from Dalmonech et al. 2022).

3.5 Forest and Carbon Dynamics

The traditional view of forest dynamics in undisturbed ecosystems describes an initial stepwise increase in productivity, followed by stabilisation and a further slight decline (Kira and Shidei, 1967; Odum, 1969). Several studies have shown that 3D-CMCC-FEM follows this general behaviour with GPP, R_a, and NPP increasing at increasing age till GPP stabilises and levels off at canopy closure, with R_a and NPP that alternatively start to increase and decrease in a feed-forwarding behaviour, but with a general trend mirrored in a slight NPP and R_a decrease for middle-aged classes to the old ones. Likewise, C-stocks increase sharply during juvenile stages and then slightly stabilise (Collalti et al. 2018; Dalmonech et al. 2022; Testolin et al. 2023; Vangi et al. 2024a, 2024b). Conversely, Tang et al. (2014; following Ryan et al. 1997 and Drake et al. 2011 and the 'hydraulic limitation' hypothesis), argued, in contrast to this foundational principle of ecosystem ecology, that NPP declines with age (mostly above-ground NPP), not because of increases in R_a but rather because of GPP declines as forest ages and that the NPP:GPP should remain fairly constant within a biome and along with ageing. Therefore, to this view, GPP should decrease and this would lead also R_a to decrease to maintain overall the NPP:GPP ratio invariant. Somewhat into the 3D-CMCC-FEM, the GPP declines with forest development as the age effect is already inherently embedded through the use of f_{age} a modifier that accounts for the age effect both in the LUE model (by directly reducing the maximum potential canopy quantum efficiency parameter α_{max}) as well as in the FvCB (by indirectly reducing in the Jarvis formulation the maximum stomatal conductance parameter $g_{s\,max}$). However, many tests accounting for the effects of a reduction in the GPP, and a theoretical decrease in R_a, into the model showed the larger effect of

biomass accumulation and R_a increase than a GPP reduction in the NPP:GPP behaviour as forest age (see **Figure *21***). Understanding the correct role of each component in the NPP will be crucial as elevated atmospheric carbon dioxide (CO_2) levels might enhance the carbon (C)-sink in forests by amplifying GPP, assuming it regulates the decline in NPP. However, rising temperatures could diminish this carbon sink if factors like R_a would show to play a dominant role in the decline of NPP (Drake et al. 2011).

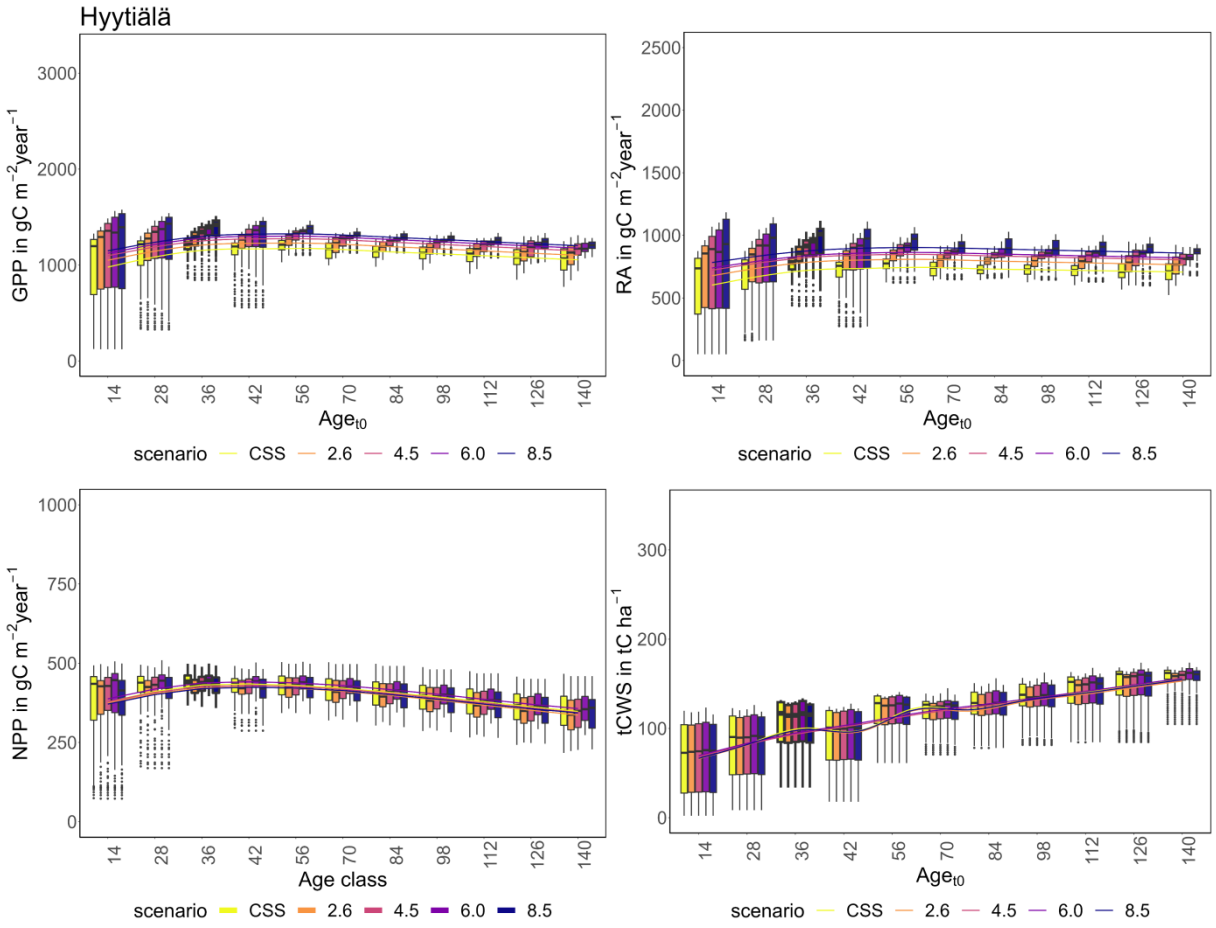

Figure 21 Boxplots GPP and NPP (Gross and Net Primary production, gC m^{-2} $year^{-1}$) R_a (Autotrophic Respiration, gC m^{-2} $year^{-1}$) and tCWS (Total Carbon Woody Stocks, tC ha^{-1}) by age classes at the Hyytiälä site in the four RCPs scenario compared to the CCS (Current Climate Scenario, i.e. no climate change scenario) one for the different 11 age classes. The thick line corresponds to the real stand, while the others come from the CFM approach. Lines are fitted throughout the median of the GPP, NPP, R_a, and tCWS values using a generalised additive model. 'Age classes' represent the stand age at the beginning of simulations (figure from Vangi et al. 2024b).

3.6 Carbon-Use and Biomass-Production Efficiency

(subroutine: *cue.c*)

The Carbon Use Efficiency (CUE) is the ratio of NPP to GPP and reflects the capacity of the plants to use the photosynthates to build plant tissues and synthesise non-structural and secondary compounds (Collalti and Prentice 2019). Differently, Biomass Production Efficiency (BPE) reflects how efficiently plants use assimilated carbon to build (only) plant organs (biomass production, BP) (Vicca et al. 2012; Campioli et al. 2016; Collalti et al. 2020b see **Figure 22**). These two metrics are inherently close, but not identical. Ultimately, given that the current 3D-CMCC-FEM versions do not account for BVOCs (Biogenic Volatile Organic Compounds) or root exudates, the main differences BP and NPP rely on the consideration of NSCs, which are not accounted for in the BP definition.

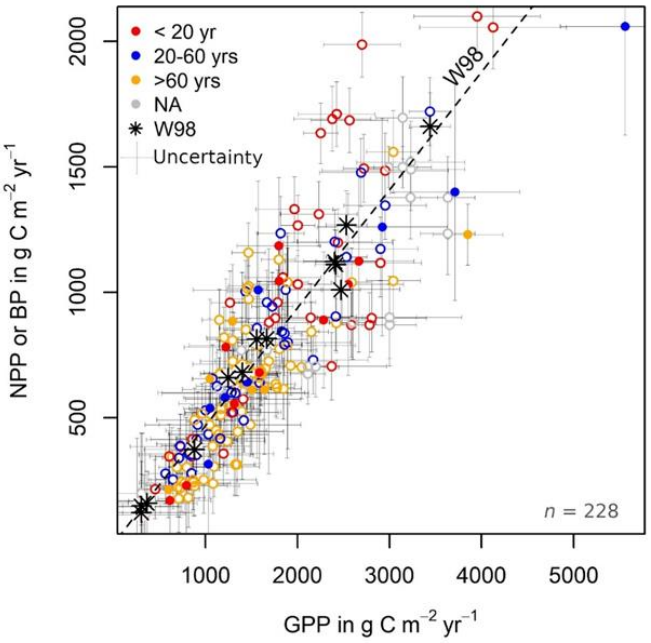

Figure 22 Scatter plot of net primary production (NPP, gC m^{-2} year^{-1}) or biomass production (BP, gC m^{-2} year^{-1}) versus gross primary production (GPP, gC m^{-2} year^{-1}) (n = 228). Open circles: BP, filled circles: NPP. Stars represent data points from Waring et al. (1998). The line marked with 'W98' represents a CUE (i.e. NPP:GPP) of 0.47. Age classes are marked by colours (see top left of the figure); NA stands for 'age not available'. The uncertainty (gC m^{-2} year^{-1}) of the data points is indicated by bars (figure from Collalti et al. 2020b).

Around the constancy or not to the NPP:GPP (or BP:GPP) ratio, there is a long-lasting debate with one school of thought emphasising its tight conservative nature close to 0.47 ± 0.04 (SD) (e.g. Waring et al. 1998; Gifford 2003; Litton et al. 2007; Van Oijen et al. 2010; Tang et al. 2014; Landsberg et al. 2020), with many forest or

vegetation models using this less complex approach (reviewed in Collalti and Prentice 2019). A different school of thought argues that the observations show a broad variation in the NPP:GPP ratio (0.46 ± 0.12 SD and a total range of 0.22-0.79) that is too large to be disregarded or considered as 'conservative' (Collalti and Prentice 2019; Collalti et al. 2020b) and then suggests for a mechanistic, and more complex, representation of R_a (and thus of the NPP:GPP ratio). Indeed, a long line of observations has shown that CUE (and BPE) varies largely because of, among others, stand age, species, forest management, soil fertility, and climate (e.g. Mäkelä and Valentine 2001; DeLucia et al. 2007; Vicca et al. 2012; Campioli et al. 2015; Collalti et al. 2018, 2020a, 2020b; Collalti and Prentice 2019; Luo et al. 2024). In addition, in a climate change context, assuming that R_a may vary in a constant and fixed proportion with GPP would imply assuming that these two processes acclimate at the same rate, although it has been shown they have different temperature responses (Drake et al. 2016; Reich et al. 2016). However, several studies (e.g. van Oijen et al. 2010; Collalti et al. 2020a, see **Figure *23***) have shown that there is a tight coupling between GPP and R_a because, ultimately, '*plants cannot respire what they do not have synthesised before*' (Gifford 2003).

All these factors (apart from soil fertility) are taken into account explicitly in the 3D-CMCC-FEM while computing GPP and R_a and, thus, NPP. The 3D-CMCC-FEM model commonly calculates both CUE and BPE, at various temporal scales, spanning daily, monthly, and annual scales using this last one (but read below), thus considering NPP as the result of GPP and R_a where R_a is mechanistically represented. With R_a computed, the 3D-CMCC-FEM relies on the NPP:GPP equation, for the BPE the BP is computed first (BP is the daily NPP going to stem, branch and bark, fruits, fine and coarse roots and leaves C-pools) and then divided by the GPP.

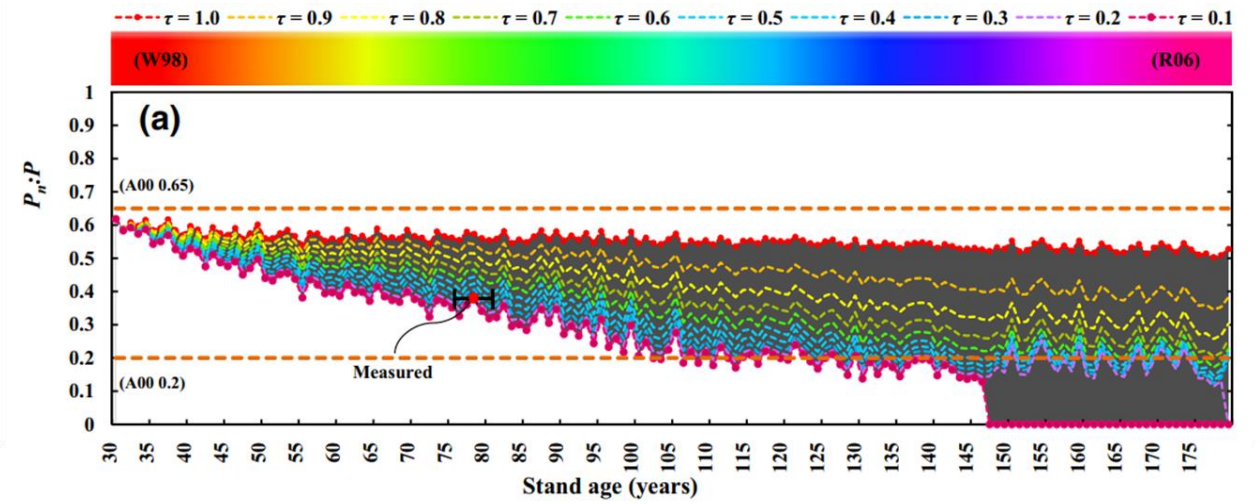

Figure 23 Model results for P_n:P ratio (dimensionless), performed with varying τ (live biomass turnover ratio, coloured lines). The beginning of simulations corresponds to 1950 (stand age 30 years), and the end of simulations corresponds to 2100 (stand age 180 years). The dark-pointed red line can be considered as a mechanistic representation of Waring

et al.'s (1998; W98) fixed Pn:P ratio (τ = 1 year^{-1}), while the dark pink line approximates Reich et al.'s (2006; R06) metabolic scaling relationship between R and biomass (τ = 0.1 year^{-1}). Orange dotted lines represent Amthor's (2000)(A00) 'allowable' range for the Pn:P ratio (0.65–0.2). The red dots give the average measured values (Wu et al. 2013) at the site for P_n:P ratio. The shaded area represents the overall uncertainty of model results (figure from Collalti et al. 2020a). In this case, P stands for GPP and P_n for NPP.

Note, much of the 3D-CMCC-FEM model instability (which reflects in the mortality of the stand during simulations) in model runs often relies on the activation of the 'growth efficiency' mortality which is turned on any time NSC is fully depleted, and current assimilates are not able to replenish and the maintenance respiration to be fuelled. This is generally due to too low GPP values and/or too high level of R_a values (and detectable by very low CUE values in the model outputs) in most of the cases caused by, for non-practitioner users, an erroneous calibration of biomass during initialization phase (see paragraph 1.4 Model Initialization: the Forest Structure and the Pools).

3.7 WATER-USE EFFICIENCY

(subroutine: *wue.c*)

The Water Use Efficiency (WUE) is the ratio of carbon gain during plant photosynthesis to water loss during evapotranspiration. Understanding WUE is essential for studying the interaction of water and carbon cycles in forest ecosystems (Puchi et al. 2024).

The 3D-CMCC-FEM model calculates different WUEs at various temporal scales, spanning from daily, monthly, and annual scales. Its computation can be performed at both the tree and ecosystem levels. At the tree level, the 3D-CMCC-FEM estimated three distinct types of WUE. The 3D-CMCC-FEM model incorporates various factors such as tree height, DBH, age, and species (deciduous or evergreen). Additionally, the model discriminates if the leaves are intolerant or shade-tolerant for accurate WUE estimations. Several WUE are considered the 3D-CMCC-FEM which are:

- Water Use Efficiency (WUE) at the tree level, which is calculated as the ratio of Net Primary Productivity (NPP) to canopy transpiration (g_C; i.e. NPP:g_C).
- Intrinsic Water Use Efficiency (iWUE) at the ecosystem level which is calculated as the ratio of Gross Primary Production (GPP) to canopy transpiration (g_C; i.e. GPP:g_C). Distinguishes between sunlit and shaded conditions, offering a better understanding of tree-level Water Use Efficiency.
- Stomatal Water Use Efficiency (g_sWUE) is derived from tree-level calculations and is calculated as the ratio of Gross Primary Production (GPP) to stomatal conductance (g_s; i.e. GPP:g_s).

3.8 PHENOLOGY, PARTITIONING AND ALLOCATION AND TURNOVER

3.8.1. Phenology

(subroutines: *phenology.c*)

The 3D-CMCC-FEM considers, for deciduous tree species, the length of the vegetative period by the variables T_{start} and '*MinDayLength*', i.e. the length of the day at which the senescence starts, for the beginning and the end of it. At the end of each day, the amount of new biomass is partitioned and allocated among the main tree carbon compartments: leaf, fine and coarse root, stem, branch, and fruit. The woody compartments are further subdivided into sapwood, heartwood, and live and dead wood. Another pool is represented by Non-Structural-Carbon (starch, and sugars) that is stored in the whole tree. NSC is used as a carbon reserve pool during periods of negative carbon balance (for example, during the dormant season, periods of stress or natural or artificially induced defoliation episodes, to combat pathogens, and fire scars, and injuries, which are, however, not accounted for by the 3D-CMCC-FEM). In these stress periods NSC is remobilized and transported from the sites of phloem loading (parenchyma rays in conifers; von Arx et al. 2015, 2017), while during periods of positive carbon balance plants preferentially allocate recently assimilated carbon to replenish NSC (Merganičová et al. 2019; Collalti et al. 2020a, 2021; D'Andrea et al. 2020, 2021). The minimum NSC is a set fraction of dry matter total sapwood mass (which is generically equal to 0.11 and 0.05 for deciduous and coniferous, respectively) as in Forest v.5.1 model (Schwalm and Ek 2004; but see also Barbaroux et al. 2003; Hoch et al. 2003) and as in Hybrid (v.3.0) model (Friend et al. 1997). The 3D-CMCC-FEM assumes that potentially all NSC can be actively remobilized and used under carbon-deficit periods to buffer C-demand as during leaves formation for deciduous in spring (Arora and Boer 2005) or under stress periods (Carbone et al. 2013). As a general principle, at any period of the year, if NSC concentration falls below this critical value, all photosynthates (if present, and once respiration costs are satisfied) are firstly allocated in the storage pool to reach the minimum NSC concentration value.

Allocation of assimilates to the other C pools is done at a daily scale and is strongly regulated by the 3D-CMCC-FEM phenological scheme, which is temperature- and photoperiod-dependent (Collalti et al. 2016, 2018; Marconi et al. 2017).

The 3D-CMCC-FEM, for deciduous species, considers four phenological transitions, i.e. that drive the seasonal progression of vegetation through phases of dormancy/quiescence, bud-burst and leaf growth, active growth, and senescence as in the following:

1. Budburst phase. During this green-up phase, the primary organs receiving remobilization of NSC are leaves and fine roots. The leaf (and fine root) onset is controlled and triggered by two species-specific parameters, which are a threshold thermic sum (the sum of the T_{day} exceeding the threshold T_{base} value of 5 °C; Bonan

2019) and a threshold day-length and, as generally assumed by many other models. Therefore, leaf and fine root onset start from quiescence when the thermic sum exceeds a species- and site-specific temperature threshold value. During the budburst phase and leaf and fine root development, which is controlled by a parameter regulating the number of days for this phase, newly synthesised carbon from photosynthesis and the remobilization of previously synthesised carbon (i.e. the NSC) are allocated to the foliage and fine root pools as long as the balance between GPP and maintenance autotrophic respiration is positive. Otherwise, the 3D-CMCC-FEM model first fuels the respiration, and then the remaining photosynthates, are used for leaf and fine root development. The target of the plant in this phase is to reach the maximum LAI (which is computed through the 'pipe model theory'; Shinozaki et al. 1964a, 1964b).

2. Normal growth or steady growth phase. During the succeeding growth phase and lasting up to the beginning of leaf senescence, some carbon is allocated to fruits (i.e. the 10% of daily allocable NPP, Sitch et al. 2003; Krinner et al. 2005; Bonan 2019) — provided that NSC is above a certain safety value — and the trees have overcome the sexual maturity age limit. It follows the allocation into the NSC pool, (to refill the reserves for the coming years), stem, branches, and coarse root, as long as the balance between GPP and maintenance respiration is positive. Otherwise, no growth occurs, and NSC is used. If the NSC level is below a minimum threshold, to avoid losses of starch and sugars (undistinguished in the model), defoliation occurs.

3. Leaf fall phase. When day length (in hours) is shorter than a species-specific threshold parameter value, the leaf fall and fine root senescence phase begins. The leaf fall and fine root senescence follow a sigmoid function which leads to the removal of all leaves and fine roots in a defined number of days. Fallen leaves enter the litter and subsequently, parallel to dead fine roots, into the soil pool. During the leaf fall phase, the total positive carbon balance (i.e. newly photosynthates less maintenance respiration costs) is allocated to the NSC pool and some (i.e. 10%) of the NSC in these two pools is also re-mobilised and transferred to the overall NSC pool (Campioli et al. 2013; Collalti et al. 2016).

4. Dormancy phase. Finally, during the dormant season, trees consume NSC for fueling maintenance respiration outside the growing season (Merganičová et al. 2019).

For evergreen species, the 3D-CMCC-FEM follows a similar but much more simplified approach simulating two phases:

1. First growth phase. When the 3D-CMCC-FEM allocates NPP to leaf up to reach the expected peak LAI. The amount of carbon allocated to the fine root pool is proportional to the amount allocated to the leaf pool. If the maximum attainable LAI is achieved in this first phenological phase, the excess of allocatable C is partitioned to the stem, coarse roots, and the branch and bark pools. If the NSC is below a minimum value, priority in allocation is given to this pool.

2. Second growth or steady growth phase. In the second growing phase, the 3D-CMCC-FEM allocates the NPP to all pools, i.e. leaf, fine and coarse root, branches and stem, and fruit pool (as 10% of allocable daily NPP; Bossell 1996), if trees have reached sexual maturity. If the NSC is below a minimum value, priority in allocation is given to this pool.

3.8.2. Carbon (and Nitrogen) Partitioning/Allocation

(subroutines: *C-evergreen-partitioning.c*, *C-deciduous-partitioning.c*)

Carbon partitioning and allocation (i.e. the amount of GPP allocated to a specific pool; Litton et al. 2007) in 3D-CMCC-FEM follows the 'Functional Balance' principles of allocation of biomass (Merganičová et al. 2019) which postulates that the resources for growth are supplied in amounts that ensure that the needs for growth and proper functioning of plant tissues are met. Carbon partitioning between pools is based on species-specific parameters that are dynamically regulated by abiotic factors (i.e. light and water availability) as:

$$a_{S_{x,y,k\,\epsilon\,z}} = \frac{\varepsilon_{S_x} + \omega_x(1 - L_{x,y,k\,\epsilon\,z})}{1 + \omega_x(2 - L_{x,y,k\,\epsilon\,z} - f_{\psi_{x,y,k\,\epsilon\,z}})} \qquad \textit{Eq.22}$$

and

$$a_{R_{x,y,k\,\epsilon\,z}} = \frac{\varepsilon_{R_x} + \omega_x(1 - f_{\psi_{x,y,k\,\epsilon\,z}})}{1 + \omega_x(2 - L_{x,y,k\,\epsilon\,z} - f_{\psi_{x,y,k\,\epsilon\,z}})} \qquad \textit{Eq.23}$$

and

$$a_{L_{x,y,k\,\epsilon\,z}} = \frac{\varepsilon_{L_x}}{1 + \omega_x(2 - L_{x,y,k\,\epsilon\,z} - f_{\psi_{x,y,k\,\epsilon\,z}})} = 1 - a_{S_{x,y,k\,\epsilon\,z}} - a_{R_{x,y,k\,\epsilon\,z}} \qquad \textit{Eq.24}$$

Where a_S, a_R, a_L account for actual allocation under suboptimal current conditions of 'allocable NPP', i.e. the NPP after that the maintenance respiration costs of the current live biomass are accounted for (but that not still account for the growth respiration costs which are related to the newly produced tissues), into the stem (S), and coarse root (R) and leaf (L) (or NSC) pools. Otherwise, ε_S, ε_R, ε_L are species-specific parameters and define the allocation fractions in non-limiting conditions, while ω controls the 'sensitivity' of allocation to changes in light and soil water availability of a species, by mean of the factors *L* and the scalar f_ψ, respectively, as in the CASA, CTEM models (Friedlingstein et al. 1999; Arora and Boer 2005). *L* is the unabsorbed light (varying between 0 and 1) by the species *x* for the diameter class *y,* age class *k,* and canopy layer *z* (Collalti 2011; Collalti et al. 2014, 2016; see **Figure 24**).

$$L_{x,y,k \in z} = e^{-k_x \cdot LAI_{x,y,k \in z}} \quad \textit{Eq.25}$$

For the limiting case of $\omega = 0$ constant optimal allocation fractions are obtained. For deciduous trees, the 3D-CMCC-FEM follows a similar scheme, but during phase 2, the fraction of carbon not allocated to stem, coarse root, and fruit pools is allocated to replenish the NSC pool.

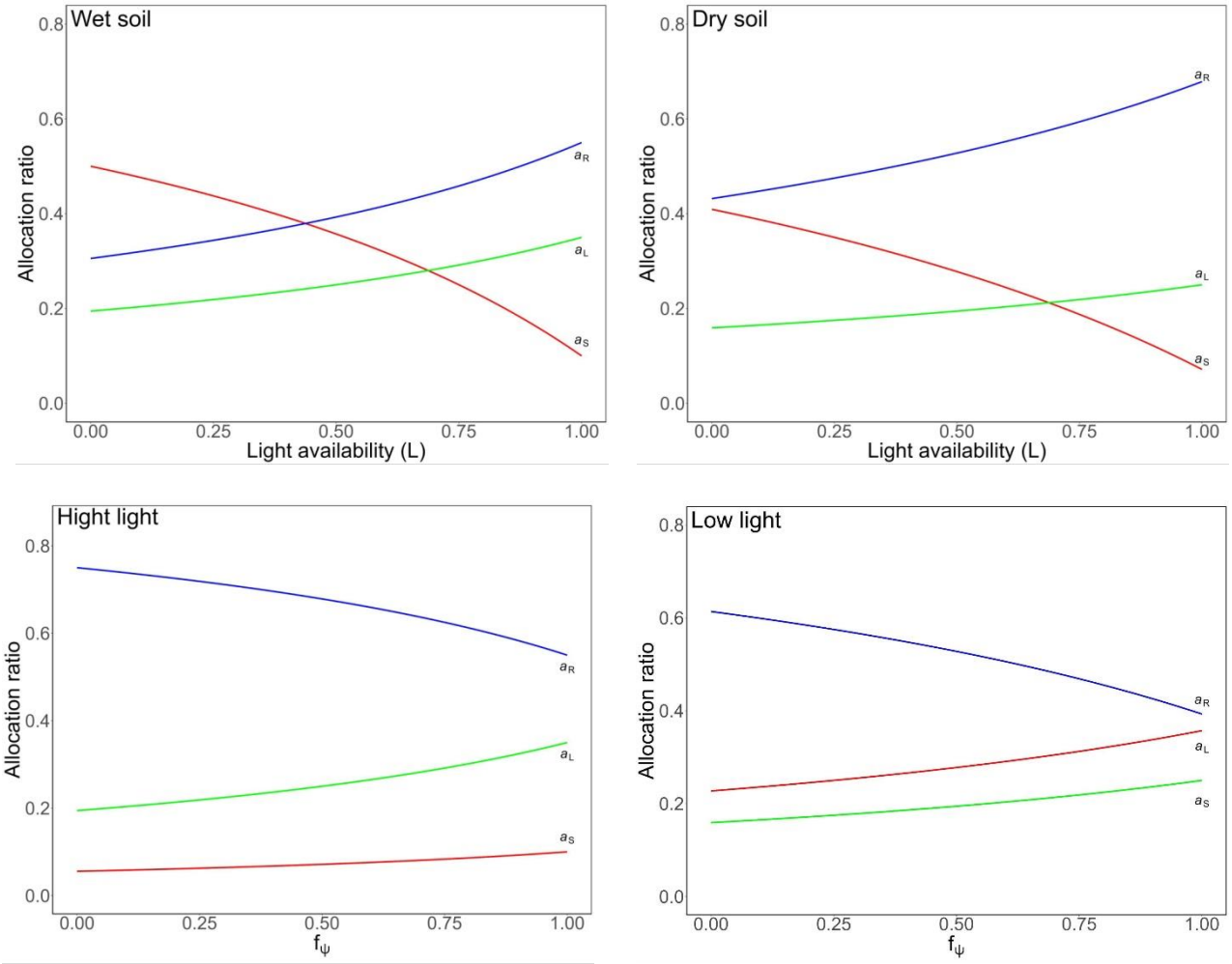

Figure 24 Allocation ratios for Stem (a_S), Coarse Root (a_R), and Leaf (a_L) at: varying light availability (L) with $f_\psi = 1.0$ (left above panel; 'wet soil') and $f_\psi = 0.5$ (right above panel; ''dry soil'); varying Soil water (f_ψ) with L = 1.0 (left below panel; 'high light') and L = 0.5 (right below panel; 'low light') both with $\varepsilon_S = 0.1$, $\varepsilon_L = 0.35$ and $\varepsilon_r = 0.55$ and $\omega = 0.8$.

The daily LAI is based on the amount of carbon allocated to the leaves, the specific leaf area (as the branch and bark fractions vary based on age), and the single tree canopy coverage (see paragraph 1.4.2 and Eq.1).

The maximum annual attainable LAI is computed at the beginning of each simulation year based on the current sapwood area and is controlled by the 'pipe-model' theory, to optimise photosynthesis (Shinozaki et al. 1964a, 1964b). The functional interdependence between sapwood and leaves states that the increment in the bole cross-sectional area at a given tree height is (or should be) proportional to the leaf area above this point to optimise stem hydraulic conductance (Landsberg and Sands 2011).

The carbon (and the nitrogen) allocated to the branch and bark pool is instead considered as a fraction varying with age (as in 3-PG model, Landsberg and Waring 1997) of the carbon allocated to the stem pool.

The carbon that is allocated daily into woody tissues (i.e. branch, stem, and coarse root) is considered sapwood. Heartwood is considered as the difference between total woody and sapwood biomass as in Forest v.5.1 model (Schwalm et al. 2004). The livewood pool is conceptually different from sapwood since it includes only live cells, not all of the sapwood biomass — e.g. it excludes lignin and cellulose. The livewood pool is used to compute autotrophic respiration, whereas the sapwood area is used to compute the leaf area index. Although the 3D-CMCC-FEM treats sapwood biomass and NSC pools separately, they are interrelated via the minimum NSC content, which is specified as a fraction of sapwood dry mass (Hoch et al. 2003; Genet et al. 2010; Wiley et al. 2017; Collalti et al. 2021).

3.8.3. Turnover

(subroutines: *turnover.c*)

While sapwood biomass (and area) and livewood biomass re computed during the initialization phase following an empirical relationship that links sapwood and DBH (the remaining biomass is considered as heartwood) and sapwood and livewood biomass, during the simulation run the sapwood and heartwood and the livewood and deadwood dynamics are computed more mechanistically. In the most recent version of the model (i.e. 'v.5.6'), any carbon allocated to the stem, coarse root, and branch is considered as new sapwood (for the stem, coarse and branch pools considered separately). Some of the previous years' sapwood (and not just the previous year's one as in the former model versions; see Collalti et al. 2020a) is converted to heartwood because of turnover ($\tau_{sapwood}$). Similarly, some of the current livewood (which are a fraction of the overall new sapwood) is added to the previous years livewood pool (for the stem, coarse and branch pools considered separately) while some of the previous years livewood die and are are added to deadwood because of turnover ($\tau_{livewood}$). Turnover, both for sapwood and for livewood, is computed daily. Heartwood and deadwood, are the remaining carbon pools that are no longer involved in any metabolic processes up to the tree is considered alive, otherwise, it becomes carbon woody debris and are considered into the litter/soil decomposition process.

The age-dependence of sapwood (and presumably also for livewood) turnover has been observed in several species (Pretzsch 2009). Indeed, both Norway spruce (*Picea abies* (L.) H.Karst), Scots pine (*Pinus sylvestris* L.), Sessile oak (*Quercus petraea* (Matt.) Liebl.), and European beech (*Fagus sylvatica* L.) show a species-specific decrease in the proportion of sapwood ($F_{sapwood}$ in %) from 100% (all stem biomass is sapwood) in the juvenile phase to 25-50% (or even less) in the mature phase. The 3D computer tomography model of the proportion of sapwood:heartwood yields heartwood volume percentages ($F_{sapwood}$ in brackets) of 0% in the juvenile phase of the tree ($F_{sapwood}$ = 100%), 1-35% at DBH = 10-15 cm ($F_{sapwood}$ = 99-65%) and 3-56% at DBH = 30–50cm ($F_{sapwood}$ = 97-44%) (Pretzsch 2005). To account for the age in sapwood turnover in the 3D-CMCC-FEM an age-dependent sapwood turnover rate is computed as follows:

$$\tau_{sapwood_{x,y,k\in z}} = \tau_{sapwood-mature_x} + (\tau_{sapwood-juvenile_x} - \tau_{sapwood-mature_x}) \cdot e^{-ln2\cdot(age_{x,y,k\in z}/\tau_{age_x})^2} \quad \textit{Eq.26}$$

where $\tau_{sapwood\text{-}juvenile}$ and $\tau_{sapwood\text{-}mature}$ represent the turnover rate for mature trees (e.g. 0.02 $year^{-1}$ depending on species) and juvenile trees (i.e. 0.01 $year^{-1}$ corresponding to 50% of the mature), τ_{age} the age at which the turnover has a median value between the two juvenile and mature turnover rates (**Figure *25***). The value of ≈0.02 $year^{-1}$ (mean residence time ≈50 years) for mature trees is close to the value adopted in LPJ by Poulter et al. (2010) and to the values of 0.05 $year^{-1}$ (mean residence time ≈20 years) for Douglas-fir and 0.01 $year^{-1}$ (mean residence time ≈100 years) for European beech reported by Bartelink (1998).

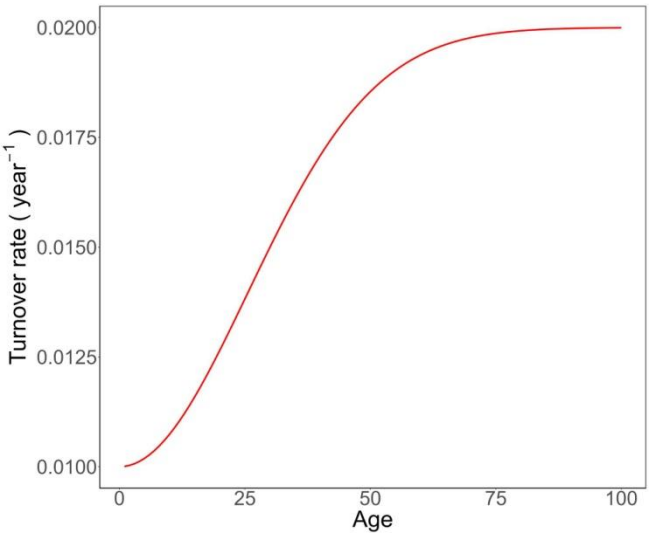

Figure 25 Variation in the sapwood (and livewood turnover) rate at varying ages with $T_{sapwood\_mature}$ = 0.02 ($years^{-1}$), $T_{sapwood\_juvenile}$ = 0.01 ($years^{-1}$) and T_{age} 30 (years).

Most vegetation models operate under the assumption of maintaining certain parameters constant, one of which is the rate of sapwood turnover. However, the lack of precise information regarding this parameter has proven to be a significant source of uncertainty in estimating the carbon balance within vegetation stands (Goulden et al. 2011; Malhi 2012; Collalti et al. 2019). Additional sources of uncertainty stem from various factors. One such factor is the omission of a size- or age-related decline in the ratio of living to dead cells, which implies a potential decline in the sapwood turnover rate over time (Ceschia et al. 2002; Damesin et al. 2002). Furthermore, changes in climate could transiently increase τ, reducing maintenance costs to favour growth (Doughty et al. 2015). Shifts in tissue nitrogen and NSC concentrations also contribute to uncertainty (Machado and Reich 2006; Thurner et al. 2017). Additionally, there is likely a genetically controlled down-regulation of basal respiration rates with cell ageing (Carey et al. 2001; Wiley et al. 2017). It is probable that both τ and basal respiration rates (R_g and R_m) vary among different tree biomass pools (Reich et al. 2008). Respiratory carbon losses per unit plant mass might adjust to sustain growth in response to increasing plant size or changing climate (Smith and Stitt 2007). While these hypotheses are all theoretically grounded, empirical support for them is, to date, limited (Collalti et al. 2020a).

Note, a new formulation and a new parameterization in the 'v5.6' — that more closely matches with the reality — now consider the possibility that both sapwood and, especially, livewood cells can have a much longer lifespan than in the previous model formulations and parameterizations. This means that the turnover rate both for sapwood ($\tau_{sapwood}$) and for live cells ($\tau_{livewood}$) has been lengthened much if compared to Collalti et al. (2020a). The current model version departures from the previous model's formulations and parameterizations for $\tau_{sapwood}$ and $\tau_{livewood}$ built upon the idea that both sapwood and mostly livewood cells had a much shorter lifespan, i.e. few years, with the turnover applied only to the last sapwood rings (i.e. the cambium or phloem) as in BIOME-BGC, CLM4.5, ORCHIDEE models. Spicer and Holdbrook (2007) have, however, shown in conifers that even 64-year-old sapwood respires and that 5-year-old parenchyma cells respired at the same rate as in the 25-year-old cells showing no inherent or intrinsic decline in respiration as a result of cellular ageing. Angiosperms have shown similar behaviours but with a bit more pronounced age effect with reduced respiration in older tissues. Such a change in the model formulation and parameterization is, ultimately, perfectly in line with the assumption (see paragraph 1.4 Model Initialization: the Forest Structure and the Pools), as currently embedded into the model, that all NCS can be used for metabolic functioning including the maintenance respiration from decade-old livewood cells in the inner parts of the wood (see also Diaz-Espejo and Hernandez-Santana 2017).

In 3D-CMCC-FEM, the livewood pool is conceptually different from the sapwood pool since it includes only live cells, not all of the sapwood biomass – it excludes lignin and cellulose. Ultimately, livewood biomass is used to compute respiration, and sapwood area is used to compute LAI. However, the same formulation for turnover, i.e. varying with age, is adopted for the livewood turnover by substituting the sapwood biomass with the livewood biomass.

In evergreen species, fine roots and leaf turnover ($\tau_{leaf\_fineroot}$), which is based on needle lifetime, occur daily all year long with $\tau_{leaf\_fineroot}$ varying between species (e.g. $\tau_{leaf\_fineroot}$ = 0.25 year^{-1} for *Pinus sylvestris* L.; Mäkelä 1997). In deciduous species $\tau_{leaf\_fineroot}$ equals to 1 year^{-1}.

Before senescence, and in the case of defoliation, a fraction (i.e. 10%) of the NSC in leaves and fine roots is re-mobilized and translocated into the overall NSC pool (see **Figure *26*** for the overall allocation scheme at different sites).

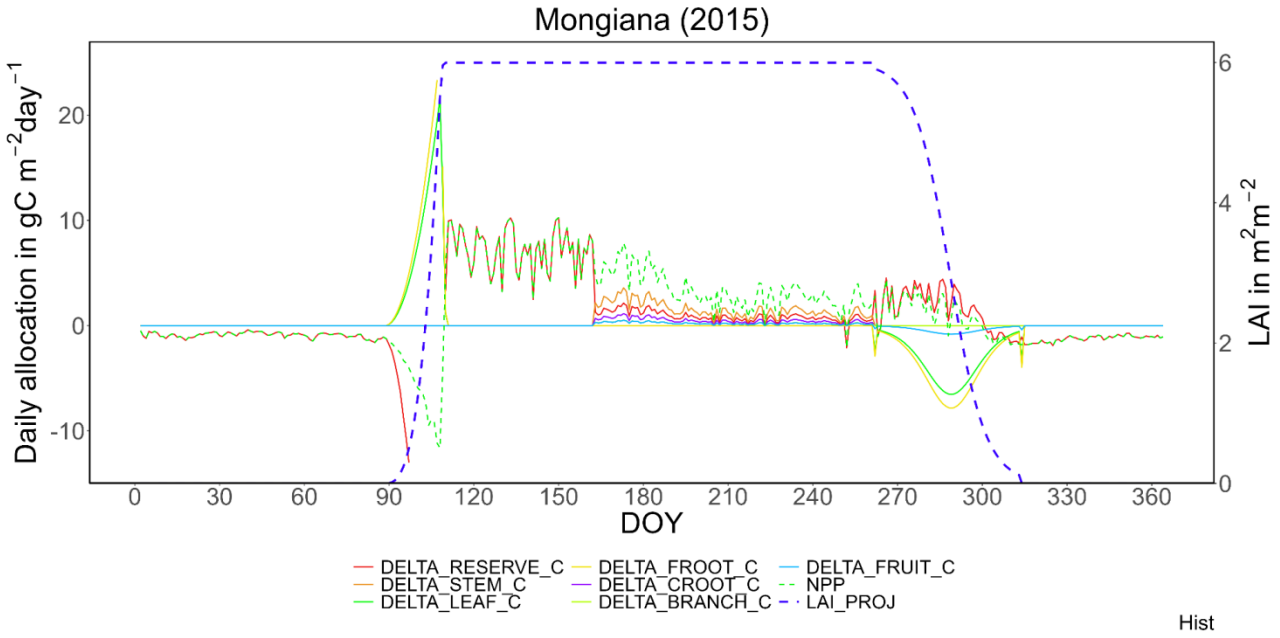
Mongiana (2015)
Daily allocation in gC m^{-2}day^{-1}
LAI in m^{2}m^{-2}
DOY
DELTA_RESERVE_C
DELTA_STEM_C
DELTA_LEAF_C
DELTA_FROOT_C
DELTA_CROOT_C
DELTA_BRANCH_C
DELTA_FRUIT_C
NPP
LAI_PROJ
Hist

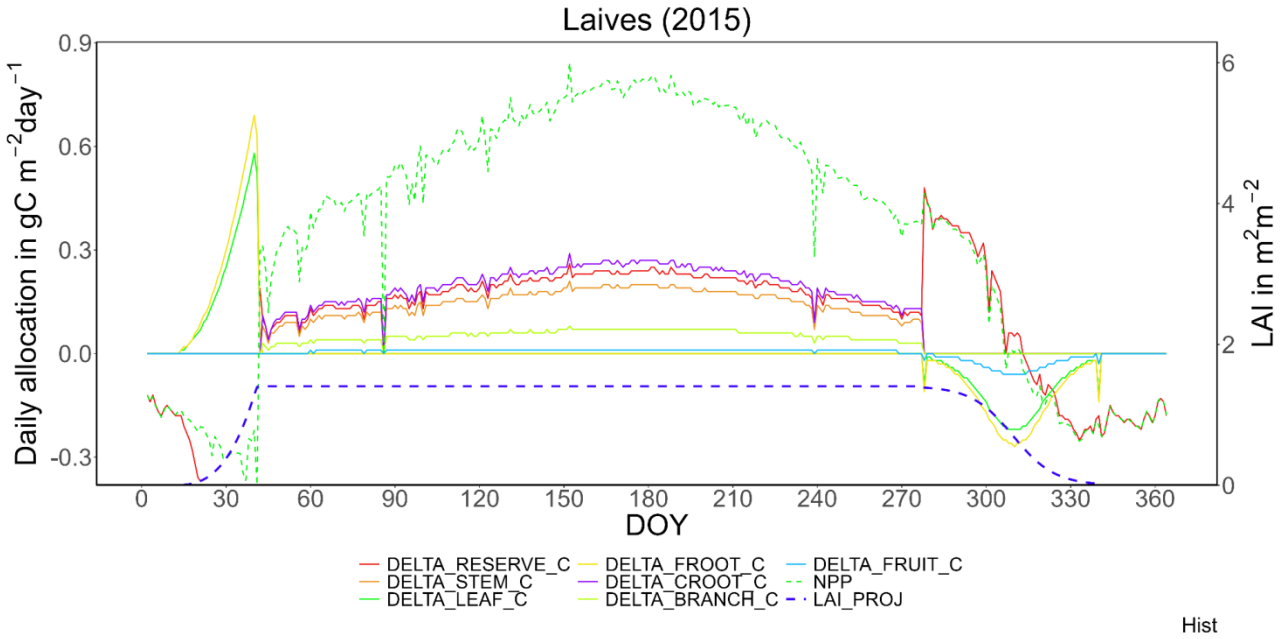
Laives (2015)
Daily allocation in gC m^{-2}day^{-1}
LAI in m^{2}m^{-2}
DOY
DELTA_RESERVE_C
DELTA_STEM_C
DELTA_LEAF_C
DELTA_FROOT_C
DELTA_CROOT_C
DELTA_BRANCH_C
DELTA_FRUIT_C
NPP
LAI_PROJ
Hist

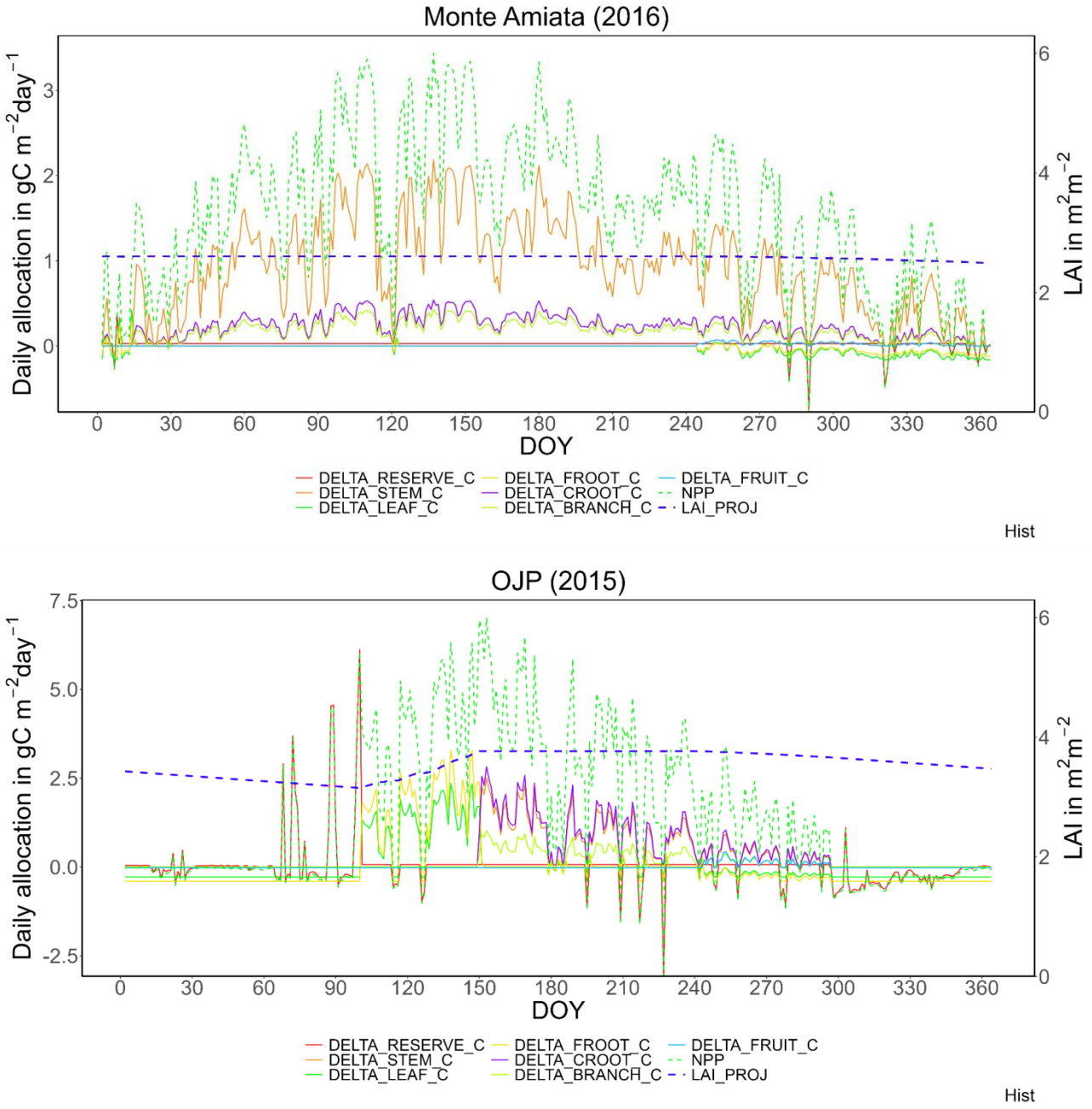

Figure 26 Examples of 3D-CMCC-FEM daily carbon fluxes, NPP, and NSC dynamic (gC m^{-2} day^{-1}) and LAI (m^2 m^{-2}) in the 93 years-old *Fagus sylvatica* L. stand of Mongiana site in Italy in 2015 (above); in the 20 years-old *Quercus pubescens* Wild. stand of Laives site in Italy (middle); in 91 years old the *Pinus banksiana* Lamb. stand of Old Jack Pine boreal stand (OJP) in Canada in 2016 (middle); and in the 56 years-old *Pinus nigra* J.F. Arnold stand of Monte Amiata in the 2016 site in Italy (below). The figure displays the net allocation of carbon within different carbon pools over the year. Each pool represents a distinct component of the trees carbon storage system, including leaves (DELTA_LEAF_C), fine roots (DELTA_FROOT_C), coarse roots (DELTA_CROOT_C), stem (DELTA_STEM_C), branches (DELTA_BRANCH_C), fruits (DELTA_FRUIT_C) and Non-Structural Carbon (NSC). The daily net primary productivity (NPP) reflects the daily carbon gain by the trees through photosynthesis; the Leaf Area Index (LAI_proj) represents leaf development and phenology. Positive values denote periods of growth, while negative values indicate pool senescence, e.g. shedding, or turnover; 'DELTA_x', represents the daily net flux in specific carbon pools, such as leaves, coarse roots, fine roots, stem, branches,

fruit, and NSC (serves as reserves of tree growth and metabolism). Positive values indicate the partitioning of GPP and carbon accumulation, while negative values indicate carbon loss because of turnover or retranslocation. The allocation of carbon to different pools varies throughout the year, reflecting seasonal changes: during spring and early summer high photosynthetic activity reflects carbon allocation to the leaf and fine root pool, and the relative changes in LAI (LAI_proj tends to increase as leaves expand and develop). Conversely, in late summer and autumn, carbon allocation to the leaf pool may decrease due to leaf and fine root pool may decrease due to leaf and fine root senescence (in evergreen species).

The N-pools in biomass are updated daily in parallel with the C-pools according to a fixed C:N stoichiometric ratio for each pool, i.e. based on the relative amount of carbon allocated within each single pool.

3.9 Non-Structural Carbon

Since the most recent daily versions of 3D-CMCC-FEM, the NSC-pool has been added to avoid carbon imbalances and losses of mass (see '*Principle of the Conservation of Energy and Mass*' section) during the bud break period or during periods where respiration may exceed photosynthesis. The NSC pool or reserve pool, which includes starch and sugars undistinguished, has not an identified and precise location within the tree but is shared between compartments depending on their relative biomass (Collalti et al. 2016). The inclusion of this new pool was necessary to represent NSC mobilisation and consequently leaf phenology (e.g. leaf production during spring for deciduous trees) and carbon imbalances. Non-structural carbohydrates are a surprisingly poorly known component of the whole-tree carbon balance and are commonly disregarded in vegetation models (Merganičová et al. 2019; Schiestl-Aalto et al. 2019) that is the reason why, although other pools are only described generically here, we pay attention to this pool.

Overall, the ability of trees to prioritise storage over growth depends on the role of NSC in allowing temporal asynchrony between carbon demand and carbon supply (Fatichi et al. 2014). Such imbalances are assumed to be buffered by drawing down NSC reserves in the 3D-CMCC-FEM. Indeed, recent studies support this assumption, showing that during periods of negative carbon balance (for example, during the dormant season, periods of stress, or natural or artificially induced defoliation episodes where NPP can become negative), NSC is remobilized and transported from the sites of phloem loading, while during periods of positive carbon balance plants preferentially allocate recently assimilated carbon to replenish NSC. Only afterwards is 'new' carbon used to sustain growth (Weber et al. 2018; Huang et al. 2019). Because ultimately plant survival depends more on metabolic carbon demands than on growth, some have argued that all positive carbon flows should be used to replenish NSC at the expense of growth until a minimum NSC pool size (30%–60% of the seasonal maximum, Martínez-Vilalta et al. 2016) is reached ('active' storage: Sala et al. 2012), thus maintaining a safety margin against the risk of carbon starvation (Huang et al. 2019; Wiley and Helliker 2012) (see 'DELTA_RESERVE_C' for NSC dynamic in **Figure *26***). Note that this assumption departs from the notion that NSC is a mere reservoir for excess supply of carbon relative to growth demand ('passive'

storage: Kozlowski 1992). It is assumed in the 3D-CMCC-FEM that a minimum NSC threshold level concentration (11% of sapwood dry mass for deciduous and 5% for evergreen species: Genet et al. 2010) has necessarily to be maintained for multiple functions including osmoregulation, cell turgor, vascular integrity, organ-specific phenology (leaf and fine-root formation), and — more importantly — tree survival (reviewed in Hartmann and Trumbore 2016). The greater the sapwood mass, the greater the minimum NSC threshold (in absolute terms) must be (Dietze et al. 2014). Such patterns of whole-tree seasonal NSC dynamics have been all recently confirmed by Furze et al. (2019) and Fierravanti et al. (2019), and a similar phenological and carbon partitioning/allocation scheme has been adopted by other models (e.g. CTEM model, Arora and Boer 2005; ORCHIDEE model, Krinner et al. 2005). Although it has been suggested that a considerable fraction of NSC (mostly starch) in the inner part of wood may become compartmentalised and sequestered away from sites of phloem loading — i.e. not more available for metabolic functions (Sala et al. 2012) — others have found that more than a decade-old NSC can be remobilised and used (Muhr et al. 2019). In 3D-CMCC-FEM all NSC accumulated over the years can be used when necessary.

3.10 MORTALITY

(subroutine: *mortality.c*)

In the 3D-CMCC-FEM, mortality is simulated within different routines acting at different temporal scales. An age-dependent mortality which considers the probability for a tree to die off which increases based on species-specific maximum lifespan MAX_{age} in a logistic regression form, as similar to the LPJ-GUESS model (Smith et al. 2001), according to the equation (see also **Figure *27***):

$$M_{age_{x,y,k\in z}} = \left(\frac{-(3\cdot ln(0.001))}{MAX_{age_x}}\right) \cdot \left(\frac{age_{x,y,k\in z}}{MAX_{age_x}}\right)^2 \qquad \textit{Eq. 27}$$

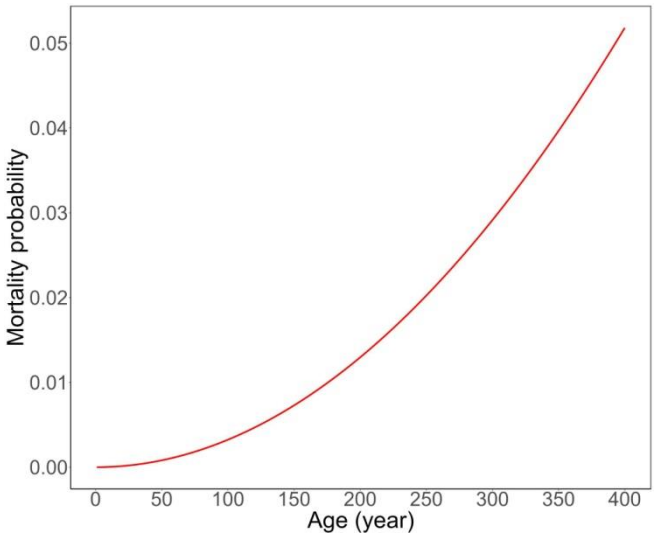

Figure 27 Variation of the mortality probability at ageing with MAX_{age} = 400.

A 'background' mortality, which stochastically accounts for the probability for a random tree to die because of e.g. fire occurrence or pests, is also included as a fixed yearly mortality rate as:

$$M_{b_{x,y,k \in z}} = 0.01 \qquad \textit{Eq. 28}$$

The 0.01, i.e. 1% of trees die each year, is close to the value of 0.014 (1.4%) assumed in the FATES model (Fisher et al. 2015).

A third mortality function takes into account the tree (over) crowding competition, and it is a mortality function based on the light tolerance of a species-specific parameter describing the shade (or light) tolerance of a species, and, thus, it represents the 'physiological-structural' mortality in the 3D-CMCC-FEM. Indeed, to avoid the sum of crown areas exceeding the '*Light_tol*' parameter in a specific layer (i.e. overcrowding), the 3D-CMCC-FEM activates first the self-pruning function and by reducing the crown diameter, if DBHDC is already at the $DBHDC_{min}$ value (see paragraph 1.4.1) the self-thinning mortality activates. Therefore, starting from the less shade-tolerant species, the model iteratively reduces the number of single trees till the sum of all crown areas falls below the '*Light_tol*' threshold value. To some extent, such an approach is not far from Yoda et al.'s (1963) —3/2 power self-thinning rule but is applied to forest structure rather than to plant biomass in a more mechanistic way.

A fourth mortality links the balance between the depletion of Non-Structural Carbohydrates through substrate-dependent maintenance respiration and its accrual through NPP (the balance between carbon assimilation and plant maintenance respiration) and it is commonly called 'growth efficiency' mortality. At any time of the simulation, when the NSC pool is fully depleted (thus mimicking the 'carbon starvation' hypothesis; McDowell 2011; Rowland et al. 2015; Adams et al. 2017), the 3D-CMCC-FEM removes those trees (or cohorts). Frequent meteorological extreme events such as drought or heat waves act indirectly on the mortality occurrence, affecting stomatal conductance and thus causing an imbalance between carbon assimilation, and maintenance respiration. This type of mortality operates on long temporal scales because of extremes-induced carry-over effects which do not account immediately and change much of the forest structure during long-simulation run.

The first three mortality types are computed annually and are applied additively, while the latter mortality is iteratively solved and computed on daily time scales and represents the 'physiological-environmental' mechanistic mortality.

The model also simulates self-pruning as well, at the daily time scale, which accounts for when overcrowding occurs over a certain threshold value (see above the '*Light_Tol*' parameter). Therefore the 3D-CMCC-FEM starts reducing crown diameter (and proportionally branch, leaf, and fine root biomass which go to the litter and soil pools) up to the $DBHDC_{min}$ value. In the case that the current DBHDC is already at the minimum value the model activates the self-thinning mortality described above.

3.11 REGENERATION (UNDER DEVELOPMENT)

(subroutine: *new_forest_class.c*, *C-fruit_partitioning.c*, *regeneration.c*, *recruitment.c*)

When the tree age within the stand reaches sexual maturity (a species-specific parameter), a fraction of the annual Net Primary Productivity (NPP) is converted to fruit C-pool according to the equation:

$$C_{fruit_{x,y,k\,\epsilon\,z}} = \begin{cases} NPP_{x,y,k\,\epsilon\,z} \cdot \alpha_x \; with \; age_{x,y,k\,\epsilon\,z} \geq Sexage_x \\ 0, \qquad\qquad else \end{cases} \qquad Eq.\ 29$$

where α_{seed} is the fixed fraction of the species-specific NPP value (5% according to Fernández-Martínez et al. 2016) produced and directly allocated for fruits during the normal growth phase (Bossel 1996). Recent studies

have, indeed, shown no evidence of carbon storage usage for seed production but that it rather depends on recently synthesised sugars (Igarashi et al. 2024).

Note that when the 3D-CMCC-FEM runs in a spatial context over a landscape, cells do not interact with each other, and there is no exchange of seeds (or fruits) between grid-cells, i.e. each cell is a distinct model run and does not interact in any way with other cells and, thus — if not prescribed by the user — the model does not consider itself the expected changes in future species composition (Noce et al. 2016).

To convert C-fruit biomass into a number of seeds, the 3D-CMCC-FEM computes as follows:

$$n_{fruit_x} = \frac{C_{fruit_x} \cdot 10^6}{W_{fruit_x}} \qquad \textit{Eq. 30}$$

where 10^6 is the correction factor (from Mg of dry matter to grams of dry matter), and W_{fruit} is the weight of a single fruit (grams dry matter), a species-specific parameter, assuming here that for each fruit only one seed is available.

In cases where fruits contain more than one seed, the species-specific parameter can be set to take into account the average number of seeds ($FRUIT_{\_seed}$) contained in a fruit (e.g. *Fagus sylvatica* L., $FRUIT_{\_seed}$ = 2) to obtain the correct estimation of seed production.

Currently, the 3D-CMCC-FEM does not have a seed bank, a pool where the model accumulates seed production of the previous years over time, thus, seeds can germinate only in the year next of production and not over.

To represent the germination of the seeds, the 3D-CMCC-FEM calculates the thermic sum in spring (STs, from March to May). When the STs exceeds a species-specific value for seed germination (GDD_{seed}, e.g. 60°C for *Fagus sylvatica* L.), seed germination is stimulated. The actual number of seeds that can germinate depends on an intrinsic species-specific parameter controlling the percentage of empty seeds (β_{seed}) as described by Wang (2003), and by a species-specific germination capacity (γ_{seed}) as in Nielsen (1977). Thus, the actual number of seeds is computed as follows (see also **Figure 28**):

$$n_{germ-seed_x} = \begin{cases} \left(n_{seed_x} \cdot 1 - \beta_{seed_x}\right) \cdot \gamma_{seed} & with \;\; ST_s \geq GDD_{seed_x} \\ 0, & else \end{cases} \qquad \textit{Eq. 31}$$

The germinated seeds will form a new layer of seedlings that can grow in the understory and over the years become saplings. During this phase, the seedlings are vulnerable to environmental factors such as light and temperature, which drive their survival (Vacchiano et al. 2018).

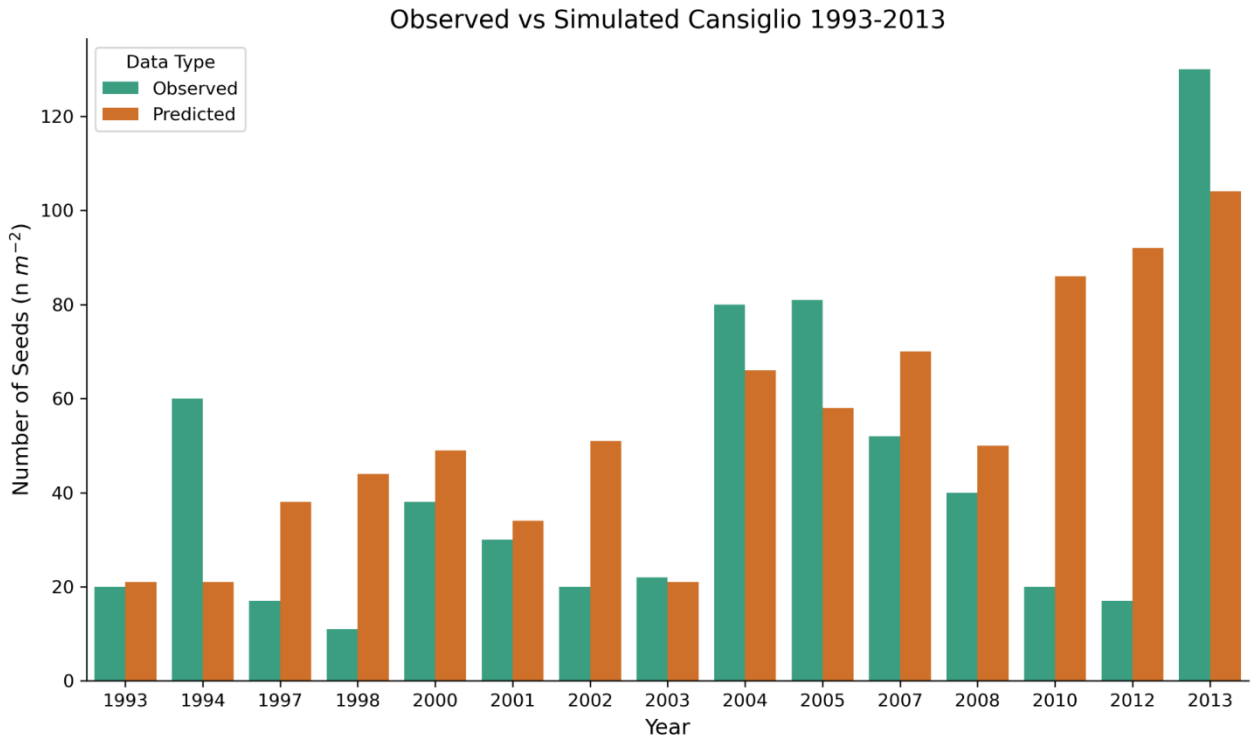

Figure 28 Comparison between observed versus 3D-CMCC-FEM modelled data for the number of seeds at the Cansiglio site (Veneto region, IT) (Saponaro et al. in prep).

Specific thresholds for each species (Muffler et al. 2021) establish the survival rate of the seedlings, guided by these abiotic factors as follows:

$$n_{seedlings_x} = \begin{cases} n_{seed_x} \cdot 0.7 & PAR_{soil} \geq PAR_{soil_{seed}} \quad and \; T_{avg} \leq T_{avg_{seed}} \\ n_{seed_x} \cdot 0.5 & PAR_{soil} \geq PAR_{soil_{seed}} \quad and \; T_{avg} > T_{avg_{seed}} \\ n_{seed_x} \cdot 0.3 & PAR_{soil} < PAR_{soil_{seed}} \quad and \; T_{avg} < T_{avg_{seed}} \\ n_{seed_x} \cdot 0.2 & PAR_{soil} < PAR_{soil_{seed}} \quad and \; T_{avg} > T_{avg_{seed}} \end{cases} \qquad Eq.32$$

where PAR_{soil} is the daily PAR reaching the soil after passing through the canopies and $PAR_{soilseed}$ a species-specific parameter controlling the minimum PAR needed for seedlings survival and development to saplings, T_{avg} is the average temperature and $T_{avgseed}$ is the maximum temperature for seedlings survival and

development to saplings (Muffler et al. 2021). The number of seedlings that survived at the end of the year will be recruited into the stand as 1.3 m high and 1 cm DBH saplings and will follow the same growth and mortality dynamics of adult trees (see **Figure 29**).

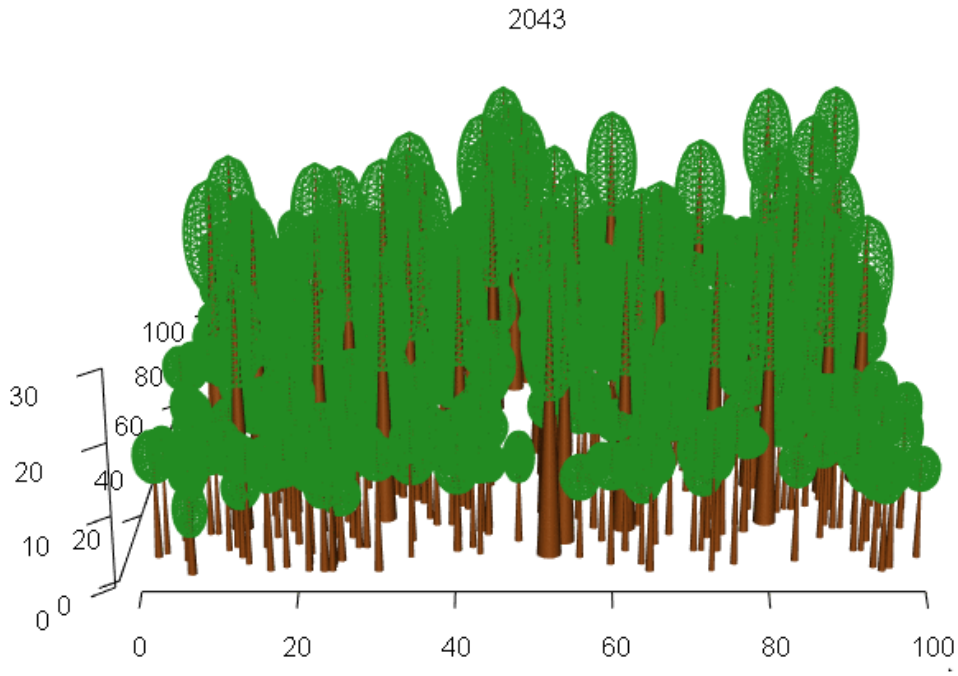

Figure 29 Simulated tree regeneration process for *Fagus sylvatica* L. species at the Cansiglio site (Veneto region, IT) in a 2010-2099 simulation run (here, the forest structural conditions for the year 2043).

We are aware that this is an over-simplistic yet unavoidable assumption in the model as the DBH is a mandatory variable for characterising the DBH class. Seeds are assumed to be distributed evenly across the grid cell, so the total input to the seed pool is, therefore, the sum of all of the reproductive output of all the classes within the grid cell.

Theoretically, in this way, every year provided that there are favourable conditions for seedling and sapling establishment, the 3D-CMCC-FEM model can produce a new generation of trees which necessarily generate, over long simulations, a massive number of classes. As in the FATES model (Fisher et al. 2015) we plan to fuse equivalent classes and cohorts every *x* number of years into single model entities (by a weighted mean procedure) to save memory and computational time. This feature relies on the establishment of criteria defining functional equivalence, which inherently involves a degree of subjectivity. These criteria serve, however, as a method for simplifying reality into a more manageable mathematical framework.

3.12 Litter Organic Matter Decomposition

(subroutines: *litter_carbon_balance.c*, *litter_nitrogen_balance.c*, *littering.c*)

Litter (and soil) carbon pools are split into conceptual 4 pools defined by different mean residence times (the inverse of the decomposition rate), mirroring the degree of decomposability of the organic matter in a conceptually similar manner as in BIOME-BGC (**Figure *30***). The litter pool includes fresh litter, i.e. fallen leaves and dead fine roots, and a deadwood carbon pool, i.e. coarse woody debris. The fresh litter pool is additionally split into a labile, cellulose, and lignin pool according to their species-specific C:N ratio. A fraction of cellulose is shielded by lignin. The deadwood pool (Coarse Woody Debris, CWD), instead, is firstly subjected to physical fragmentation and enters the cellulose and lignin pool but it is considered only into the soil pool.

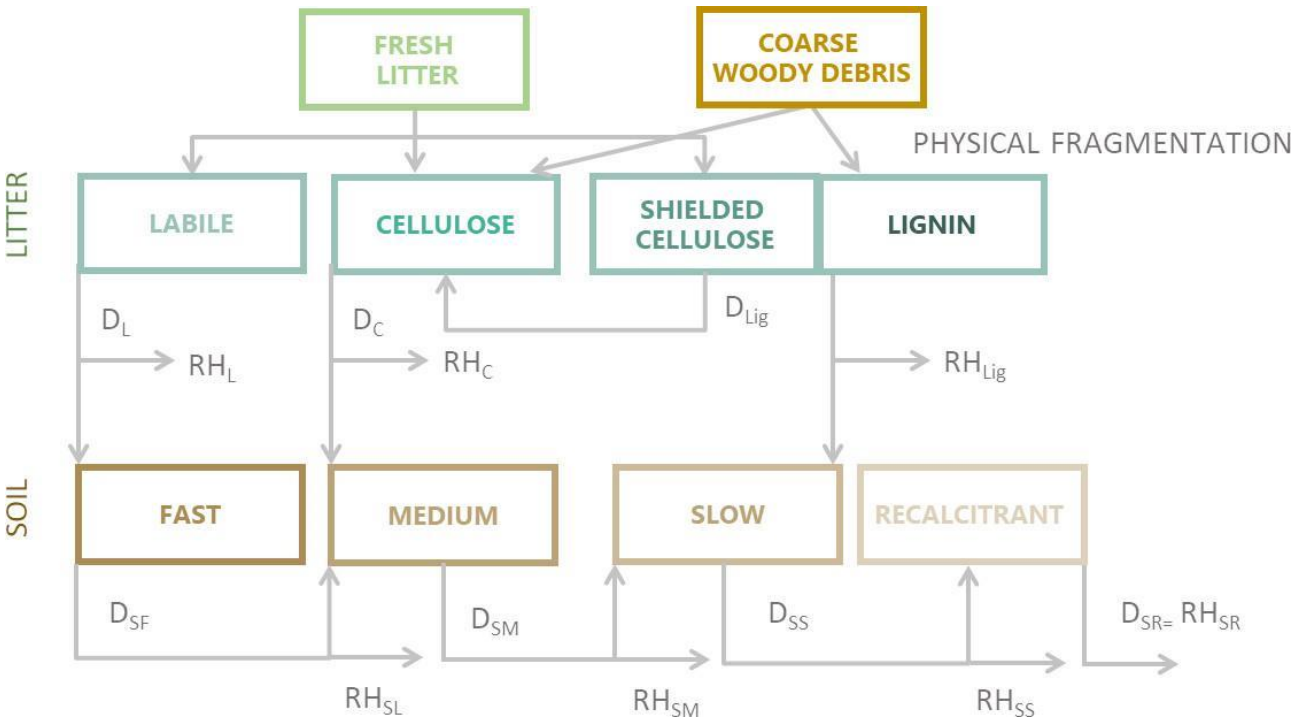

Figure 30 Conceptual model of litter and soil organic matter decomposition. D represents the decomposition rate fluxes from each carbon pool, while RH represents the respired fraction of the decomposition fluxes, i.e. heterotrophic respiration R_h). Fresh litter is split in the labile, cellulose and lignin pool according to the C:N ratio decomposition.

The general daily mass balance of the litter organic C-pools is written as:

$$C_l = C_{l_{t-1}} + I - D_{l_i} \qquad \textit{Eq. 33}$$

Where C_l is the carbon in the specific pool of interest, e.g. labile, cellulose pool etc, at day t and $t—1$. The variable I is the input flux into the pool and D_l is the decomposition flux.

The carbon organic matter decomposition carried by the microorganism community, follows the scheme and the kinetic as presented in Thornton and Rosenbloom (2005) for BIOME-BGC, which embeds a simplified version of the CENTURY model (Parton et al. 1987, 1993, 1994, 1996).

The decomposition dynamic follows a linear kinetic, where the flux scales linearly with the organic carbon mass according to the following general equation:

$$D_l = fs_T \cdot fs_\theta \cdot k_l \cdot C_l \qquad \textit{Eq. 34}$$

where k_l is the decomposition rate constant, characteristics of each litter carbon pool, fs_T is a scalar describing the abiotic effect of soil temperature T_{soil} and soil moisture θ on the decomposition dynamic (see paragraph 3.13 Soil Organic Matter Decomposition). The microbial pool is not explicitly represented, and it is assumed that within each carbon pool the decomposition rate is homogeneous.

In the litter pool, the input is constituted by each fresh litter constituent and coarse woody debris fraction. The flux of shielded cellulose to the cellulose pool is driven by the lignin decomposition rate.

The decomposed carbon which is transferred among litter pools is defined as:

$$I_l = \alpha_l \cdot D_l \qquad \textit{Eq. 35}$$

where the fraction α_l depends on the specific decomposability degree of each litter carbon pool. It follows that the fraction of decomposed organic carbon respired to the atmosphere, i.e. the heterotrophic respiration R_{hl} by litter microorganisms is defined as:

$$R_{h_l} = (1 - \alpha_l) \cdot D_l \qquad \textit{Eq. 36}$$

The total heterotrophic respiration carbon flux from litter is the sum of all carbon resealed during the decomposition of each litter organic pool.

3.13 Soil Organic Matter Decomposition

(subroutines: *decomposition.c*; *het_respiration.c*, *soil_respiration.c*, *soil_carbon_balance.c*, *soil_nitrogen_balance.c*)

Similarly to the litter pool, the soil pool is constituted by 4 different conceptual pools characterised by different decomposability degrees: a fast, a medium, a slow and a recalcitrant carbon pool. The general daily mass balance of the soil organic C-pools is written as:

$$C_s = C_{s_{t-1}} + I_s - D_s \qquad \textit{Eq. 37}$$

where C_s is the carbon in the specific soil pool of interest, e.g. fast, slow pool, etc, at day t and $t—1$. The variable I_s is the input flux into the soil pool, and D_s is the decomposition flux.

Following the same dynamics shown for litter, the soil decomposition flux is written as:

$$D_s = fs_C \cdot fs_T \cdot fs_\theta \cdot k_s \cdot C_s \qquad \textit{Eq. 38}$$

where k_s is the decomposition rate constant, characteristics of each soil carbon pool, and fs_C is a scalar which depends on the soil texture (i.e. %sand, %clay, %silt) and describes the physical effect of protection to soil decomposition due to the mineral matrix. The fully interactive soil nitrogen cycle with its down-regulating effect on carbon decomposition is under development.

Each soil carbon pool receives as input the decomposed carbon flux from litter and/or from the less recalcitrant carbon pool, e.g. from fast to slow pool, at the net of the respiratory cost (

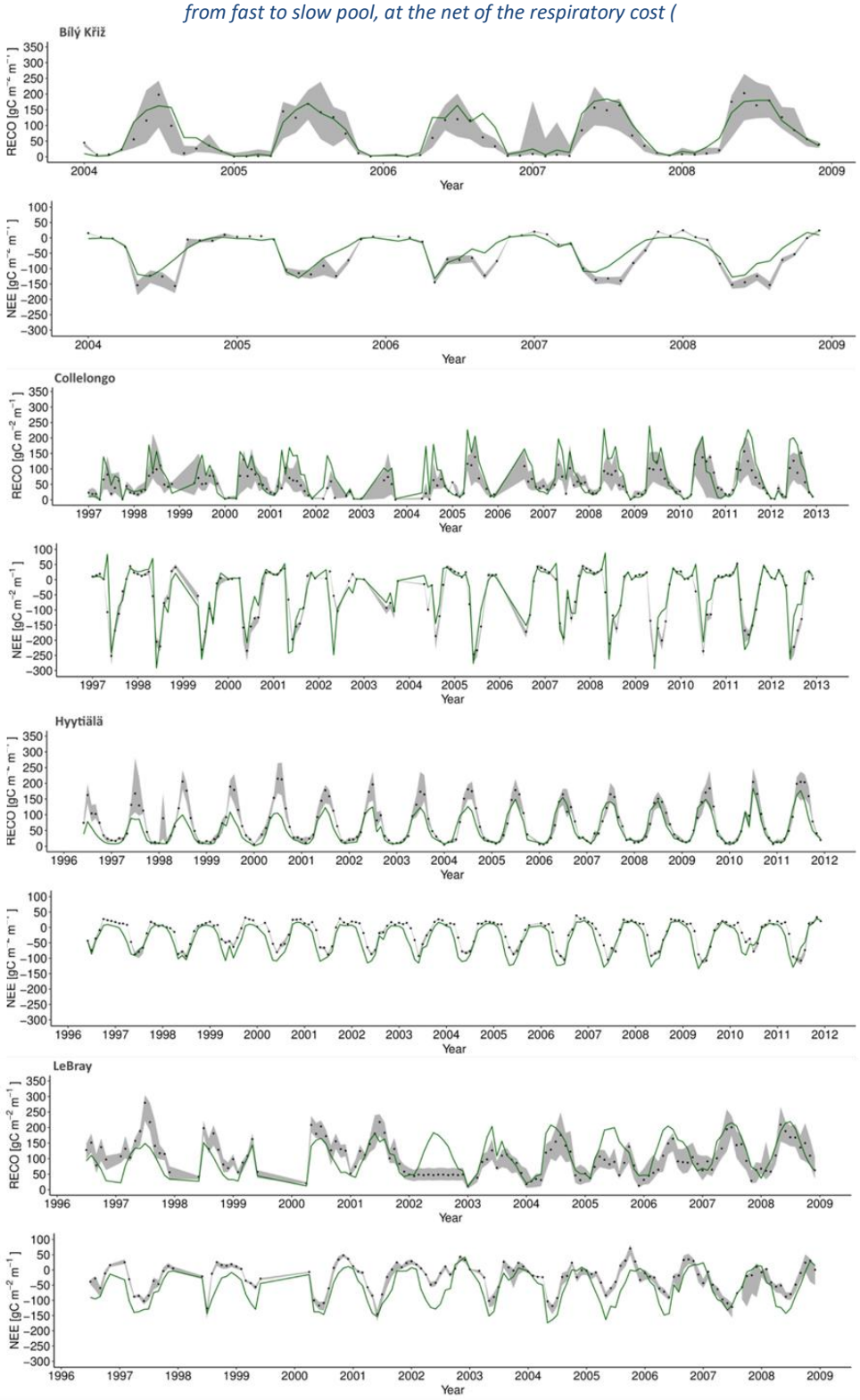

Figure *31*) The decomposed soil carbon which is transferred among soil pools is defined as:

$$I_s = \alpha_s \cdot D_s \qquad \textit{Eq. 39}$$

where the fraction α_s depends on the specific decomposability degree of each carbon pool. It follows that the fraction of decomposed organic carbon respired to the atmosphere, i.e. the heterotrophic soil respiration Rh_s by soil microorganisms, is defined as:

$$R_{h_l} = (1 - \alpha_s) \cdot D_s \qquad \textit{Eq. 40}$$

The total heterotrophic respiration carbon flux is the sum of all carbon resealed during the decomposition of each litter and soil organic pool, R_{hl} and $R_{hs,}$ respectively. When R_h is summed up to the autotrophic respiration it is considered as ecosystem respiration (R_{eco}) and NEE is computed by the models (as GPP — R_{eco}).

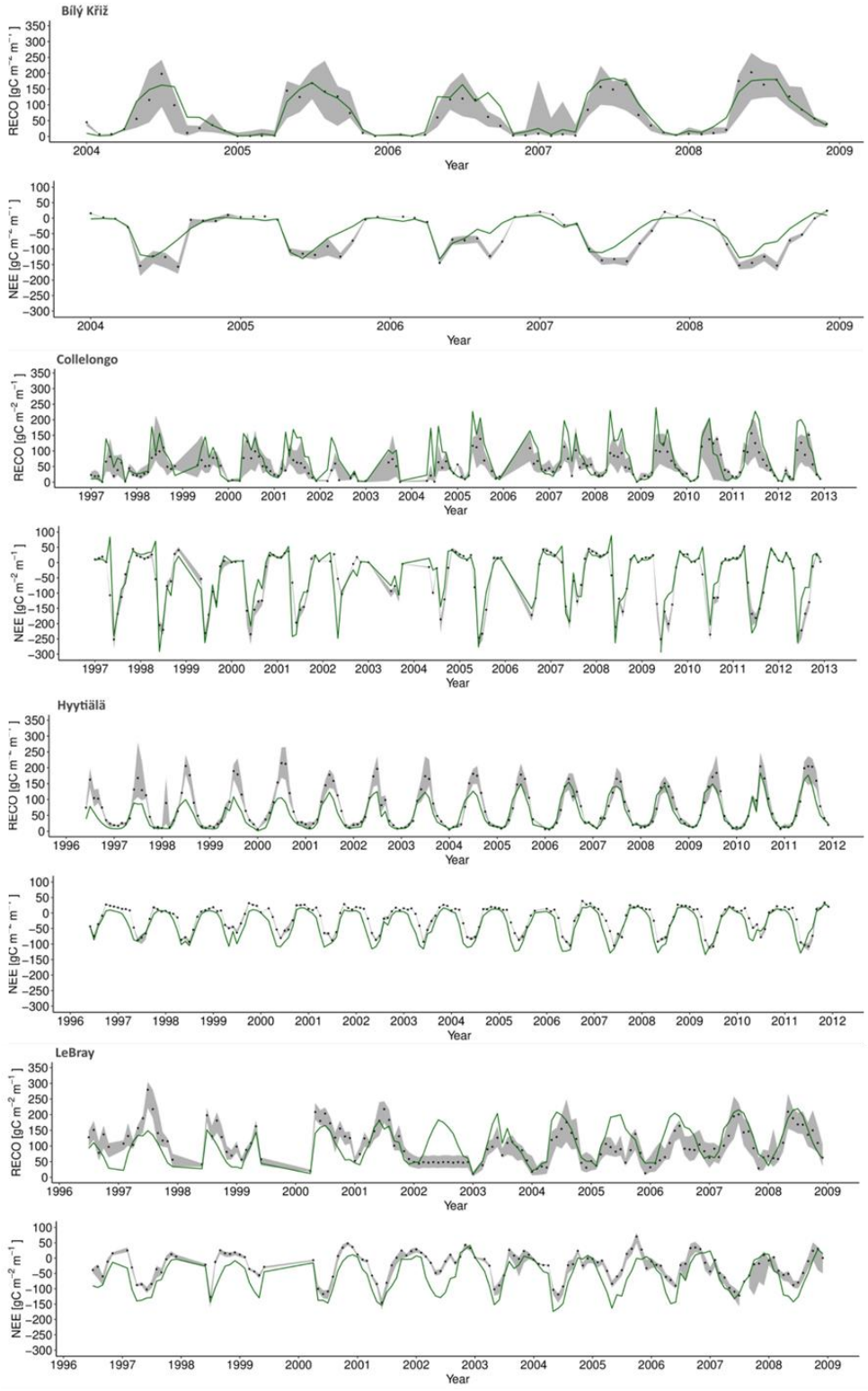

Figure 31 Patterns in monthly R_{eco} and NEE (gC m^{-2} $month^{-1}$) computed for four forest stands on a site level. Black dots represent measured R_{eco} and NEE from eddy covariance (FLUXNET dataset) and the grey shaded area represents the interval between the 5th and 95th percentile value (Pastorello et al. 2020). The green line represents the modelled R_{eco} and NEE (figure from Morichetti et al. 2024).

4. WATER BUDGET

4.1 WATER CYCLE

(subroutine: *water_balance.c*)

The vertically resolved water budget considered, as similarly as in the radiation budget, all different vertical layers that can compose a specific forest structure to simulate. The overall water budget in the 3D-CMCC-FEM is the result of incoming water (i.e. precipitation; both in the form of rain if the temperature exceeds 0 °C or in the form of snow when the temperature is below 0 °C) and the outgoing water, the remaining water is the one remaining in the soil (or temporarily to the canopy if there are not the conditions for the complete evaporation). The incoming precipitation is routed to several potential compartments, some is directly intercepted by the canopies, and some goes directly to the soil (also because of snowmelt) and becomes available to the roots (**Figure 32**). The outgoing fluxes are represented by canopy evaporation, canopy transpiration, and soil evaporation, which collectively represent evapotranspiration at the cell level. The difference between incoming and outgoing water is stored in the soil (or in the canopy). Any excess to the soil water holding capacity is considered lost for runoff. As for the carbon the water cycle has by abstraction its budget with several levels of 'budget' depending on the level of representation, which in 3D-CMCC-FEM are at tree- and cell-level which also include litter- and soil-level.

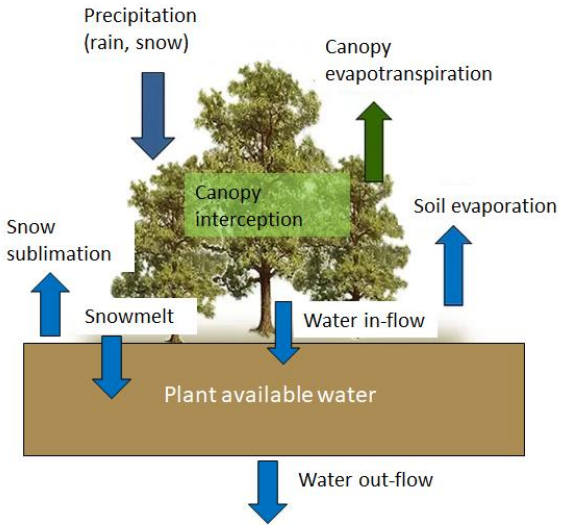

Figure 32 Water balance in a forest ecosystem, illustrating processes like precipitation, evapotranspiration, interception, soil evaporation, and plant-available water. It visually represents how water flows interact within the ecosystem, highlighting pathways such as canopy evaporation and runoff.

4.2 Rain and Snow Canopy Interception

(subroutine: *canopy_interception.c*)

Firstly, some (if not all) incoming precipitation, both as rain or snow, is intercepted by the canopy. In the 3D-CMCC-FEM, when T_{avg} is above 0°C, all incoming precipitation is considered as rainwater, otherwise, for T_{avg} below 0°C is considered as snow. The amount of intercepted rainwater follows Jiao et al. (2016) by a nonlinear regression relationship which accounts for the maximum interceptable rain and follows the general first principles previously described for light interception and absorption, as follows:

$$IntMaxRain_{x,,y,k \in z} = 0.284 + 0.092 \cdot LAI_{x,y,k \in z} \cdot (1 - e^{-0.231 \cdot rain}) \cdot CC_{x,y,k \in z} \quad \textit{Eq. 41}$$

where *rain* is the incoming rain (and not that interceptable by the species *x*, the DBH *y* and the tree height *k* (**Figure *33***).

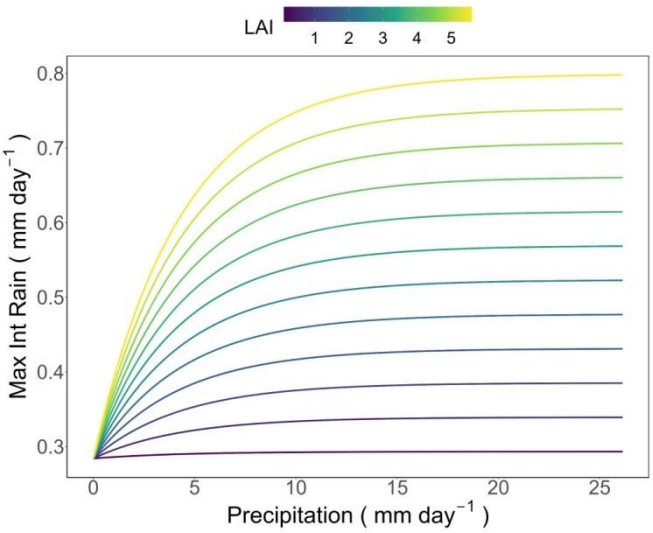

Figure 33 Variation of maximum interceptable rainwater from the canopy at varying LAI with CC = 1.

The actual amount of intercepted rain by the canopy is computed by:

$$IntRain_{x,y,k \in z} = min\,(IntMaxRain_{x,y,k \in z}, Rain_{x,y,k \in z}) \quad \textit{Eq. 42}$$

where *Rain* is the actual rain incoming from above (the net from those arriving from the sky and that potentially intercepted by the above canopies, if any). If there is more than enough water to fill the canopy interception pool ('*IntRain*'), the excess water is considered to have fallen and entered the soil water pool. The intercepted water can evaporate directly from the canopy. At the cell level, the 3D-CMCC-FEM sums up all the intercepted rain by all canopies of different classes and N layers as:

$$IntRain = \sum_{z=1}^{N} IntRain_{x,y,k} \qquad \textit{Eq. 43}$$

Snow interception is also simulated following Pomeroy et al. (1998) and Hedstrom and Pomeroy (1998) by first computing the maximum interceptable snow through (see also **Figure *34***):

$$IntMaxSnow_{x,y,k \in z} = 4.4 \cdot LAI_{x,y,k \in z} \qquad \textit{Eq. 44}$$

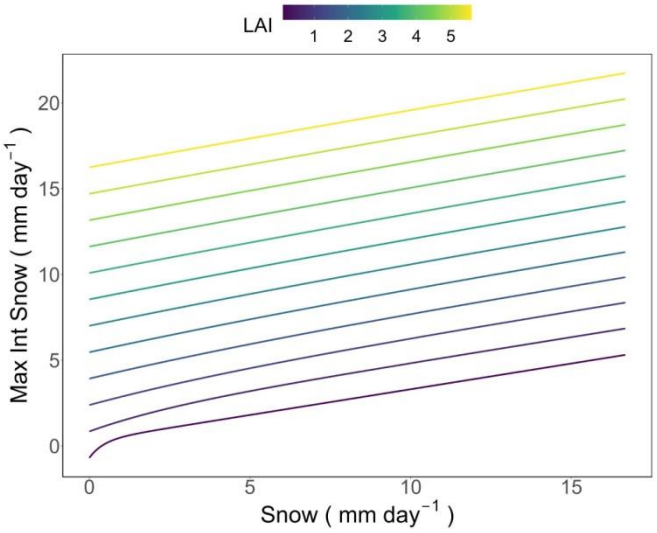

Figure 34 Variation of maximum interceptable snow from the canopy at varying LAI and at varying Snow amount (mm day^{-1}).

and the actual amount of snow intercepted is modelled as:

$$IntSnow_{x,y,k\in z} = Snow_{x,y,k\in z} + 0.7 \cdot ((IntMaxSnow_{x,y,k\in z} - Snow_{x,y,k\in z}) \cdot (1 - e^{-\frac{Snow}{IntMaxSnow_{x,y,k\in z}}})) \cdot CC_{x,y,k\in z}$$

Eq. 45

Likewise rainwater, at the cell level the 3D-CMCC-FEM sums up all the intercepted snow by all canopies of different classes and N layers as (**Figure 35**):

$$IntSnow = \sum_{z=1}^{N} IntSnow_{x,y,k}$$

Eq. 46

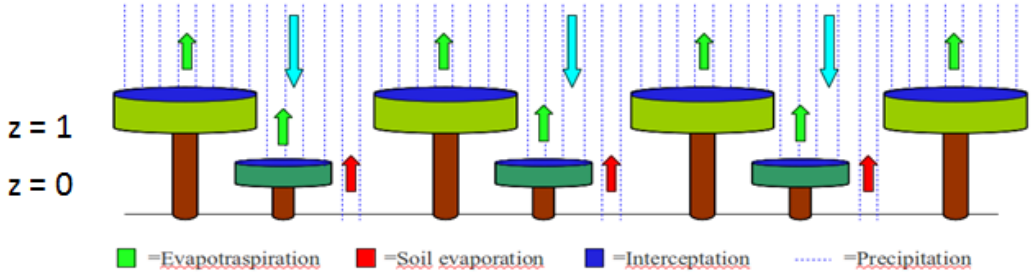

Figure 35 Conceptual scheme adopted in 3D-CMCC-FEM for Evapotranspiration, Canopy Interception and Soil Evaporation (figure from Collalti 2011).

When the intercepted rain or snow does not evaporate or sublimate in the day the remaining part is considered as stored water above the canopy until meteorological conditions do not favour their complete evaporation in the coming days.

4.3 Snow Dynamics

(subroutine: *snow.c*)

In the case of snow presence, i.e. when snow is diverse from 0 and if T_{avg} is higher than 0 °C, considering the melting point as in Running and Coughlan (1988) and Marks et al. (1992), the rate of daily snowmelt is estimated by:

$$Snow_{melt} = (t_{coeff} \cdot T_{avg}) + \left(Rad_{soil} \cdot \frac{\varepsilon_{snow}}{H_{fus}}\right)$$

Eq. 47

where t_{coeff} is the snowmelt coefficient (0.65 Kg m^{-2} °C^{-1} day^{-1}), ε_{snow} is the absorptivity of snow (0.6), H_{fus} is the latent heat of fusion (335 kJ kg^{-1}) and Rad_{soil} is the incident net radiation at the soil surface (kJ m^{-2} day^{-1}) accounted for the amount reflected by the snow albedo (ρ_{snow}). Otherwise, if T_{avg} is lower than 0 °C, snow sublimation is computed by:

$$Snow_{subl} = \left(Rad_{soil} \cdot \frac{\varepsilon_{snow}}{H_{sub}}\right) \quad \textit{Eq. 48}$$

where H_{sub} is the latent heat of sublimation (2845 kJ kg^{-1}). The model does not consider ice.

4.4 Leaf and Canopy EvapoTranspiration

(subroutine: *canopy_evapotranspiration.c*)

All evaporative processes (canopy evaporation of intercepted water and transpiration and soil evaporation) are calculated at daily time scales using the Penman-Monteith Equation — PME as modified by Waring and Running (2007) and Monteith and Unsworth (2008). The PME uses characteristics of a particular surface (e.g. surface resistances) and current meteorological data (e.g. incoming radiation, vapour pressure deficit, air temperature, air pressure) to calculate an instantaneous heat balance, in terms of heat loss or gain, of an object. This equation calculates the latent heat fluxes of evaporation and transpiration (W m^{-2}) as a function of incoming radiation, vapour pressure deficit (VPD), and the conductances associated with the evaporation surface as follows:

$$\lambda E_{x,y,k\,\epsilon\,z} = \frac{\Delta e \cdot Rn_{x,y,k,\epsilon\,z} + \frac{\rho_{air} \cdot C_P \cdot VPD}{rhr}}{\Delta e + \gamma \frac{rv}{rhr}} \quad \textit{Eq. 49}$$

where R_n is the net radiation (W m^{-2}), VPD is the vapour pressure deficit of the air (kPa), ρ_{air} is the mean air density as a function of temperature (kg m^{-3}), c_p is the specific heat of the air (W m^{-2}), Δe represents the slope of the saturation vapour pressure-temperature relationship (Pa °C^{-1}), γ is the psychrometric constant (kPa °C^{-1}), and *rhr* and *rv* (sec meter^{-1}) are the combined, i.e. in parallel, resistance to convective and

radiative heat transfer and the resistance to water vapour flux respectively (Campbell and Norman 1998). The slope of the saturation pressure is approximated numerically as the slope in the neighbourhood of T_{air}. The flux is then converted from W m^{-2} to mm m^{-2} day^{-1} dividing by the latent heat of the vaporisation of water. At the cell level, the 3D-CMCC-FEM sums up all the evaporations by all canopies of different classes and *n* layers as:

$$\lambda E = \sum_{z=1}^{N} \lambda E_{x,y,k} \qquad \textit{Eq. 50}$$

4.4.1. Stomatal Conductance

The stomatal conductance g_s is parametrized via the empirically based multiplicative Jarvis model (Jarvis 1976; Frank et al. 2015; Hidy et al. 2016) which expresses the species-specific $g_{s\ max}$ as its theoretical maximum value which is reduced by a product of factors f_i varying from 0 (totally limiting) to 1 (not limiting) (see paragraph 5). These factors are functions of environmental variables such as light, atmospheric CO_2 concentration, air temperature, soil water content, VPD, and age, respectively. The stomatal conductance is in addition corrected for the direct effect of temperature and atmospheric CO_2 on conductance, *via* fc_{CO2} and fc_T as follows:

$$g_{s_{x,y,k\in z}} = g_{s\,max_x} \cdot f_{L_{x,y,k\in z}} \cdot fc_{CO_{2_x}} \cdot fc_{T_x} \cdot f_{\psi_{x,y,k\in z}} \cdot f_{T_x} \cdot f_{VPD_x} \cdot f_{age_{x,y,k\in z}} \qquad \textit{Eq. 51}$$

Leaf conductance per unit projected LAI, both for sun and shaded leaves, is finally derived from stomatal and cuticular conductance (gl_C) in parallel with each other, and both in series with leaf boundary layer conductance (gl_{bl}) as follows:

$$g_{L_{x,y,k\in z}} = \frac{gl_{bl_x} \cdot (g_{s\,max_x} + gl_{C_x})}{gl_{bl_x} + g_{s\,max_x} + gl_{C_x}} \qquad \textit{Eq. 52}$$

The 3D-CMCC-FEM considers water competition as an asymmetric competition, although to a different degree. The degree to which each species 'competes' for water is indirectly defined by how species-specific parameters define the modifiers applied to the stomatal conductance. The way each species responds to the

soil moisture conditions and regulates directly the competition for water under limiting conditions, i.e. drought, is embedded in the modifier f_ψ (see paragraph 5).

4.5 SOIL EVAPORATION

(subroutine: *soil_evaporation.c*)

Soil water evaporation is determined by adjusting the potential evaporation, computed through the Penman-Monteith Equation, with a factor that accounts for the duration since the last rainfall event. This adjustment acknowledges the soil's increased retention of water as moisture becomes scarce, consequently reducing the potential for evaporation (Taiz and Zeiger, 2006). Unlike leaves, which possess distinct resistances to convective and water vapour flux regulated by stomatal activity, soil exhibits a unified resistance to vapour flux equal to its resistance to sensible heat flux (i.e. *rh* and *rv*) equal to boundary layer resistance (rbl), with *rbl* = 107 · r_{corr}. The initial step involves deriving this resistance by calculating a correction factor for sensible heat conductance based on temperature and pressure conditions with standard conditions assumed to be 20 °C, 101300 Pa (Jones 1992):

$$r_{corr_{soil}} = \frac{1}{\left(\frac{T_{day}+273.15}{293.15}\right)^{1.75} \cdot \left(\frac{101300}{P}\right)} \qquad \textit{Eq. 53}$$

after that, PME the potential evaporation of soil can be computed. As in the BIOME-BGC model when precipitation (both in terms of rainwater or melted snow) equals or exceeds soil potential evaporation, actual evaporation is assumed to be 60% of the potential evaporation. Alternatively, if precipitation falls short, the counter for days since the last rain event (*Days Since Rain*) is incremented. The actual proportion of evaporation is subsequently determined as follows:

$$SoilEvapo = \frac{0.3}{Days\ Since\ Rain^2} \cdot SoilPotEvapo \qquad \textit{Eq. 54}$$

4.6 EVAPOTRANSPIRATION

(subroutine: *evapotranspiration.c*)

At cell level the total evapotranspiration rate (ET) is the sum of all intercepted (and evaporated) water (both as rainwater or melted snow), all the water transpired by the canopies of all classes (i.e. tree height, dbh,

ages classes) and species simulated in the stand and the soil evaporation. The 3D-CMCC-FEM capacity for simulating ET has been in the past as also recently tested in several sites around Europe (Collalti et al. 2014; Mahnken et al. 2022a).

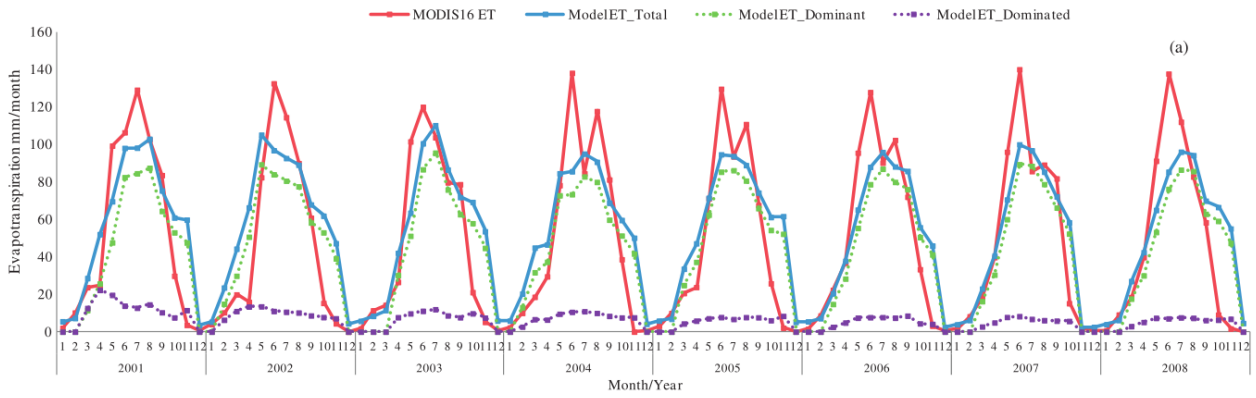

Figure 36 Comparison of Modis monthly evapotranspiration (MODIS16 ET) and 3D-CMCC-FEM total monthly evapotranspiration (mm month^{-1}), from dominant and dominated layer in the double-layered Turkey oak (*Q. cerris* L.) forest at the Torre di Feudozzo (Italy) (figure from Collalti et al. 2014).

4.7 Soil Water Balance

(subroutine: *soil_water_balance.c*)

Snow accumulates in a snow water pool during sub-freezing temperatures and melts when the temperature is above-freezing, seeping into the soil. Snow can also undergo to sublimation when exposed to sub-freezing temperatures depending on the amount of incoming solar radiation it receives.

The 3D-CMCC-FEM considers the soil as one bucket layer (i.e. one single layer) in which the water balance is computed on a daily time step considering inputs and outputs. Incoming water flux is constituted by daily precipitation at the net of the canopy-intercepted water, irrigation, whereas water leaves the soil through total evapotranspiration represented by canopy transpiration, canopy evaporation, and soil evaporation (collectively called 'evapotranspiration', ET), and through free drainage as surface runoff of the soil when soil water availability is higher than the field capacity. Note that when the 3D-CMCC-FEM runs in a spatial context over a landscape, cells do not interact with each other, i.e. each cell is a distinct model run and does not interact in any way with neighbouring cells, and the hydrology dynamic is one-dimensional.

The Available Soil Water (ASW, in mm) and the water budget is, thus, overall determined as:

$$ASW = ASW_{t-1} + Precipitation + Irrigation - ET \qquad Eq.\ 55$$

where Precipitation is the amount of daily rainwater or, if any, daily melted snow (snow is considered as long as it remains as snow not available for plants and has its own balance) reaching the soil, where *t* indicates the generic day of simulation and *t*—1 the day before. Irrigation is the amount of water in the form of irrigation (when and if set by the user), ET is the Evapotranspiration (in mm). When incoming water fluxes increase the ASW over the field capacity, water is lost from the soil as lateral surface (or subsurface) runoff or for infiltration to deep soil layers (groundwater); these processes are, however, not simulated explicitly within the model.

Canopy transpiration flux, defined as the sum of the canopy transpiration from all the canopy layers, is modulated by the soil moisture availability, through the soil matric potential.

The current soil water matric potential ψ (MPa) is a function of the water in the soil in relation to texture and the soil's saturated water holding capacity according to Clapp and Hornberger (1978) and Cosby et al. (1984), as follows:

$$\psi = \psi_{sat} \cdot \left(\frac{VWC}{VWC_{SAT}}\right)^{b} \qquad \textit{Eq. 56}$$

where ψ_{sat} is the soil water matric potential at saturation, expressed as a function of the soil texture, computed as:

$$\psi_{sat} = -(exp((1.54 - 0.0095 \cdot \%sand + 0.0063 \cdot \%silt) \cdot log(10)) \cdot 9.81e - 5) \qquad \textit{Eq. 57}$$

where *b* is a parameter, function of soil texture:

$$b = -(3.10 + 0.157 \cdot \%clay - 0.003 \cdot \%sand) \qquad \textit{Eq. 58}$$

Saturated soil water and field capacity soil water holding, expressed as Volumetric Water Content VWC (%), is defined based on the soil texture and depth (as specified in the site initialization file – percentage sand, silt, clay, and depth) as:

$$VWC_{sat} = (50.5 - 0.142 \cdot \%sand - 0.037 \cdot \%clay)/100 \quad \textit{Eq. 59}$$

with

$$VWC = \frac{ASW}{\left(\frac{SD}{100}\right) \cdot 1000} \quad \textit{Eq. 60}$$

where SD is the soil depth (in cm) and 1000 is a conversion factor. Likewise, the available soil water at field capacity is defined as:

$$ASW_{FC} = \left(\frac{SD}{100}\right) \cdot VWC_{FC} \cdot 1000 \quad \textit{Eq. 61}$$

and

$$VWC_{FC} = VWC_{sat} \cdot \left(\frac{-0.015}{\psi_{SAT}}\right)^{1/b} \quad \textit{Eq. 62}$$

when incoming precipitation (or irrigation, or both) exceeds its water holding capacity this water is considered lost for lateral surface (or subsurface) runoff or infiltration into the deep soil (groundwater) and not more available for tree roots.

5. MULTIPLIERS

(subroutine: *modifiers.c*)

Several multipliers (or modifiers, '$f_{variable}$') are used by the 3D-CMCC-FEM both in the Light Use Efficiency approach for GPP calculation as even in the Jarvis model (and then also for the BGC version) for stomatal conductance.

The modifier of the stomatal conductance accounting for the atmospheric CO_2 effect follows Frank et al. (2013), and it is expressed as:

$$fc_{CO_2} = \left(\frac{39.43}{0.9116}\right) \cdot Ca^{-0.64} \qquad \textit{Eq. 63}$$

and C_a is the atmospheric CO_2 concentration (µmol mol^{-1}) (**Figure *37***).

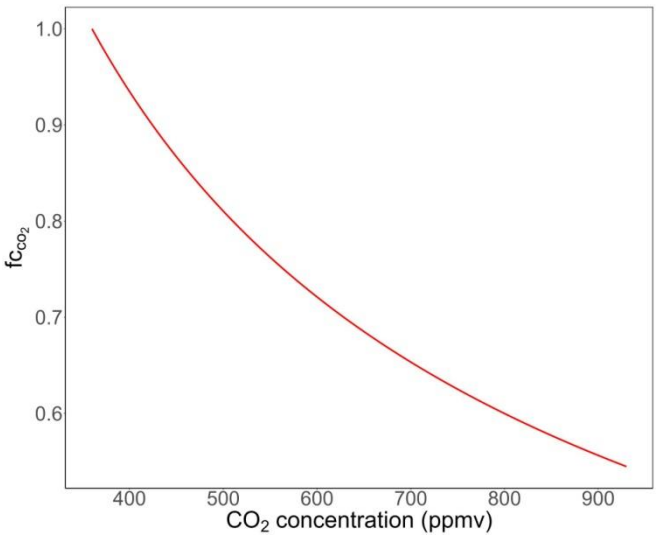

Figure 37 Changes in the stomatal conductance CO_2 modifier fC_{CO2} at varying atmospheric CO_2 concentration (µmol mol^{-1}).

The correction factor of the stomatal conductance for temperature and pressure follows the rationale of the BIOME-BGC model, and it is defined as:

$$fc_T = \left(\frac{T_{day} + 273.13}{293.15}\right)^{1.75} \cdot \frac{101300}{P} \qquad \textit{Eq. 64}$$

where T_{day} is the daytime average temperature, and *P* is the air pressure at the surface corrected for elevation (**Figure 38**).

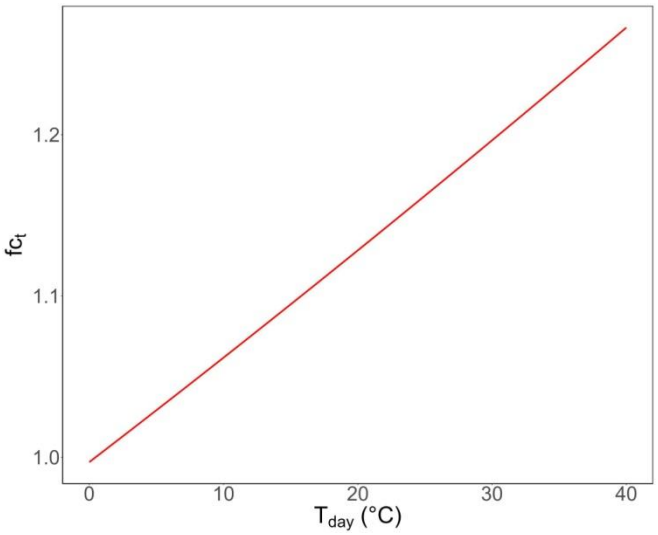

Figure 38 Variations in the stomatal conductance for temperature and pressure modifier f_{Ct} at varying T_{day} (°C) with P = 89733 P_a (at 1000 a.s.l.).

In 3D-CMCC-FEM T_{day}, that is daylight daily air temperature, is computed as in Running and Coughlan (1988) and Collalti et al. (2016) as:

$$T_{day} = 0.45 \cdot (T_{max} - T_{avg}) + T_{avg} \qquad \textit{Eq. 65}$$

while T_{night}, the night-time daily air temperature (for leaf maintenance respiration), is computed as:

$$T_{night} = \frac{T_{day} + T_{min}}{2} \qquad \textit{Eq. 66}$$

and T_{avg} is defined as in Running (1997) and Collalti et al. (2016):

$$T_{avg} = 0.606 \cdot T_{max} + 0.394 \cdot T_{min} \qquad \textit{Eq. 67}$$

The soil temperature (T_{soil}), if not provided as input meteorological forcing data, is computed as the 10-day running weighted average of the daily average temperature T_{avg}.

In the LUE model version, a CO_2-dependent modifier is applied directly to the light use efficiency parameter, and it is defined, independently of species, following Veroustraete (1994) and Veroustraete et al. (2002) and Collalti et al. (2018) and is computed as:

$$f_{CO_2} = \frac{[CO_{2\,curr}] - \frac{[O_2]}{2\tau_{CO2O2}}}{[CO_{2\,ref}] - \frac{[O_2]}{2\tau_{CO2O2}}} \cdot \frac{K_m^{CO_2} \cdot \left(1 + \frac{[O_2]}{K_0}\right) + [CO_{2\,ref}]}{K_m^{CO_2} \cdot \left(1 + \frac{[O_2]}{K_0}\right) + [CO_{2\,curr}]} \qquad \textit{Eq. 68}$$

where where $[O_2]$ is the atmospheric oxygen concentration (%), K_m^{CO2} (µmol mol^{-1} CO_2) and K_O (%O_2) are the Michaelis-Menten Rubisco affinity coefficients for CO_2 and the Michaelis-Menten inhibition coefficient for O_2 (µmol mol^{-1} O_2), respectively, and τ_{CO2O2} is the CO_2:O_2 specificity ratio (dimensionless). As shown by Badger and Collatz (1977), Veroustraete (1994, 2002), $KmCO_2$ and K_o are controlled by daily average temperature [K], according to an Arrhenius relationship:

$$K_m^{CO_2} = A \cdot e^{-\frac{E_a}{R_{gas} \cdot T_{day_K}}} \qquad \textit{Eq. 69}$$

Veroustraete (1994) showed that CO_2 fertilisation has two phases and hence two sets of parameters that are used in the model, based on daily average air temperature. The two phases originate from a conformational change of Rubisco in the membranes and are incorporated as functions of daily mean temperature T_{avg}:

1. for $T_{day} \geq 15$ °C Ea = 59.4 (KJ mol^{-1}) and A = 2.419 × 1013

2. for $T_{day} < 15$ °C Ea = 109.6 (KJ mol^{-1}) and A = 1.976 × 1022

The inhibition constant K_O for the oxygen concentration O_2 is computed as:

$$K_0 = A_0 \cdot e^{-\frac{E_{a0}}{R_{\square\square\square} \cdot T_{day_K}}} \qquad \textit{Eq. 70}$$

with A_0 = 8240 and Ea_0 = 13913.5 (KJ mol^{-1}). For both the equations of $KmCO_2$ and K_o, R_{gas} is the gas constant (8.314 J·mol^{-1}·K^{-1}) and T_{day_K} is the daily average air temperature in Kelvin. The temperature dependence of τ is computed as:

$$\tau = A_\tau \cdot e^{-\frac{E_{a\tau}}{R_{gas} \cdot T_{day_K}}} \quad \textit{Eq. 71}$$

wherein A_τ = 7.87 × 105 and $E_{a\tau}$ = 42896.9 (KJ mol^{-1}) (**Figure 39**).

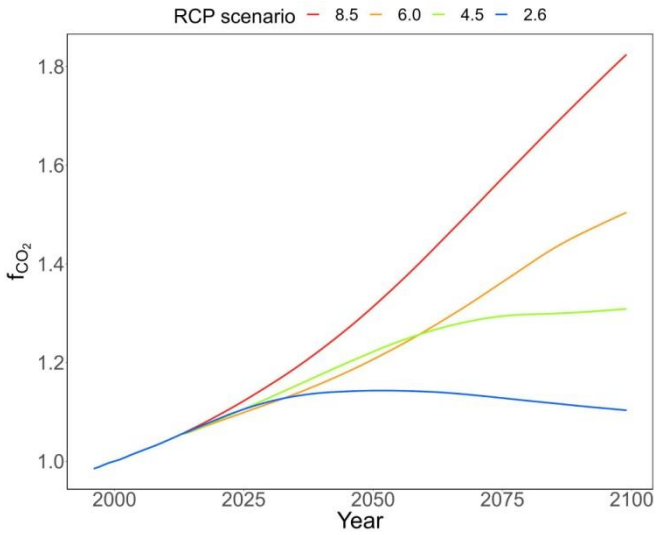

Figure 39 Trends for the f_{CO2} modifier for assimilation as a function of different atmospheric CO_2 concentration scenarios associated (CMIP5 Representative Concentration Pathways: RCPs 2.6, 4.5, 6.0, 8.5) with reference atmospheric CO_2 concentration = 370 µmol mol^{-1} and T_{day} = 20 °C.

Soil water modifiers depend on the current soil matric potential (Ψ). It is assumed that at daily time scale, canopy experiences a matric potential equal to the soil matric potential. The soil water modifiers is computed daily as similarly as in the BIOME-BGC model as follow:

$$f_{\psi_{\square}} = max\left(\frac{\psi l_{close_{\square}} - \psi}{\psi l_{close_{\square}} - \psi l_{open_{\square}}}, 0.3\right) \quad \textit{Eq. 72}$$

where ψl_{close} is the leaf matric potential of stomatal total closure and ψl_{close} is the leaf matric potential, both species-specific, at which stomatal starts closing. The value 0.3 is the minimum allowed stress factor in order to avoid e.g. zero transpiration (and zero photosynthesis). Similarly, the JULES model (Clark et al. 2011)

adopts the value of 0.2. However, transpiration is forced to be 0, in the extreme case where no soil water is available for plants.

The modifier f_ψ is linear in ψ, however, ψ varies highly non-linearly with soil water content, depending on the soil texture. How these modifiers behave in relationship to the species-specific parameters ψl_{close} and ψl_{open}, define the degree of anysohydricity/isohydricity of the species.

$$f_{VPD_x} = e^{-Ccond_x \cdot VPD} \qquad \textit{Eq. 73}$$

where *Ccond* is a species-specific parameter defining the closure degree of stomata with daily vapour pressure deficit VPD in hPa (Landsberg and Waring 1997) (**Figure *40***). The latter two factors concur in defining the isohydric/anisohydric spectrum to characterise plant drought responses and recovery process.

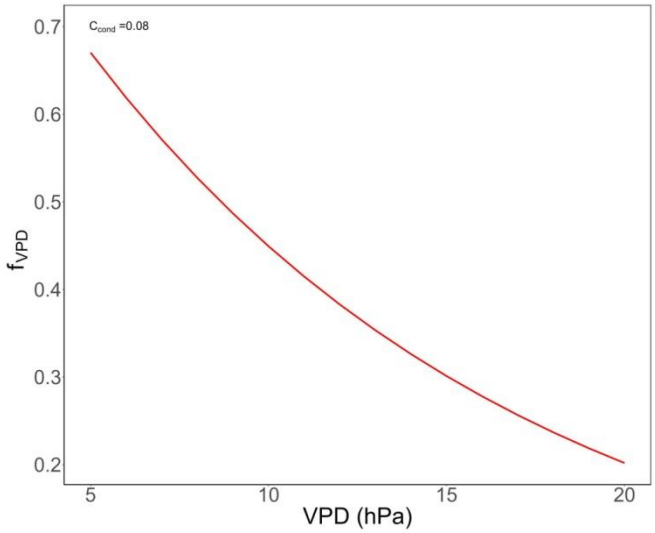

Figure 40 Variations in the VPD modifier f_{VPD} at varying VPD (hPa) with C_{cond} = 0.08.

The modifier f_L represents the photosynthetic photon flux density conductance control (Körner et al. 1995) and it is expressed in its general formula as:

$$f_{L_{x,y,k\in z}} = \frac{APAR_{x,y,k\in z}}{PARD50 + APAR_{x,y,k\in z}} \qquad \textit{Eq. 74}$$

where PARD50 is the PAR value at which the 50% of the stomatal closure occurs and is set at 6.48 molPARm^{-2} day^{-1} (**Figure *41***). The light modifier f_L is computed separately for sunlit and shaded leaves because the amount of absorbed PAR is different.

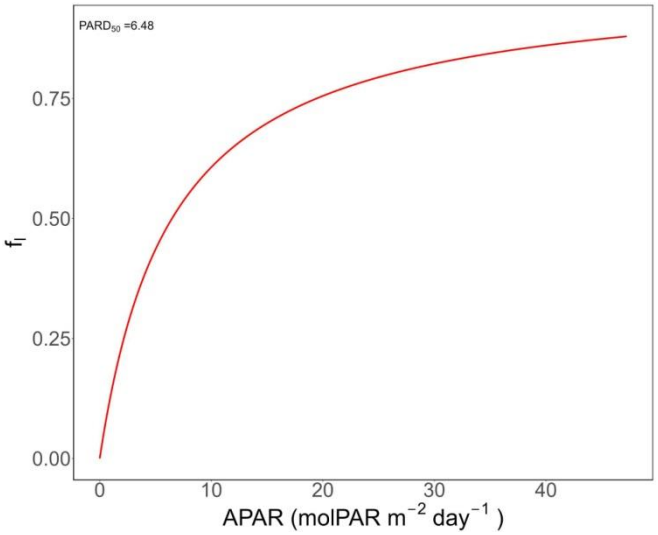

Figure 41 Variations in the Photosynthetic Photon Flux Density modifier f_L at varying APAR (molPAR m^{-2} day^{-1}).

Introduced in the 3-PG model by Landsberg and Waring (1997), the modifier function of age, assumes that with age (and indirectly by assuming an increase in tree height), the hydraulic resistance increases and the stomatal conductance decreases, reflecting a decrease in forest productivity (the so-called 'age-related' decline). In 3D-CMCC-FEM the age modifier is expressed as in the 3-PG model through:

$$f_{age_{x,y,k\in z}} = \frac{1}{1+\left(\frac{Relage_{x,y,\in z}}{Rage_x}\right)^{Nage_x}} \qquad \textit{Eq. 75}$$

where:

$$Rel_{age} = \frac{age_{x,y,\in z}}{MAX_{age_x}} \qquad \textit{Eq. 76}$$

with MAX_{age} the expected lifespan of the species considered (**Figure 42**). *Rage* and *Nage* are species-specific parameters, following Landsberg and Waring (1997). This modifier is used in the Jarvis model of stomatal conductance and, thus, in the FvCB photosynthesis model, and directly in the LUE one.

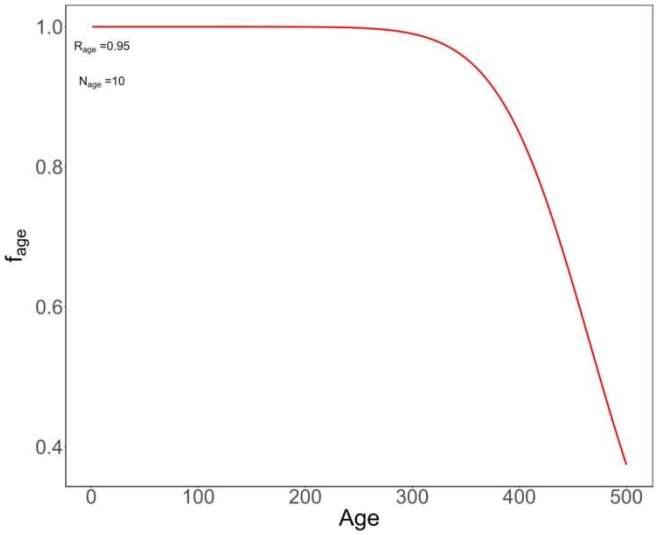

Figure 42 Variations in the Age modifier f_{AGE} at varying age with R_{age} = 0.95 and N_{age} = 10.

The temperature-dependent modifier f_T is defined as:

$$f_{T_x} = \left(\frac{T_{day} - T_{min_x}}{T_{opt_x} - T_{min_x}}\right) \cdot \left(\frac{T_{max_x} - T_{day}}{T_{max_x} - T_{opt_x}}\right)^{(T_{max_X} - T_{opt_x})/(T_{opt_x} - T_{min_x})} \qquad \textit{Eq. 77}$$

with f_T = 0 when T_{day} >= T_{max} or T_{day} <= T_{min} where, in this case, $T_{min\ x}$, $T_{max\ x}$, and $T_{opt\ x}$ are species-specific parameters defining the temperature dependence of photosynthetic plant activity (Waring and McDowell, 2002) at stomatal level (**Figure 43**).

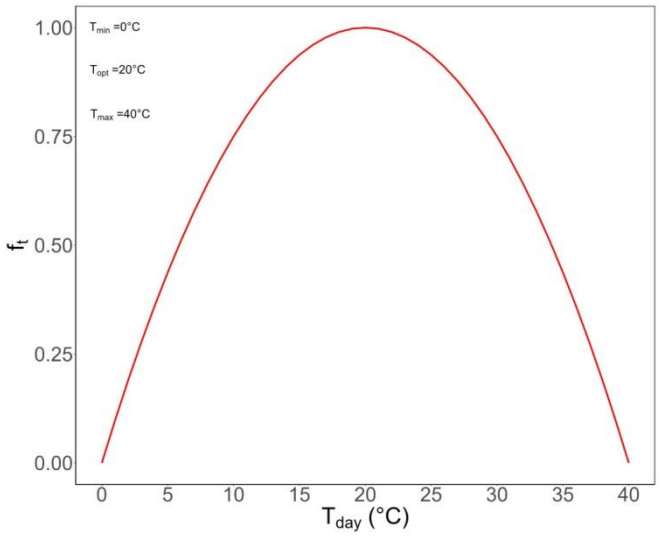

Figure 43 Variations in the Temperature modifier f_T at varying Tday (°C) with T_{opt} = 20°C, T_{min} = 0°C, T_{max} = 40°C.

The modifier fs_T describes the effect of soil temperature on the decomposition of litter and soil organic carbon pools (Parton et al. 1987) as follows:

$$fs_T = \left(\frac{C45 - T_{soil}}{T_b}\right)^2 \cdot e^{0.076 \cdot \left(1 - \left(\frac{45-}{T_b}\right)^{bb}\right)} \qquad \textit{Eq. 78}$$

where T_{soil} is the soil temperature (**Figure *44***). The constant T_b is set to 20 and 10 (both in °C) for litter and soil respectively; *bb* is set to 4.9 and 2.63 for litter and soil respectively.

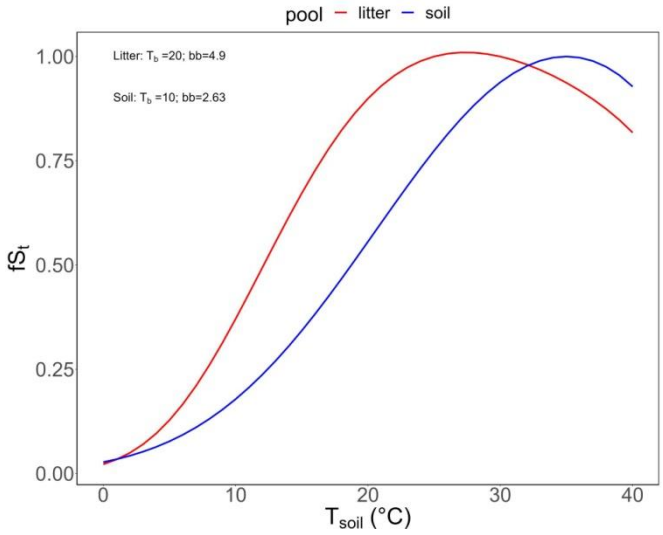

Figure 44 Variations in the Litter and Soil temperature decomposition modifier f_{St} at varying T_{soil} (°C) with Litter T_b = 20 and Litter bb = 4.9; Soil T_b = 10 and bb = 2.63.

Similarly, the modifier $f_{s\theta}$ describes the effect of soil water availability on the organic matter decomposition and is defined as (see also **Figure *45***):

$$fs_\theta = \frac{1}{1+30 \cdot e^{-8.5 \cdot \left(\frac{ASW}{ASW_{FC}}\right)}} \qquad \textit{Eq. 79}$$

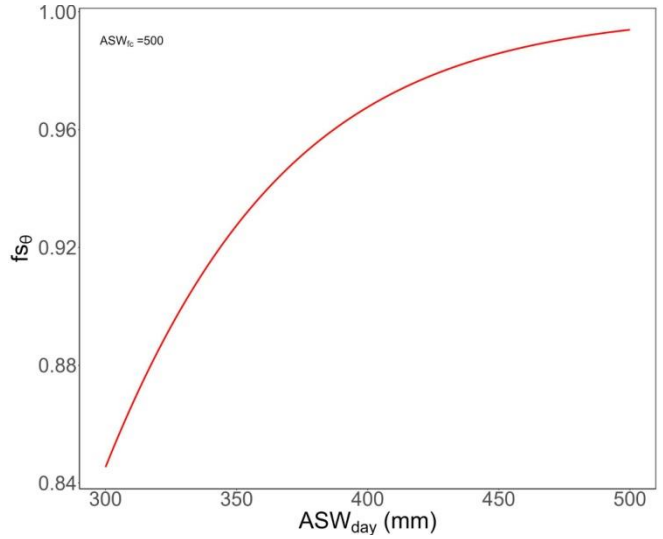

Figure 45 Variations in soil water availability on the organic matter decomposition modifier $f_s\theta$ at varying ASW_{day} (mm) with ASW_{fc} = 500 mm.

The soil organic matter decomposition modifier f_{sc}, which depends on the soil matrix, is defined as (see also **Figure 46**):

$$f_{sc} = \left(1 - 0.75 \cdot \left(\frac{\%clay}{100} + \frac{\%silt}{100}\right)\right) \quad \textit{Eq. 80}$$

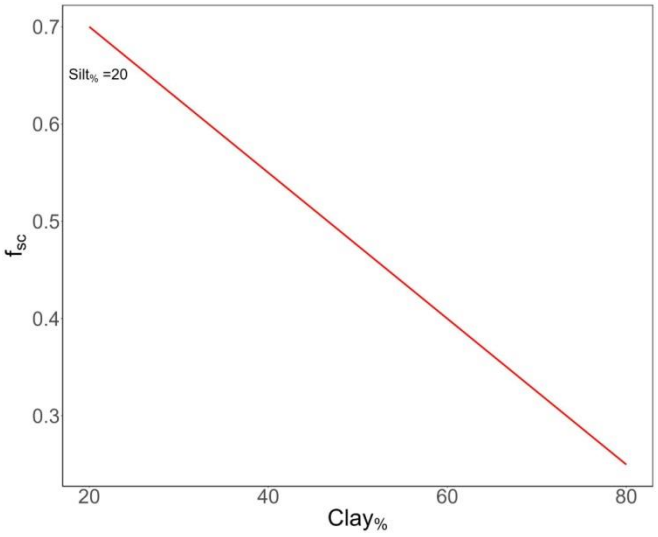

Figure 46 Variations in soil organic matter decomposition modifier f_{sc} at varying clay% (and silt%)

The 'cold acclimation' modifier f_t is defined as in Luo et al. (2003), and it is the result of a differential equation of the delayed daily temperature X at day t, here solved explicitly for each year as:

$$f_t = min\left(\frac{S_t}{S_{max}}, 1\right) \quad \textit{Eq. 81}$$

Where S is the acclimation state and S_{max} is a species-specific parameter which sets the minimum temperature threshold at which the photosynthetic process is no more inhibited by low temperatures.

S is described as:

$$S \quad = max(X \quad - X_0, 0) \quad \textit{Eq. 82}$$

X_0 is a species-specific parameter that is the minimum temperature threshold above which the modifier is higher than 0. The value of X is solved dynamically during the year as:

$$X \quad = X_{t-1} + \frac{1}{\tau}(T_{min} - X_{t-1}) \qquad \textit{Eq. 83}$$

with the initial condition

$$X_{t=1} = T_{min,t=1} \qquad \textit{Eq. 84}$$

Following Luo et al. (2023), T_{min} is the daily minimum temperature of the day t, and τ[day] is a parameter that defines the time scale needed for the leaf to acclimate to the new temperature (**Figure *47***).

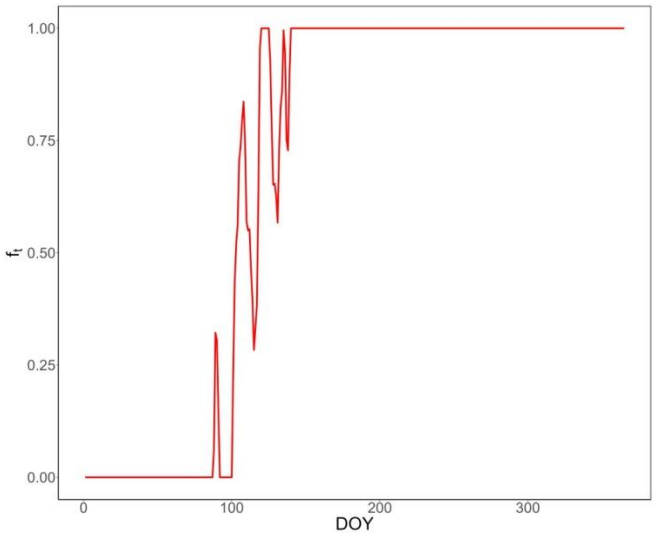

Figure 47 Example of the yearly variations of the cold acclimation multiplier for the canadian OJP *Pinus banksiana* site

6. FOREST DENDROMETRIC AND STRUCTURAL ATTRIBUTES

(subroutine: *allometries.c*, *dendrometry.c*, *canopy_cover.c*)

Model updates the tree and forest structural attributes such as tree DBH, tree height, and crown area or canopy cover (i.e. the sum of all tree crown areas within the grid-cell) some at daily, some at monthly and others at the annual scale. Such changes in forest structural attributes are computed by the model through species-specific and possibly generic (i.e. non stand-based) power-law allometric equations. Recent studies (e.g. Collalti et al. 2019) showed that 3D-CMCC-FEM is particularly sensitive to parameters used in the allometric equations described below as these equations control both in the initialization as during the model runs the amount of biomass and its accumulation over the years and then the amount of autotrophic respiration and the use of reserve (see also paragraph 3.9 Non-Structural Carbon). Caution should be then paid in the analysis of these values adopted during the parameterization.

6.1 STEM BIOMASS - DBH RELATIONSHIP

The relationship between DBH and stem biomass (kg dry matter) is expressed via a power function (see e.g. Cannell 1984 and Forrester et al. 2017) as follows:

$$STEM_{biomass_{x,y,k \in z}} = STEM_{const_x} \cdot DBH_{x,y,k \in z}^{STEM_{power_x}} \quad \textit{Eq. 85}$$

where $STEM_{const}$ and $STEM_{power}$ are fitting parameters (**Figure 48**). The formula considering stem biomass as the variable to predict is used during the initialization procedure given that DBH is one of the mandatory input data requested by the 3D-CMCC-FEM.

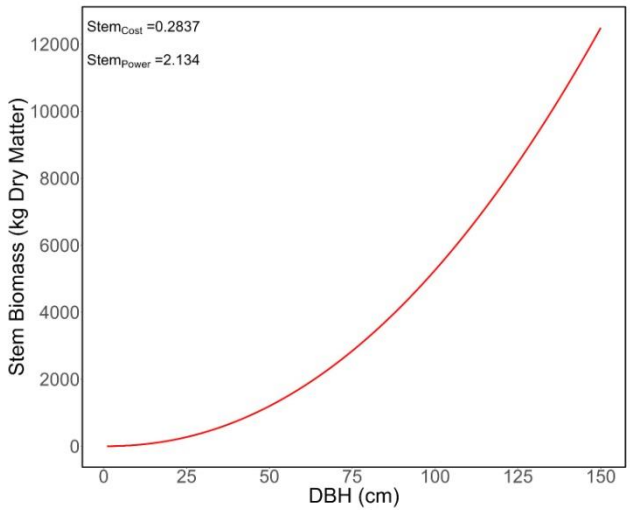

Figure 48 Variation of Stem Biomass (kg dry matter) with respect to diameter at breast height (DBH, cm) with $Stem_{const}$ = 0.2837 and $Stem_{power}$ = 2.314.

Conversely, during the model run, given that stem biomass increments are computed through the allocation of partitioned daily NPP to the stem biomass pool (and converted in dry matter) the same formula is transformed to compute the new daily DBH into the equivalent (see also **Figure *49***):

$$DBH_{x,y,k \in z} = \left(\frac{STEM_{biomass_{x,,y,k \in z}}}{STEM_{const_x}}\right)^{1/STEM_{power_x}} \quad \textit{Eq. 86}$$

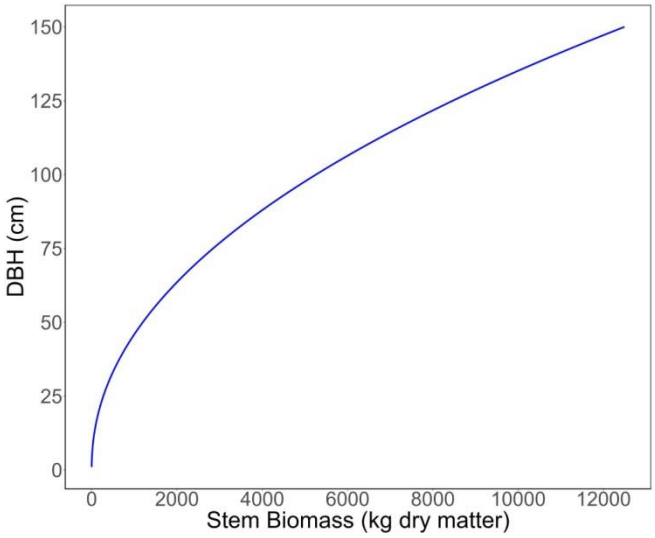

Figure 49 Variation of diameter at breast height (cm) for Stem Biomass (kg dry matter) with $Stem_{const}$ = 0.2837 and $Stem_{power}$ = 2.314

The 3D-CMCC-FEM capacity on simulating DBH (or its annual increments as well as the Basal Area and its annual increments) has been tested in several sites around Europe over the years (Collalti 2011; Collalti et al. 2014; Mahnken et al. 2022a; Testolin et al. 2023; Vangi et al. 2024a, 2024b*;* Puchi et al. *in prep.*; and see **Figure 50** and **Figure 51**).

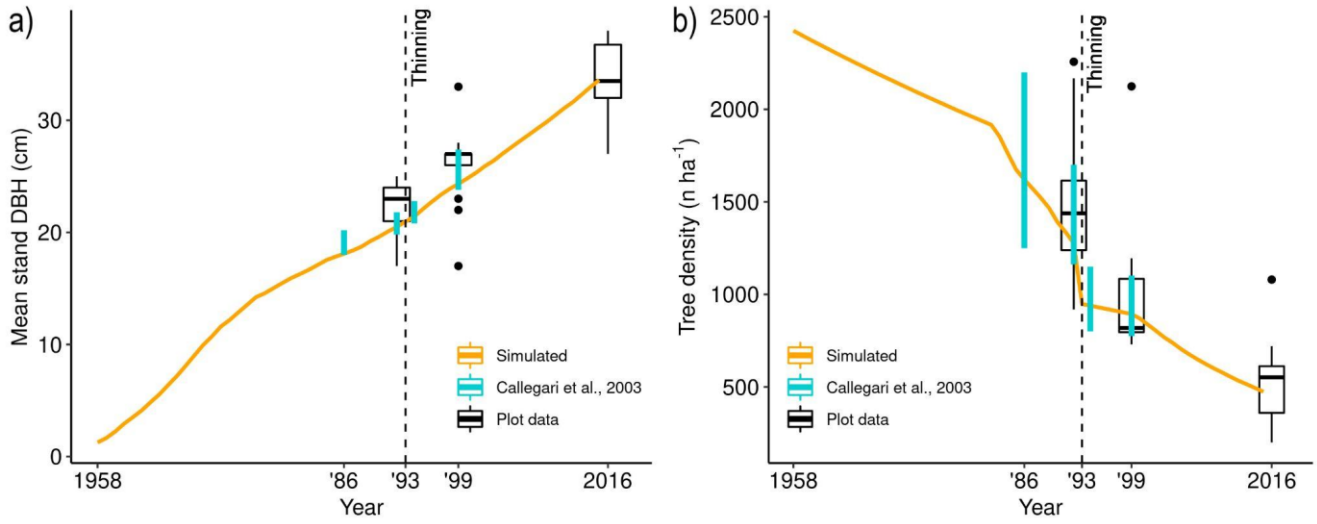

Figure 50 Evaluation of (a) simulated mean stand DBH (cm) and (b) tree density (n trees ha^{-1}) against the values reported by Callegari et al. (2003) and measured within the sampling plots (figure from Testolin et al. 2023).

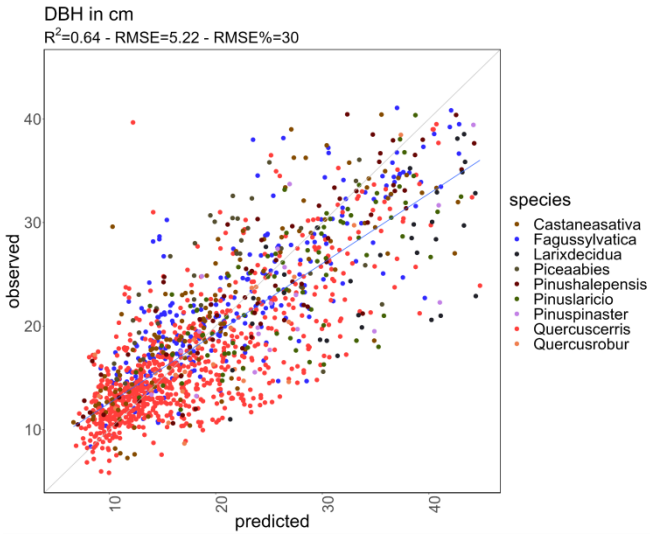

Figure 51 Comparison between modelled and observed DBH (cm) from NFI data at the species level (Vangi et al. in prep.).

6.2 Tree Height - DBH Relationship

The Chapman-Richard equation (Bertalanffey 1957) describes the relationship between the DBH and tree height in the form of :

$$h_{x,y,k \in z} = h_{ref} + CRA_x \cdot (1 - e^{-CRB_x \cdot DBH_{x,y,k \in z}})^{CRC_x} \quad \textit{Eq. 87}$$

where h is the tree height (m), DBH is the average tree diameter (cm), CR_A, CR_B and CR_C are fitting species-specific parameters of the equation with h_{ref} = 1.3 m. This equation should be applied for trees which are at least 1.3 m height (**Figure *52***).

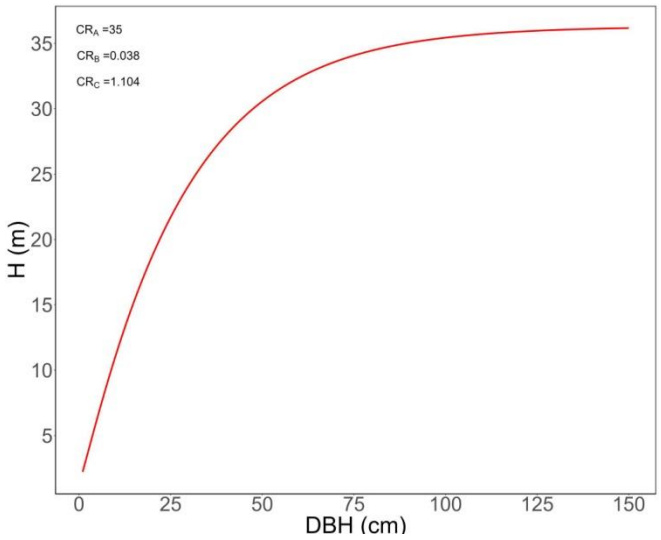

Figure 52 Variation of tree height (m) with respect to diameter at breast height (DBH, cm) with CR_A = 35 (m) , CR_B = 0.038, CR_C = 1.104

The 3D-CMCC-FEM capacity on simulating tree height (or its annual increments) has been recently tested in several sites around Europe over the years (Mahnken et al. 2022a; Vangi et al. *in prep*).

6.3 Sapwood Area - DBH Relationship

The relationship between DBH (cm) and sapwood area (cm^2) is described by a power function as follows (see e.g. Thurner et al. 2019):

$$SAPWOOD_{area_{x,y,k \in z}} = SAP_{A_x} \cdot DBH_{x,y,k \in z}^{SAP_{B_x}} \quad \textit{Eq. 88}$$

where SAP_A and SAP_B are species-specific parameters. This equation is only used in the initialization phase while during the entire simulation the sapwood increases (or decreases) controlled by the balance between the new stem biomass and the one that goes to heartwood because of turnover (τ) (**Figure 53**).

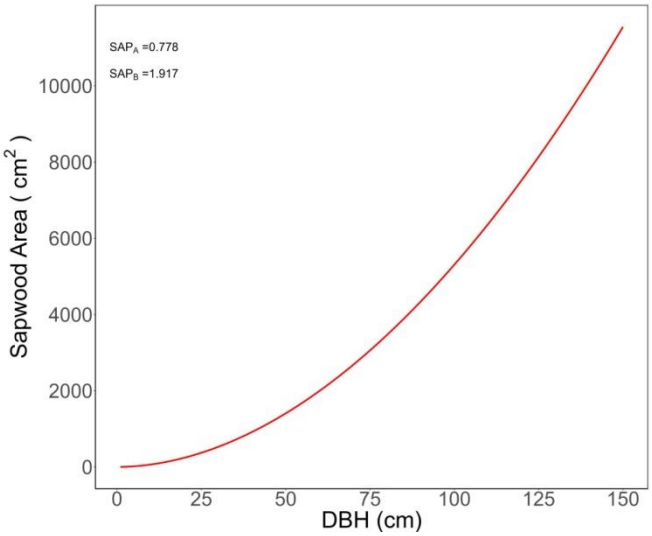

Figure 53 Variation of Sapwood Area (cm^2) with respect to diameter at breast height (DBH, cm) with SAP_A = 0.778 and SAP_B = 1.917.

6.4 Crown Development Constraints

First the variable DBHDC (dimensionless) is defined as DBH to Crown Diameter (DC) ratio, where crown diameter is a new variable computed according to the maximum layer coverage a species can tolerate and the total stand density (Collalti 2011; Collalti et al. 2014; **Figure *54***). Different levels of stand density set constraints on both tree survival and crown development, as trees tend to occupy the available space.

Competition for space among trees is avoided when:

$$DBHDC_{min_x} >= DBHDC_{x,y,k \in z} <= DBHDC_{max_{x,y,k \in z}} \quad \textit{Eq. 89}$$

under the condition DBHDC <= $DBHDC_{min}$, self-thinning occurs. Where $DBHDC_{min}$ is a species-specific parameter.

In case of crown competition (overlapping between crowns), constraints on crown development and expansion when e.g. there are opening gaps in the canopy, are set according to the following condition and allometric equation and computed as follows:

$$DBHDC_{x,y,k \in z} = min(DBHDC_{max_x}, DBHDC_{x,y,k \in z}) \quad \textit{Eq. 90}$$

where $DBHDC_{max}$ is computed as:

$$DBHDC_{max_{x,y,k \in z}} = \alpha_{DBHDC_x} \cdot DBH_{x,y,k \in z}{}^{-\beta_{DBHDC_x}} \quad \textit{Eq. 91}$$

where α_{DBHDC} and β_{DBHDC} are parameters which are currently set for evergreen and deciduous species. This ability to open the canopy is limited with and controlled by increasing DBH.

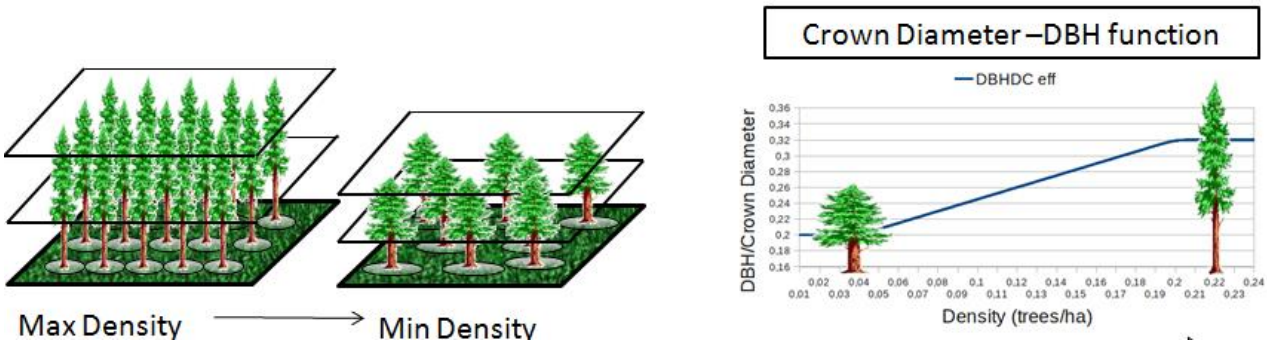

Figure 54 DBHDC density function (adapted from Collalti 2011)

Similarly, as for DBH, stem biomass and tree height (see section 6) the 3D-CMCC-FEM model updates the tree-level and forest structural attributes such as Basal and Crown, Volume, Current and Mean Annual Increment (CAI and MAI, respectively) as well as Above- and Below-Ground Biomass (AGB and BGB, respectively) at the beginning of each simulation years at the species, DBH, tree height for any layer.

6.5 Crown Diameter and Crown Area

Once accounted for and established the DBHDC, then, crown diameter can be computed simply through:

$$Crown\ diameter_{x,y,k\ \epsilon\ z} = DBH_{x,y,k\ \epsilon\ z} \cdot DBHDC_{x,y,k\ \epsilon\ z} \quad \textit{Eq. 92}$$

and crown area as:

$$Crown\ area_{x,y,k\ \epsilon\ z} = \pi \cdot \left(\frac{Crown_{diameter_{x,y,k\ \epsilon\ z}}}{2}\right)^2 \quad \textit{Eq. 93}$$

6.6 Basal Area

The basal area can be considered a productivity index of a forest stand and corresponds to the cross-sectional area of tree stem at 1.30 metres, on a given forest plot, which is commonly scaled up to 1 hectare. In the 3D-CMCC-FEM the basal area (and its annual increments) is determined using the following equation:

$$Basal\ area_{x,y,k\ \epsilon\ z} = \pi \cdot \left(\frac{DBH_{x,y,k\ \epsilon\ z}}{2}\right)^2 \cdot Ntree_{x,y,k\ \epsilon\ z} \quad \textit{Eq. 94}$$

where the model takes the diameter (DBH) and computes the stand-level basal area by factoring in the number of trees (N_{tree}) in m^2 (see **Figure 55**).

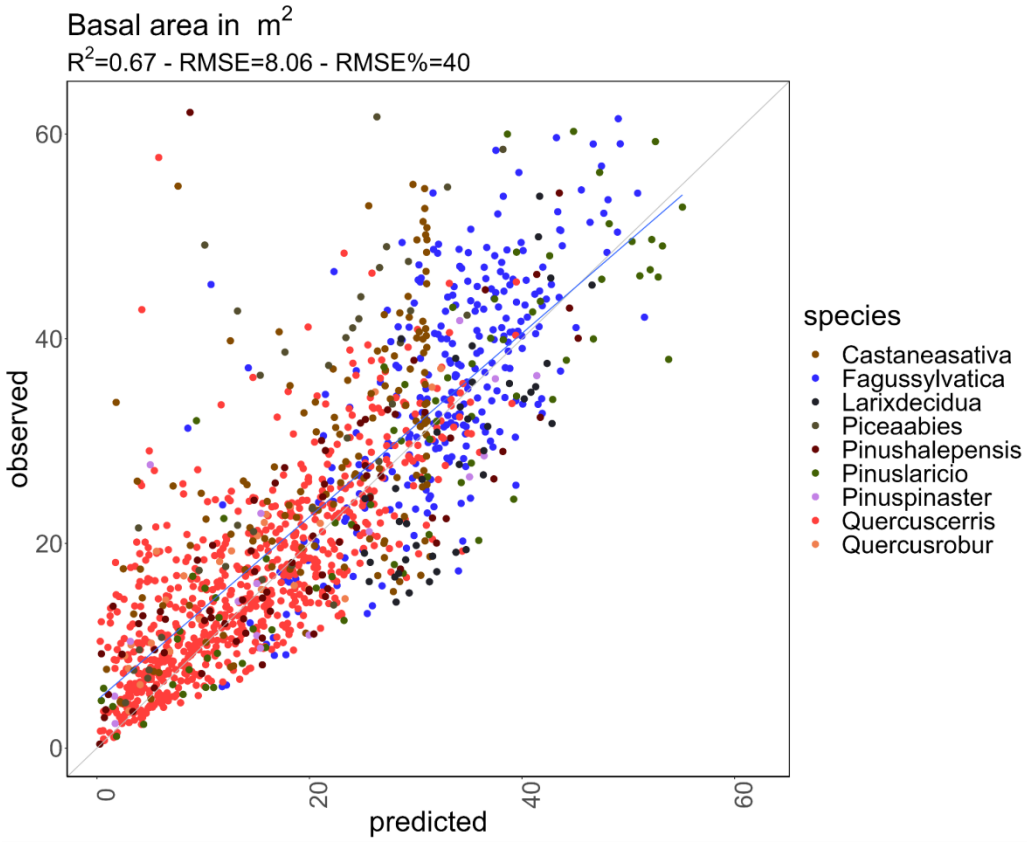

Figure 55. Comparison between modelled and observed Basal Area (m^2) from NFI data at the species level (Vangi et al. in prep.).

6.7 VOLUME

Stem volume is computed through the general formula as follows:

$$Stem\ volume_{x,y,k\,\epsilon\,z} = \pi \cdot \left(\frac{DBH_{x,y,k\,\epsilon\,z}}{2}\right)^2 \cdot h_{x,y,k\,\epsilon\,z} \cdot \varphi_x \qquad \textit{Eq. 95}$$

where *h* indicates the tree height (m), then the DBH (cm) and φ is the stem form factor which is a species-specific parameter defining the shape of the tree stem bole. The Volume at every single class is then scaled to layer and cell level as:

$$Volume_{x,y,k\,\epsilon\,z} = Stem_{volume_{x,y,k\,\epsilon\,z}} \cdot N_{tree_{x,y,k\,\epsilon\,z}} \qquad \textit{Eq. 96}$$

$$Volume = \sum_{z=1}^{N} Volume_{x,y,k} \quad \text{Eq. 97}$$

6.8 Current and Mean Annual Increment

The model computes annually the volume growth of the tree over the past year (CAI) and the average volume growth of the tree per year since its establishment (MAI) as:

$$CAI_{x,y,k \in z} = V_{x,y,k \in z_t} - V_{x,y,k \in z_{t-1}} \quad \text{Eq. 98}$$

And

$$MAI_{x,y,k \in z} = \frac{Volume_{x,y,k \in z}}{age_{x,y,k \in z}} \quad \text{Eq. 99}$$

where *t* represents the time and *t*—1 the year before (Vangi et al. 2024a)

6.9 Above-Ground Biomass

Above-Ground Biomass (both in tC and by conversion in tDM) is the sum of different above-ground pools and is computed as:

$$AGB_{x,y,k \in z} = LeafC_{x,y,k \in z} + StemC_{x,y,k \in z} + BranchC_{x,y,k \in z} + FruitC_{x,y,k \in z} \quad \text{Eq. 100}$$

while at cell level:

$$AGB = \sum_{z=1}^{N} AGB_{x,y,k} \quad \text{Eq. 101}$$

6.10 Below-Ground Biomass

Similarly, Below-Ground Biomass (both in tC and by conversion in tDM) is the sum of different below-ground pools and is computed as:

$$BGB_{x,y,k\,\epsilon\,z} = FineRootC_{x,y,k\,\epsilon\,z} + CoarseRootC_{x,y,k\,\epsilon\,z} \quad \textit{Eq. 102}$$

while at cell level:

$$BGB = \sum_{z=1}^{N} BGB_{x,y,k} \quad \textit{Eq. 103}$$

7. FOREST MANAGEMENT AND DISTURBANCES

(subroutine: *management.c*)

Forest management represents an anthropogenic perturbation to the natural dynamic of the ecosystem. The Intergovernmental Panel on Climate Change guidelines define managed land as the area where human interventions and practices have been applied to perform production, ecological, or social functions (IPCC, 2006). Recent studies have shown and discussed the profound effects of forest management on both carbon, nitrogen, and water cycle (Nolè et al. 2015; del Río et al. 2017; Akujärvi et al. 2019; Gutsch et al. 2018; Dalmonech et al. 2022; Testolin et al. 2023) and the potential role of forest management in climate change adaptation strategies (Ayan et al. 2018; De Marco et al. 2022). The 3D-CMCC-FEM model simulates several potential management practices, from the 'Business as Usual' (BAU) to diverse other ones, on high stands as those included in the ISIMIP protocol (Collalti et al. 2018; Pellicone et al. 2018; Reyer et al. 2020; Dalmonech et al. 2022; Mahnken et al. 2022a, 2022b, 2023; Saponaro et al. 2024; https://www.isimip.org/protocol/). The 3D-CMCC-FEM implemented a simple BAU management routine that simulates an intensive, even-aged approach to forest management following Duncker et al. (2012)(see **Figure 56**).

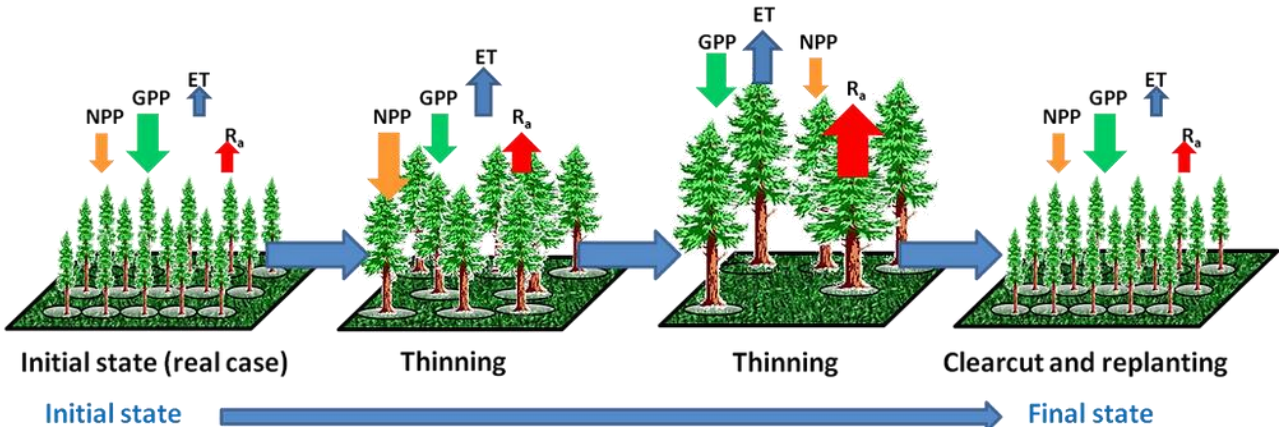

Figure 56 Graphical representation of forest management in the 3D-CMCC-FEM model

These management guidelines are characterised and in the model simulated by:

1. Thinning intensity (i.e. percentage of stand basal area to remove based on total stand basal area),

2. Thinning interval (i.e. years between operations), and

3. Rotation age (i.e. stand age at which the final harvest occurs and trees are replanted)

Each management variable represents a species-specific parameter, then characterising and gives the possibility to the user to simulate diverse species-specific management schemes that can be represented by different combinations of management variables and, thus, hypothesising, through different models runs, different management options with different model results. Both thinning and harvesting occur at the end of the year, and to close both daily, monthly, and annual carbon budgets, these trees and their associated pools are accounted for before their removal. When the stand age for final harvest is reached in a site, all trees are completely removed. At the year after harvesting (first of January), the plot is replanted with new trees of the same or different species (e.g. 6000 trees ha^{-1}, dbh = 1 cm, tree height = 1.3 m, and age = 5 years), thus, providing the mandatory initial variables needed for model runs. Note, values for replanting can be set by the user as even the change and the type in tree species to replant but not a species-specific parameter but rather as setting run parameter. Overall, three different general forest management schemes can be set into the 3D-CMCC-FEM modelling setting file ('*management*' parameter). The 'no management' (management '*off*'), which actually means that the stand is left to develop undisturbed with no management interventions; the regular management (management '*on*'), which is controlled the three above variables (i.e. '*thinning intensity*', '*thinning interval*' and '*rotation age*'), which means that the thinning operations are iteratively simulated any '*x*' years controlled by the species-specific parameter '*thinning interval*' and starting at a defined year define by the '*Year start management*' parameter. Lastly, irregular management (management '*var*'), which means that thinning and harvesting operations can be simulated not on a regular time regime, is an additional setting that can be used to simulate management, in this case, the background mortality is turned off and the number of trees to remove is provided by the user, something that can happen in the real world, but every user-defined years (this means that the user should provide in a specific file the years when applying thinning and harvesting). The last management scheme can also be used to mimic and simulate any other different type of disturbance (and not just forest management) provided that there are enough information about the intensity (number or % of trees to remove) and the interval (years of the events) of the disturbance. By acting on the intensity, the interval and the regime (and the relative combinations of these three variables) 3D-CMCC-FEM can simulate different management schemes (to that more 'close-to-nature' implying a relative continuous canopy cover, i.e. the 'continuous cover forestry') to those more intensive (see Dalmonech et al. 2022 and Testolin et al. 2023; **Figure 57**) which include clear-cut and human replanting (or through natural regeneration processes). In principle a fourth variable could be accounted for by the 3D-CMCC-FEM when simulating management, which is the 'thinning from above' (or from below) that removes trees (controlled by the intensity and intervals setting parameters) from the dominant (*above*) or dominated (*below*) layer. However, such an hypothesis in modelling forest management has never been tested in the model.

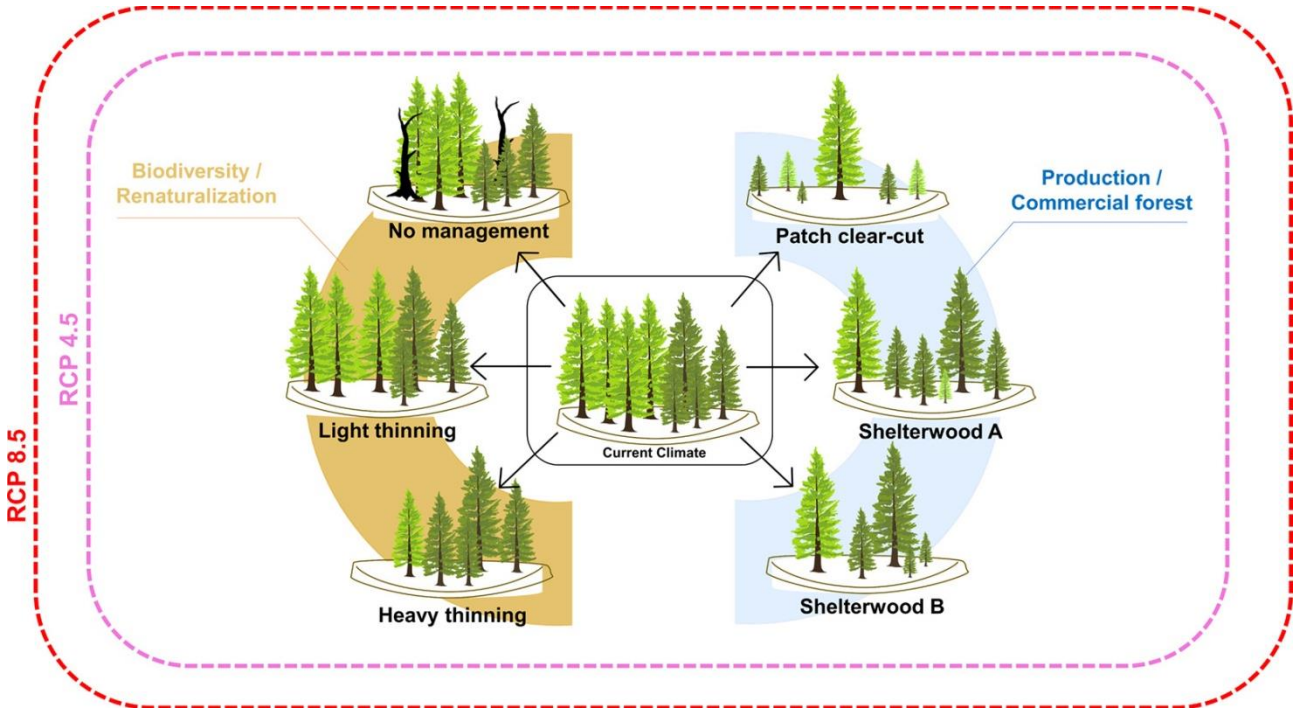

Figure 57 Graphical abstract of the different forest management schemes usable within the 3D-CMCC-FEM (figure from Testolin et al. 2023)

The comparison of model results between e.g. the Business-as-Usual (BaU) and the more or less intensive management schemes is a useful and valuable tool, especially under climate change scenarios, not only for foresters but also for the scientific community and the relative policies for the future forests. Recent studies applying the 3D-CMCC-FEM have indeed shown that under any climate change scenarios (RCP 2.6, 4.5, 6.0, 8.5) both NPP, CUE and Carbon Woody Stock increase when applying BaU management scenarios when comparing to No Management scenarios (i.e. forests are left to develop undisturbed with no human interventions) simulations (Collalti et al. 2018; **Table *1***).

	Hyytiälä		Bílý Kříž		Sorø	
RCP	Mean NF	Mean FF	Mean NF	Mean FF	Mean NF	Mean FF
			ΔGPP%			
Control	-14.66	-18.28	-10.68	-13.68	-4.17	-38.55
RCP2.6	-13.70	19.50	-9.78	-13.34	-3.26	-26.71
RCP4.5	-13.65	18.55	-9.84	-12.41	-3.15	-19.12
RCP6.0	-13.75	17.85	-10.00	-11.89	-3.11	-17.38
RCP8.5	-13.45	17.30	-9.43	-11.81	-3.19	-11.21
AVG	-13.64	18.30	-9.76	-12.36	-3.18	-18.61
			ΔR_a%			
Control	-20.27	-25.44	-19.19	-26.39	-18.31	-67.41
RCP2.6	-19.53	-23.47	-17.95	-26.10	-16.99	-60.21
RCP4.5	-19.53	-22.78	-18.03	-24.96	-16.75	-53.53
RCP6.0	-19.56	-22.46	-18.05	-24.28	-16.82	-51.28
RCP8.5	-19.38	-22.52	-17.39	-24.49	-16.78	-45.98
AVG	-19.50	-22.81	-17.85	-24.96	-16.83	-52.75
			ΔNPP%			
Control	-3.84	-2.31	5.19	15.08	20.88	29.06
RCP2.6	-1.69	2.07	6.26	19.49	20.97	63.41
RCP4.5	-1.61	3.22	6.26	20.02	20.52	66.41
RCP6.0	-2.11	2.96	5.35	19.68	20.73	61.86
RCP8.5	-1.30	7.62	5.89	25.16	20.17	77.30
AVG	-1.68	3.97	5.94	21.09	20.60	67.24
			ΔCUE%			
Control	12.56	19.68	18.28	33.99	27.14	113.92
RCP2.6	13.75	22.24	18.43	38.50	26.14	128.13
RCP4.5	13.64	22.40	18.40	37.84	25.09	110.62
RCP6.0	13.19	21.38	17.52	36.57	25.38	101.42
RCP8.5	13.69	26.25	17.53	42.61	24.70	106.84
AVG	13.57	23.07	17.97	38.88	25.32	111.75
			ΔNPP_{wood}%			
Control	7.08	18.59	13.16	31.32	33.26	71.29
RCP2.6	9.21	25.11	11.96	34.37	27.65	110.56
RCP4.5	8.95	24.42	11.98	32.28	26.54	91.47
RCP6.0	8.31	20.92	10.96	29.57	27.51	76.93
RCP8.5	8.86	28.23	10.28	35.27	25.32	90.40
AVG	8.83	24.67	11.30	32.87	26.76	92.34
			ΔCarbon woody stock%			
Control	6.90	41.58	12.32	41.45	9.34	38.09
RCP2.6	7.40	44.62	15.31	45.16	9.28	41.48
RCP4.5	7.49	44.98	15.52	45.15	8.95	40.59
RCP6.0	7.30	43.82	15.07	43.68	9.23	38.94
RCP8.5	7.50	45.71	15.19	44.99	9.01	41.38
AVG	7.42	44.78	15.27	44.74	9.12	40.60

Table 1 Percentage of Changes for Mean GPP, R_a, NPP, CUE, NPP_{woody}, and Carbon Woody Stocks between thinned vs. unthinned simulations for Near Future (NF; 2020–2050) and Far Future (FF; 2070–2099) time windows (table rewritten from Collalti et al. 2018).

Even more recent studies applying the 3D-CMCC-FEM and questioned whether different forms of management scheme combinations, with respect to the BaU, could maximise NPP while at the same time maintaining and/or increasing potential Carbon Woody Stocks (CWS; i.e. when no decay of harvested wood products occurs) in response to a range of climate change scenarios (Dalmonech et al. 2022). 28 different management scenarios were applied to three different European sites including additional virtual stands, obtained by the CFM approach (see paragraph 1.4.4). Overall, the BaU and 'No management' schemes plus 26 alternative management schemes were applied. These alternative forest management scenarios represented all the possible combinations of two thinning in-tensities, two thinning intervals, and two rotation lengths that differ from those in the BaU scenario adopted in Collalti et al. (2018). The schemes were grouped into a factorial combinations of: (1) 'more intensive' ('AM+'), where at least one out of the three management variables reflect an intensified management case relative to BaU (e.g. higher thinning intensity and/or shortened interval and/or shortened rotation length than BaU: +10% ca. in intensity, —10 years ca. in interval, —20 years ca. in rotation length), and the other one or two (or no) variables are kept as in BaU; (2) 'less intensive' ('AM–'), where at least one variable reflects lower thinning intensity (—10% ca.) and/or prolonged interval (+10 years ca.) and/or prolonged rotation length (+20 years ca.), compared to the BaU case; and (3) 'mixed schemes' ('MIX'), where at least one management variable was more intensive and at least one management variable was less intensive than the BAU scheme. Results shown that, for any combination reflecting a more intensive or less intensive scenarios both NPP as well as pCWS, BaU was the management scheme reaching the higher NPP and pCWS and that the differences between the different management schemes were much higher than those between climate scenarios, providing further evidences on the key role of forest management in shaping C-cycle in forests (**Figure 58** and **Figure 59**).

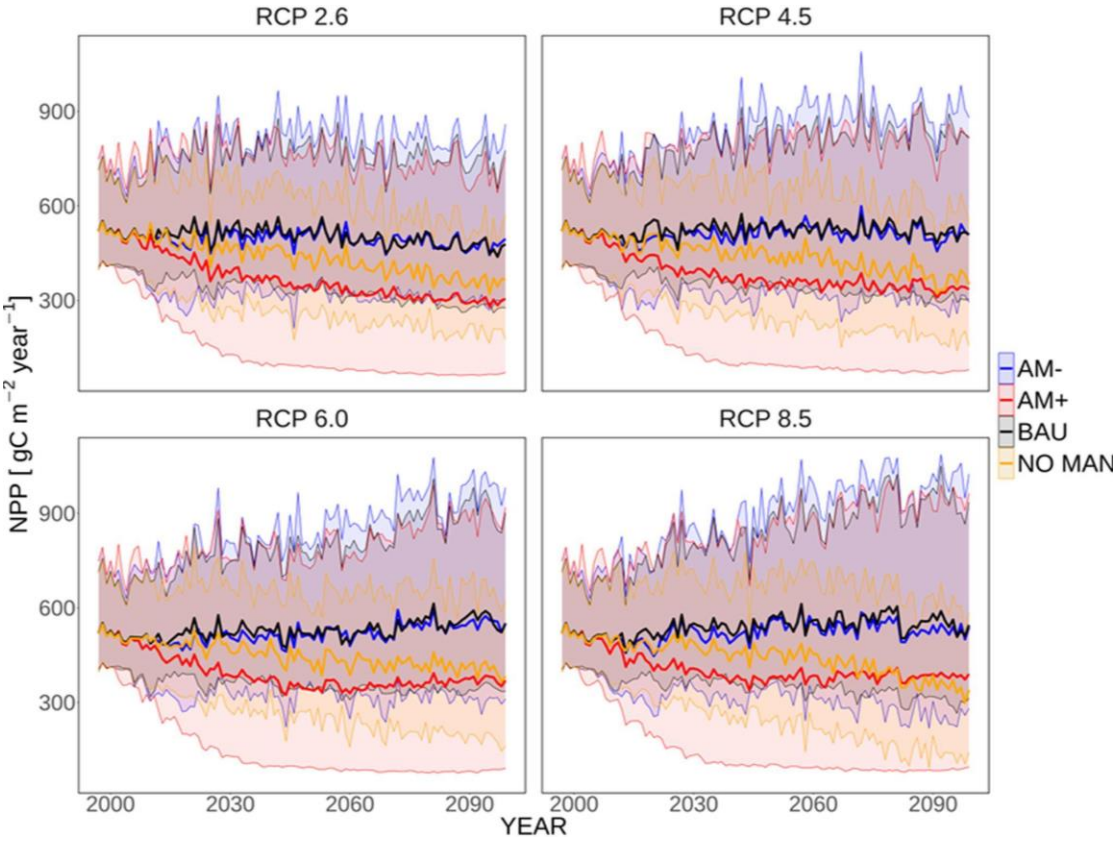

Figure 58 NPP (Net Primary Productivity, gC m^{-2} $year^{-1}$) simulations under different management scenarios (AM+, BAU, AM–) and the NO-MAN scenario for each of the four atmospheric CO_2 concentration pathways (RCPs). NPP, solid line, is averaged across the representative forests, different Earth System Models (ESMs) forcing climate and aggregated according to the management regime. Shaded areas represent the maximum and minimum values (5th and 95th percentiles) across the representative forests, different ESMs and aggregated according to the management regime (figure from Dalmonech et al. 2022).

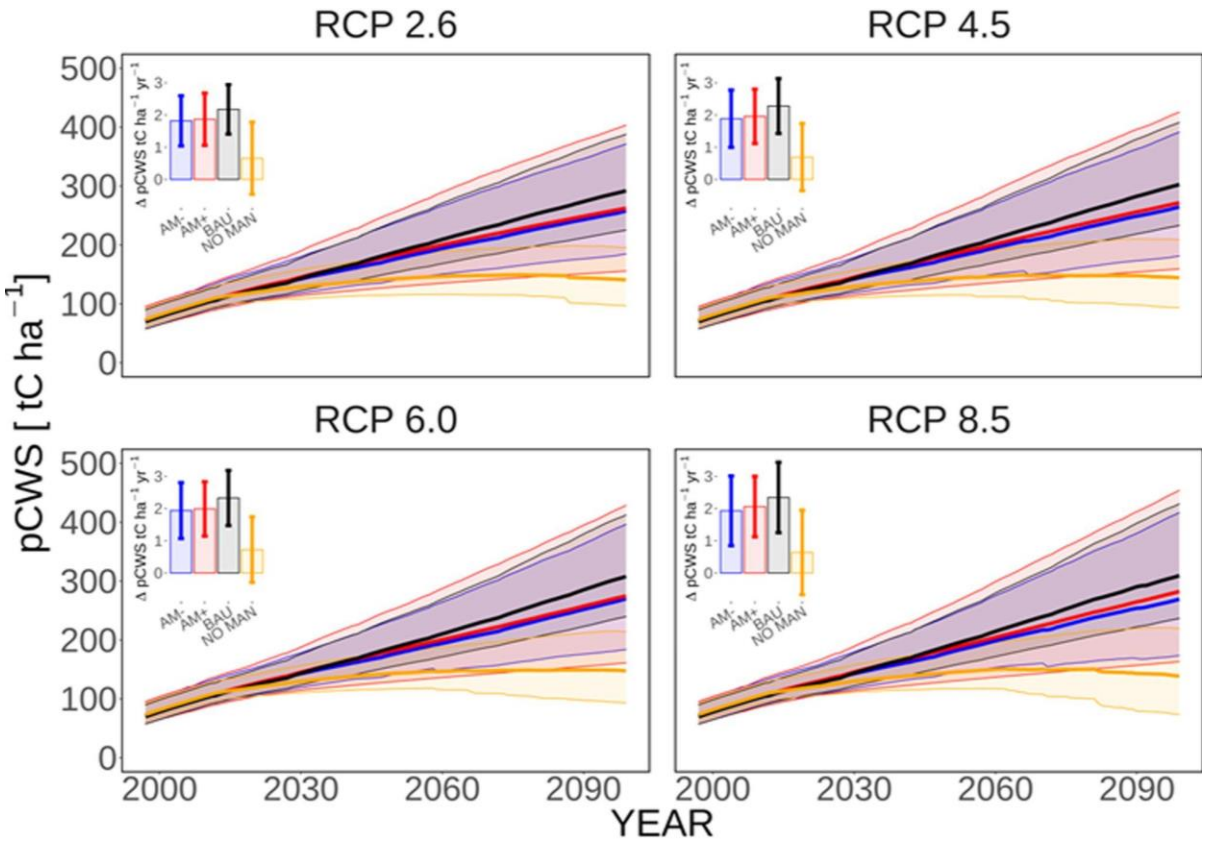

Figure 59 pCWS (potential Carbon Woody Stock = standing and potential harvested woody biomass; tC ha^{-1}) simulations under different management scenarios (AM+, BAU, AM–) and the NO-MAN scenario divided by different emission scenario RCPs. pCWS, solid line, is averaged across the representative forests, and different ESMs and aggregated according to the management regime. Shaded areas represent the maximum and minimum values (5th and 95th percentiles) across the representative forests, with different Earth System Models (ESMs) forcing climate and aggregated according to the management regime. Carbon sequestration rates (as annual increase of CWS, tC ha^{-1} year^{-1}) in the potential total woody stocks (mean and standard deviation) are reported in the bar plots (figure from Dalmonech et al. 2022).

Other studies applying the 3D-CMCC-FEM adopting different silvicultural practices and under climate change scenarios (RCP 4.5, 8.5) and in other forest stands than that from Dalmonech et al. (2022), have found similar results on the overall autotrophic C-budget (i.e. GPP, NPP, pCWS and BA)(Testolin et al. 2023). Likewise, even in this study forest management has shown large control on model outputs (more than climate change itself) and climate change and management have shown to be largely independent (i.e. no strong interaction effects)(**Figure *60***). Recently, Boukhris et al. (2024) used Testolin et al. (2023) model outputs into a comprehensive framework called 'TimberTracer' designed to explicitly simulating carbon stock in HWPs over temporal scales, substitution effects, and carbon emissions from wood decay and bioenergy.

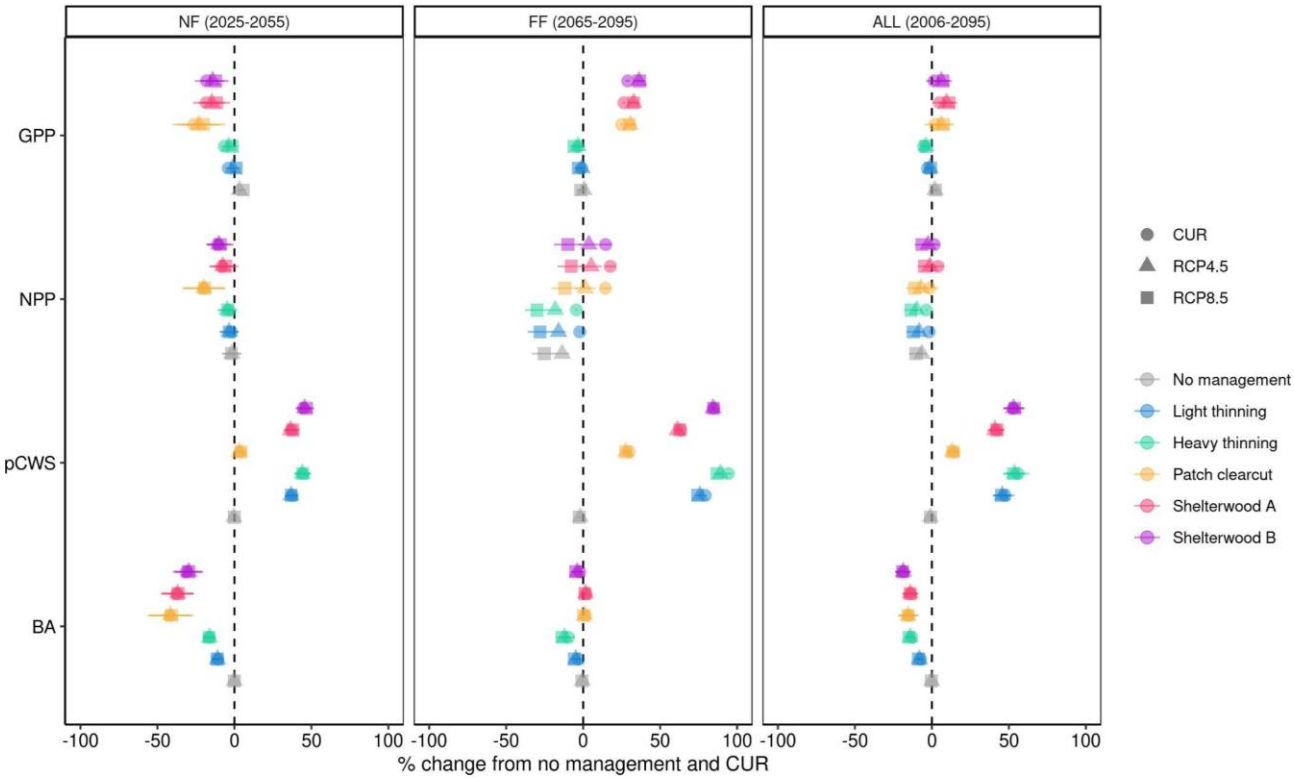

Figure 60 Relative change of modelled outputs according to six different management options (no management, light thinning, heavy thinning, patch clearcut, shelterwood A, shelterwood B) and three climate scenarios (CUR, RCP4.5, RCP8.5) compared to the baseline 'no management' option under the CUR (CUR = current climate scenario) within the NF (Near Future, 2025‑2055), FF (Far Future, 2065‑2095), and ALL (2006-2095) time windows for Gross and Net Primary Production (GPP, NPP), pCWS (potential Carbon Woody Stocks) and Basal Area (BA). The error bars are the 95 % confidence intervals (figure from Testolin et al. 2023).

Note that changes in the values of every variable during thinning and harvesting operations are uniquely the result of a change in space, light, and water availability caused by the tree removal operations and do not depend on specific modifications in model algorithms or parameters when thinning and/or harvesting are applied.

Management for coppiced forests is still under development. However, for oaks, allometric relationships for forest managed as coppice and an ad-hoc parameterization to simulate sprout growth is provided in this version of the 3D-CMCC-FEM model.

8. PRINCIPLE OF THE CONSERVATION OF ENERGY AND MASS

(routines: *tree_model_check_balance.c*, *soil_model_check_balance.c*, *litter_model_check_balance.c*, *cell_model_check_balance.c*)

In 3D-CMCC-FEM at different time-steps (i.e. daily, monthly and annual) the conservation of mass fundamental principle is checked (both for fluxes as well as for stocks). This means that the incoming energy radiation, C, N, and H_2O, must all be in balance with the amount outcoming and that stored (i.e. Balance = In – Out – Stores), at any given time. When (and if) the check balance function (‘*tree_model_balance_check.c’*) finds that the balance is not maintained the 3D-CMCC-FEM aborts and exits from the simulation with an error message (‘*...FATAL ERROR in 'Tree_model_daily' Carbon flux balance (exit)’*). The ‘check-balance’ functions for the conservation are done at each hierarchical level of tree representation (DBH, tree height, age, and species level) as well as at the cell level.

9. SENSITIVITY ANALYSIS TO PARAMETERS, INPUT DATA AND MODEL STRUCTURE

Sensitivity analysis and Factorial Analysis are methods to quantify the sensitivity in model outputs induced by changes to model inputs (Uusitalo et al. 2015) or model setting (Collalti et al. 2019; Boukhris et al. 2023). These methods are commonly the first diagnostics in assessing the uncertainty in model assumptions, process representations, and parameterizations (Collalti 2011). As diagnostic tools are considered essential to quantifying the reliability, robustness, and limitations of models suggesting directions for further improvements aiming to reduce uncertainty (Pappas et al. 2013; Pianosi et al. 2016). A recent study by Collalti et al. (2019), through the course of >100 years of simulations, found large responsiveness of the 3D-CMCC-FEM to the allometric parameters used for initialise forest carbon and nitrogen pools early in forest simulation, i.e. for NPP up to ≈37%, 256 gC m^{-2} yr^{-1} and for SWB (standing woody biomass) up to ~90%, 65 tC ha^{-1}, when compared to standard simulation, with this sensitivity decreasing sharply during forest development at decreasing NPP. At medium to longer time scales, and under climate change scenarios, the model became increasingly more sensitive to additional and/or different parameters controlling biomass accumulation and autotrophic respiration, i.e. for NPP up to ≈30%, 167 gC m^{-2} $year^{-1}$ and for SWB up to ≈24%, 64 tC ha^{-1}, when compared with simulations with standard parameterisation. Interestingly, 3D-CMCC-FEM model outputs were shown to be more sensitive to parameters and processes controlling stand development rather than those linked with climate change (i.e. warming and changes in atmospheric CO_2

concentration) itself although model sensitivities were generally higher under climate change scenarios (Collalti et al. 2019, **Figure *61***). Likewise, other sensitivity analyses for other models showed a similar degree of sensitivity to especially allometric parameters in allometric equations (Massoud et al. 2019), to be context dependent (Forrester et al. 2024), and that parameters should be free to vary with forest development (Oddou-Muratorio et al. 2020). Through a Factorial Analysis Collalti et al (2018) between climate data (both at ESM-level and RCP-level), atmospheric CO_2 concentration, and forest management (and all the possible combinations between them) found that for GPP, NPP, NPP_{woody}, R_a, and CUE the forest management, and its effects on forest structure, is far to be the more impacting factor on 3D-CMCC-FEM results (data not shown here). Likewise, Dalmonech et al. (2022) found that, on average, across the simulation time, i.e. 2006-2100, stand characteristics, as results of the management scenarios, explain most of the variability of the C-related variables (**Figure *62***).

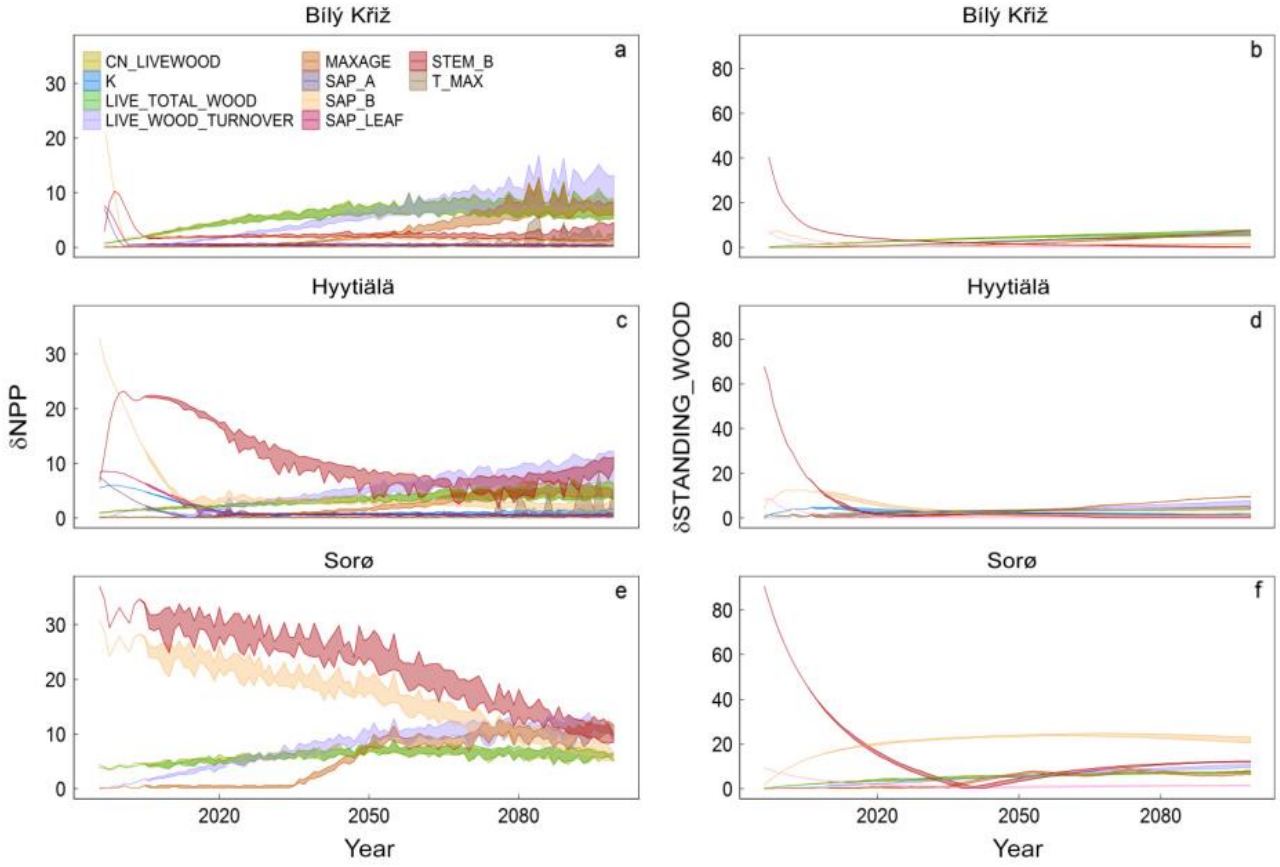

Figure 61 Sensitivity in modelled annual NPP (net primary productivity, left panel) and SWB (standing woody biomass, right panel) expressed in percentage across forest development and climate change scenarios at each of three selected sites. Shaded areas represent the maximum and the minimum relative sensitivity (in absolute values) for the most influential parameters considering that the maximum among the maximum annual values of NPP and SWB changes and the minimum among the maximum annual values of NPP and SWB changes over the climate change and present-day climate scenarios (RCPs). An arbitrary threshold of 5% level was used as the reference level (figure from Collalti et al. 2019). Parameter 'STEM_B' in the figure stands for the parameter '$STEM_{power}$' in the text.

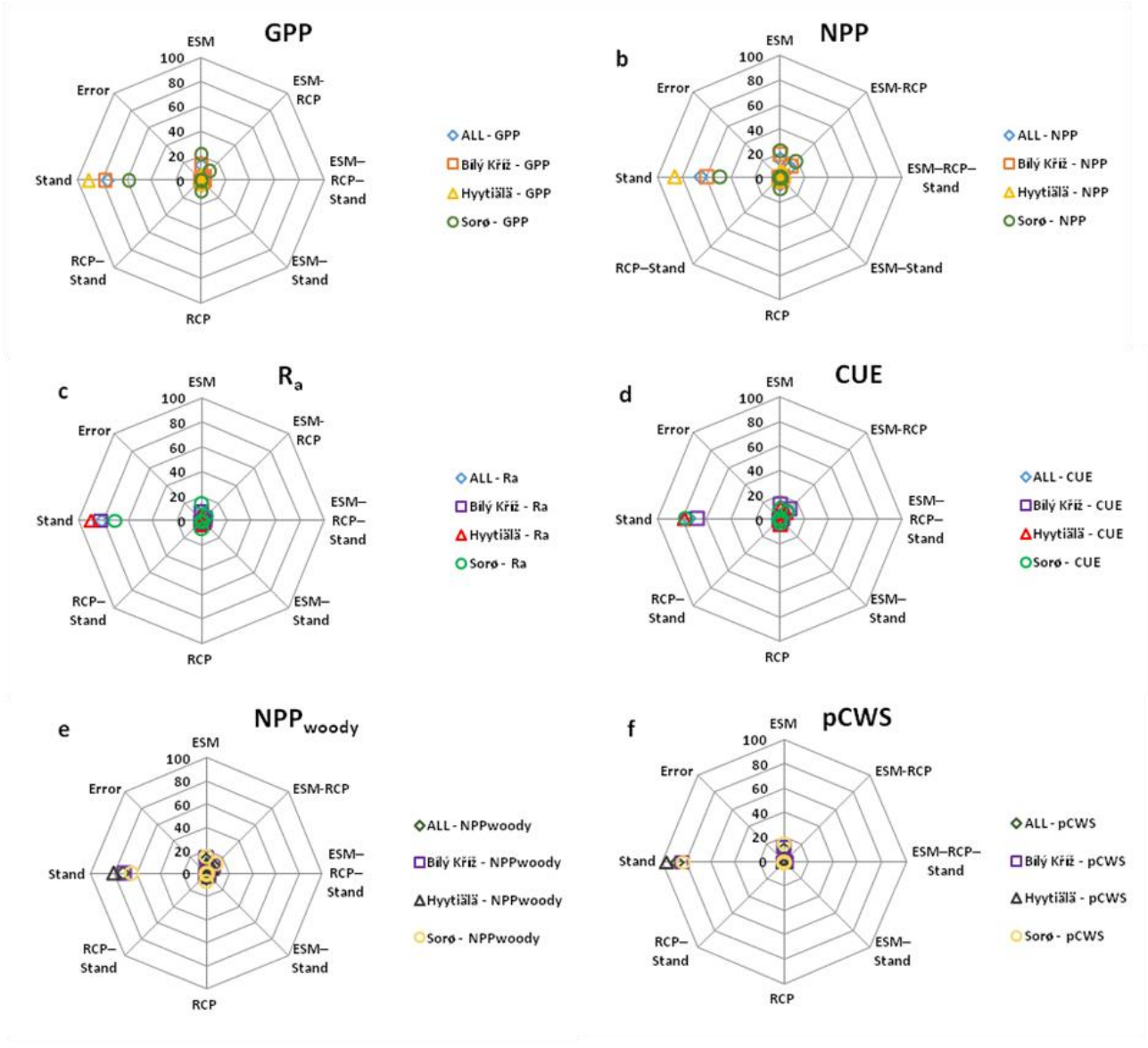

Figure 62 Factorial analysis of the factors driving the variability of GPP, NPP, RA, CUE, NPP_{woody} and pCWS, for the three study sites Bílý Kříž (square), Hyytiälä (triangle), Sorø (circle) and an average among sites (rhombus); ESMs = model forced with Earth System Models climate, RCP = emission scenarios, 'Stand' = virtual stands of the Composite Forest Matrix, i.e. simulations from each individual virtual stand, characterised by a specific age class and structure, are considered (figure from Supporting Information in Dalmonech et al. 2022).

ACKNOWLEDGEMENTS

Alessio Collalti and all other authors would like to acknowledge the substantial contributions of various experts, which are esteemed colleagues, mentors and in some case also truly friends, who, since its inception in 2007 (the first line code written), have played a significant role in the 3D-CMCC-FEM model development. Through their insightful discussions, suggestions, comments and practical support they inspired us to persist and strive for excellence: R. (Dick) Waring, P.E. Thornton, I.C. Prentice, J. Landsberg, M.G. Ryan, A. Ibrom, B.E. Medlyn, A. Mäkelä, A. Cescatti, P. Ciais, D. Papale, J.S. Amthor, T. Keenan, M. Lindner, M. Santini, B. Bond-Lamberty, D. Baldocchi, F. Loreto, L. Perugini, G. Hoch, O.A. Atkin, A. Almeida, S.W. Running, G. Scarascia-Mugnozza, F. Magnani, M. Tjoelker, G. Petit, C. Trotta, S. Marconi, M. Vitale, F. Miglietta, G. Bonan, H. Bugmann, M. Fernández-Martínez, A. Ribeca, R. Gifford, M. Mencuccini, S. Fares, M. Kirschbaum, T. Vesala, L. Montagani, S. Vicca, M. Campioli. S. Bedini, R.A. Fisher, P. De Angelis, A. Anav, C.P.O. Reyer, S. Luyssaert, M. Michetti, C. Massari, G. Battipaglia, O. Gavrichkova, A. Rita, G. Chirici, P. Corona, T. Chiti, M. Borghetti, R. Tognetti, G. Grassi, L. A. Sala, L. Todaro, G. Guidolotti, R. Valentini, F. Veroustraete, A. De Marco, E. Paoletti, F. Pagani, R. Seidl, S. Zaehle, R. Testolin, G. Matteucci, F. Giannetti, C. Calfapietra, N., C., J. and R. Gordon, J. and B. Smith, A. Bombelli, J. Curiel Yuste, A. Nolè, S. Noce, E. D'Andrea, G. Vacchiano, M.C. Rulli, G. Mengoli, D. Liberati, A. Montaghi, I.M. Tomè, I. Boukhris, N. Orefice, C. Biondo. We warmly thank Claudia Puchi for creating the 3D-CMCC-FEM new model logo. Our sincere apologies to those we might have inadvertently forgotten to acknowledge in the list.

To conclude, Alessio apologises for bothering and annoying you all — in some cases a lot — over these years with his continuous questions, concerns and doubts, any of you is a brick of this wall (or a leaf of the canopy). He is more in debt with any of you than you think.

FUNDING

This book is partially funded from the National Recovery and Resilience Plan (NRRP) project, Mission 4 Component 2 Investment 1.4 - Call for tender No. 3138 of 16 December 2021, rectified by Decree n.3175 of 18 December 2021 of Italian Ministry of University and Research funded by the European Union – NextGenerationEU under award Number: Project code CN_00000033, Concession Decree No. 1034 of 17 June 2022 adopted by the Italian Ministry of University and Research, CUP B83C22002930006, Project title 'National Biodiversity Future Centre - NBFC'.

REFERENCES

Adams, H., Zeppel, M., Anderegg, W., Hartmann, H., Landhäusser, S. M., Tissue, D. T., et al. (2017). *A multi-species synthesis of physiological mechanisms in drought-induced tree mortality*. Nature Ecology and Evolution, 1(9), 1285–1291. https://doi.org/10.1038/s41559017-0248-x

Akujärvi, A., Shvidenko, A., Pietsch, S.A., 2019. *Modelling the impacts of intensifying forest management on carbon budget across a long latitudinal gradient in Europe*. Environmental Research Letters 14, 034012. https://doi.org/10.1088/1748-9326/aaf766

Amthor, J. (2000). *The McCree-de Wit-Penning de Vries-Thornley respiration paradigms: 30 Years later*. Annals of Botany, 86, 1–20. https://doi.org/10.1006/anbo.2000.1175

Arora, V. and Boer, G. (2005). *A parameterization for leaf phenology in the terrestrial ecosystem component of climate models*. Global Change Biology, 11(1), 39–59. https://doi.org/10.1111/j.1365-2486.2004.00890.x

Atkin, O. and Tjoelker, M. (2003). *Thermal acclimation and the dynamic response of plant respiration to temperature*. Trends in Plant Science, 8, 343–351. https://doi.org/10.1016/S1360-1385(03)00136-5

Atkin, O., Bruhn, D., Hurry, V. and Tjoelker, M. (2005). *The hot and the cold: Unraveling the variable response of plant respiration to temperature*. Functional Plant Biology, 32, 87–105, https://doi.org/10.1071/FP03176

Atkin, O., Atkinson, L. and Fisher, R. (2008). *Using temperature-dependent changes in leaf scaling relationships to quantitatively account for thermal acclimation of respiration in a coupled global climate-vegetation model*. Global Change Biology, 14, 2709–2726. https://doi.org/10.1111/j.1365-2486.2008.01664.x

Badger, M. and Collatz, J. (1977). *Studies on the kinetic mechanism of RudP-carboxilase and oxygenase, with particular reference to the effect of temperature on kinetic parameters.* 1976–1677: Carnegie Institution, Annual Report.

Barbaroux, C., Brèda, E. and Dufrêne, E. (2002). *Distribution of aboveground and below-ground carbohydrate reserves in adult trees of two contrasting broad-leaved (Quercus cerris and Fagus sylvatica)*. New Phytologist, 157, 605–615. https://doi.org/10.1046/j.1469-8137.2003.00681.x

Barbati A., Scarascia-Mugnozza G., Ayan S., et al. (2018). Chapter 8, *Adaptation and Mitigation*, in: *State of Mediterranean Forests 2018*. Food and Agriculture Organization of the United Nations, Rome and Plan Bleu, Marseille, pp. 128-146. ISBN 978-92-5-131047-2, http://www.fao.org/3/CA2081EN/ca2081en.PDF

Bartelink, H.H. (1998). *A model of dry matter partitioning in trees*. Tree Physiology, 18, 91–101. https://doi.org/10.1093/treephys/18.2.91

Bernacchi, C. J., Singsaas, E. L., Pimentel, C. A. R. L. O. S., Portis Jr, A. R. and Long, S. P. (2001). *Improved temperature response functions for models of Rubisco-limited photosynthesis.* Plant, Cell and Environment, 24(2), 253-259. https://doi.org/10.1111/j.1365-3040.2001.00668.x

Bernacchi, C. J., Calfapietra, C. A. R. L., Davey, P. A., Wittig, V. E., Scarascia-Mugnozza, G. E., Raines, C. A. and Long, S. P. (2003). *Photosynthesis and stomatal conductance responses of poplars to free-air CO2 enrichment (PopFACE) during the first growth cycle and immediately following coppice*. New Phytologist, 159(3), 609-621. https://doi.org/10.1046/j.1469-8137.2003.00850.x

Bohlman, S., and Pacala, S. (2012). *A forest structure model that determines crown layers and partitions growth and mortality rates for landscape-scale applications of tropical forests*. Journal of Ecology, 100(2), 508-518. https://doi.org/10.1111/j.1365-2745.2011.01935.x

Bohn, FJ, Huth, A. (2017). *The importance of forest structure to biodiversity–productivity relationships*. R. Soc. Open sci. 4, 160521, https://doi.org/10.1098/rsos.160521

Bonan, G. B., Levis, S., Sitch, S., Vertenstein, M., & Oleson, K. W. (2003). *A dynamic global vegetation model for use with climate models: Concepts and description of simulated vegetation dynamics.* Global Change Biology, 9, 1543–1566. https://doi.org/10.1046/j.1365-2486.2003.00681.x

Bonan, G.B., et al. (2011). *Improving canopy processes in the Community Land Model version 4 (CLM4) using global flux fields empirically inferred from FLUXNET data*. Journal of Geophysical Research, 116, https://doi.org/10.1029/2010JG001593

Bonan, G. (2019). *Climate change and terrestrial ecosystem modeling*. Cambridge University Press.

Bossel, H. (1996). *TREEDYN3 forest simulation model*. Ecological modelling, 90(3), 187-227. https://doi.org/10.1016/0304-3800(95)00139-5

Boukhris, I., Lahssini, S., Collalti, A., Moukrim, S., Santini, M., Chiti, T. and Valentini, R. (2023). *Calibrating a Process-Based Model to Enhance Robustness in Carbon Sequestration Simulations: The Case of Cedrus atlantica (Endl.) Manetti ex Carrière*. Forests, 14(2), 401. https://doi.org/10.3390/f14020401

Boukhris, I., Collalti, A., Lahssini, S., Dalmonech, D., Nakhle, F., Testolin, R., ... and Valentini, R. (2024). *TimberTracer: A Comprehensive Framework for the Evaluation of Carbon Sequestration by Forest Management and Substitution of Harvested Wood Products*. bioRxiv, 2024-01. https://doi.org/10.1101/2024.01.24.576985

Bugmann, H. (2001). *A review of forest gap models. Climatic change*, 51(3), 259-305. https://doi.org/10.1023/A:1012525626267

Callegari, G., Ferrari, E., Garfi, G., Iovino, F., Veltri, A. (2003). *Impact of thinning on the water balance of a catchment in a Mediterranean environment*. For. Chron. 79, 301–306. https://doi.org/10.5558/tfc79301-2

Campbell, G.S., Norman, J.M. (1998). *An Introduction to Environmental Biophysics*. Springer-Verlag Inc., New York.

Campioli, M., Verbeeck, H., Van den Bossche, J., Wu, J., Ibrom, A., D'Andrea, E., ... Granier, A. (2013). *Can decision rules carbon allocation for years with contrasting and extreme weather conditions? A case study for three temperate beech forests*. Ecological Modelling, 263, 42–55. https://doi.org/10.1016/j.ecolmodel.2013.04.012

Campioli M, Vicca S, Luyssaert S et al. (2015) *Biomass production efficiency controlled by management in temperate and boreal ecosystems*. Nature Geoscience 8:1–7, https://doi.org/10.1038/ngeo2553

Cannell M.G.R. (1984). *Woody biomass of forest stands*. Forest Ecology and Management, 8:299-312 https://doi.org/10.1016/0378-1127(84)90062-8

Carbone, M. S., Czimczik, C. I., Keenan, T. F., Murakami, P. F., Pederson, N., Schaberg, P. G., ... Richardson, A. D. (2013). *Age, allocation and availability of non-structural carbon in mature red maple trees*. New Phytologist, 200, 1145–1155. https://doi.org/10.1111/nph.12448

Carey, E. V., Sala, A., Keane, R., & Callaway, R. M. (2001). *Are old forests underestimated as global carbon sinks?.* Global Change Biology, 7, 339–344. https://doi.org/10.1046/j.1365-2486.2001.00418.x

Ceschia, E., Damesin, C., Lebaube, S., Pontailler, J. Y. and Dufrêne, É. (2002). *Spatial and seasonal variations in stem respiration of beech trees (Fagus sylvatica)*. Annals of Forest Science, 59, 801–812. https://doi.org/10.1051/forest:2002078

Chang, C. Y. Y., Bräutigam, K., Hüner, N. P. A., & Ensminger, I. (2021). *Champions of winter survival: cold acclimation and molecular regulation of cold hardiness in evergreen conifers*. New Phytologist, 229(2), 675–691. https://doi.org/10.1111/nph.16904

Chapin, F.S., Woodwell, G.M., Randerson, J.T. et al. (2006). *Reconciling Carbon-cycle Concepts, Terminology and Methods*. Ecosystems 9, 1041–1050. https://doi.org/10.1007/s10021-005-0105-7

Clapp, R. B. and Hornberger, G. M. (1978). *Empirical equations for some soil hydraulic properties*. Water resources research, 14(4), 601-604.https://doi.org/10.1029/WR014i004p00601

Clark, D. B., Mercado, L. M., Sitch, S., Jones, C. D., Gedney, N., Best, M. J., ... and Cox, P. M. (2011). *The Joint UK Land Environment Simulator (JULES), model description–Part 2: carbon fluxes and vegetation dynamics*. Geoscientific Model Development, 4(3), 701-722. https://doi.org/10.5194/gmd-4-701-2011

Collalti, A., Santini, M., & Valentini Valentini, R. (2010). *Light competition and carbon partitioning-allocation in an improved forest ecosystem model*. In EGU General Assembly Conference Abstracts, Vol. 12, EGU2010-12135.

Collalti, A. (2011). *Sviluppo di un modello ecologico-forestale per foreste a struttura complessa.* Ph.D. Thesis, University of Tuscia. https://10.13140/RG.2.2.17900.92800; https://dspace.unitus.it/handle/2067/31328 (Italian language)

Collalti, A., Perugini, L., Chiti, T., Matteucci, G., Oriani, A., Santini, M., ... & Valentini, R. (2012). *A dynamic ecosystem growth model for forests at high complexity structure*. In EGU General Assembly Conference Abstracts Vol. 14, EGU2012-4125-2.

Collalti, A., Natali, S., Noilè, A., Mattiuzzi, M., Marconi, S., Santini, M., & Valentini, R. (2013). *Description and application of the 3D-CMCC FEM on multi-temporal NDVI satellite imagery and future scenarios*. In AGU Fall Meeting Abstracts (Vol. 2013, pp. B51G-0376).

Collalti, A., Perugini, L., Santini, M., Chiti, T., Nolè, A., Matteucci, G. and Valentini, R. (2014). *A process-based model to simulate growth in forests with complex structure: Evaluation and use of 3D-CMCC Forest Ecosystem Model in a deciduous forest in Central Italy*. Ecological Modelling, 272, 362–378. https://doi.org/10.1016/j.ecolmodel.2013.09.016

Collalti, A., Marconi, S., Ibrom, A., Trotta, C., Anav, A., D'Andrea E., Matteucci G., Montagnani L., Gielen B., Mammarella I., Grunwald T., Knohl A., Berninger F., Zhao Y., Valentini R., Santini M. (2016). *Validation of 3D-CMCC Forest Ecosystem Model (v. 5.1) against eddy covariance data for 10 European forest sites.* Geoscientific Model Development, 9(2), 479-504.https://doi.org/10.5194/gmd-9-479-2016

Collalti, A., Biondo, C., Buttafuoco, G., Maesano, M., Caloiero, T., Lucà F., Pellicone G., Ricca N., Salvati R., Veltri A., Scarascia Mugnozza G., Matteucci G. (2017). *Simulation, calibration and validation protocols for the model 3D-CMCC-CNR-FEM: a case study in the Bonis' watershed (Calabria, Italy).* Forest@, 14, 247-256.https://doi.org/10.3832/efor2368-014 (Italian language)

Collalti, A., Trotta, C., Keenan, T. F., Ibrom, A., Bond-Lamberty, B., Grote R., Vicca S., Reyer C.P.O., Migliavacca M., Veroustraete F., Anav A., Campioli M., Scoccimarro E., Sigut L., Grieco E., Cescatti A., Matteucci G. (2018). *Thinning can reduce losses in carbon use efficiency and carbon stocks in managed forests under warmer*

climate. Journal of Advances in Modeling Earth Systems, 10(10), 2427-2452. https://doi.org/10.1029/2018MS001275

Collalti, A., Thornton, P. E., Cescatti, A., Rita, A., Borghetti, M., Nolè, A., Trotta, C., Ciais, P. and Matteucci, G.. (2019). *The sensitivity of the forest carbon budget shifts across processes along with stand development and climate change.* Ecological Applications 29(2) https://doi.org/10.1002/eap.1837

Collalti, A. and Prentice, I. C. (2019). *Is NPP proportional to GPP? Waring's hypothesis 20 years on*. Tree Physiology, 39(8), 1473-1483.https://doi.org/10.1093/treephys/tpz034

Collalti, A., Tjoelker, M.G., Hoch, G., Mäkelä, A., Guidolotti, G., Heskel, M., Petit, G., Ryan, M.G., Battipaglia, G., Matteucci, G., Prentice, I.C. (2020a). *Plant respiration: Controlled by photosynthesis or biomass?* Global Change Biology, 26: 1739–1753, https://doi.org/10.1111/gcb.14857

Collalti, A., Ibrom, A., Stockmarr, A., Cescatti, A., Alkama, R., Fernandez-Martínez, M., Matteucci, G., Sitch, S., Friedlingstein, P., Ciais, P., Goll, D. S., Nabel, J. E. M. S., Pongratz, J., Arneth, A., Haverd, V. and Prentice, I. C. (2020b). *Forest production efficiency increases with growth temperature*. Nature Communications. https://doi.org/10.1101/2020.04.15.042275

Collalti, A., Todaro, L. and Rita, A. (2021). *Growth and allocation of woody biomass in forest trees based on environmental conditions*. Forests, 12(2), 154, https://doi.org/10.3390/f12020154

Collalti, A., Dalmonech, D., Marano, G., Vangi, E., Puchi, P., Grieco, E., Orrico, M. (2023). *3D-CMCC-FEM (Coupled Model Carbon Cycle). BioGeoChemical and Biophysical Forest Ecosystem - User's Guide.* CNR Edizioni; ISBN 978-88-8080-573-1 (electronic edition) https://doi.org/10.32018/3D-CMCC-FEM-2022;

Collatz, G. J., Ball, J. T., Grivet, C. and Berry, J. A. (1991). *Physiological and environmental regulation of stomatal conductance, photosynthesis and transpiration: a model that includes a laminar boundary layer*. Agricultural and Forest meteorology, 54(2-4), 107-136. https://doi.org/10.1016/0168-1923(91)90002-8

Cosby, B. J., Hornberger, G. M., Clapp, R. B. and Ginn, T. (1984). *A statistical exploration of the relationships of soil moisture characteristics to the physical properties of soils*. Water resources research, 20(6), 682-690.https://doi.org/10.1029/WR020i006p00682

Cox, P. (2001). *Description of the 'TRIFFID' Dynamic Global Vegetation Model* (pp. 1–16). Berkshire, Hadley Centre, Met Office: Bracknell.

Dalmonech, D., Marano, G., Amthor, J. S., Cescatti, A., Lindner, M., Trotta, C. and Collalti, A. (2022). *Feasibility of enhancing carbon sequestration and stock capacity in temperate and boreal European forests via changes*

to management regimes. Agricultural and Forest Meteorology, 327, 109203. https://doi.org/10.1016/j.agrformet.2022.109203

Dalmonech, D., Vangi, E., Chiesi, M., Chirici, G., Fibbi, L., Giannetti, F., Marano G., Massari C., Nolè A., Xiao J., Collalti, A. (2024). *Regional estimates of gross primary production applying the Process-Based Model 3D-CMCC-FEM vs. Remote-Sensing multiple datasets.* European Journal of Remote Sensing, 57(1), 2301657. https://doi.org/10.1080/22797254.2023.2301657

Damesin, C., Ceschia, E., Le Goff, N., Ottorini, J.-M., & Dufrêne, E. (2002). *Stem and branch respiration of beech: From tree measurements to estimations at the stand level*. New Phytologist, 153, 159–172. https://doi.org/10.1046/j.0028-646X.2001.00296.x

Díaz-Espejo, A., & Hernandez-Santana, V. (2017). *The phloem–xylem consortium: until death do them part*. Tree Physiology, 37(7), 847-850. https://doi.org/10.1093/treephys/tpx080

Dietze, M., Sala, A., Carbone, M. S., Czimczik, C. I., Mantooth, J. A., Richardson, A. D. and Vargas, R. (2014). *Nonstructural carbon in woody plants*. Annual Review of Plant Biology, 65, 667–687. https://doi.org/10.1146/annurev-arplant-050213-040054

Doughty, C. E., Metcalfe, D., Girardin, C., Amézquita, F. F., Cabrera, D. G., Huasco, W. H. ... Feldpausch, T. R. (2015). *Drought impact on forest carbon dynamics and fluxes in Amazonia*. Nature, 519, 78–82. https://

doi.org/10.1038/nature14213

Drake, J.E., Davis, S.C., Raetz, L.M., DeLucia, E.H. (2011) Mechanisms of age-related changes in forest production: The influence of physiological and successional changes. Global Change Biology 17(4):1522–1535. https://doi.org/10.1111/j.1365-2486.2010.02342.x

Drake, J., Tjoelker M., Aspinwall M., Reich P., Barton C., Medlyn B. and Duursma R.. (2016). *Does physiological acclimation to climate warming stabilize the ratio of canopy respiration to photosynthesis?.* New Phytologist, 211:850–863. https://doi.org/10.1111/nph.13978

Dufrêne, E., Davi, E., François, C., Le Maire, G., Le Dantec, V., & Granier, A. (2005). *Modelling carbon and water cycles in a beech forest. Part I: Model description and uncertainty analysis on modelled NEE*. Ecological Modelling, 185, 407–436. https://doi.org/10.1016/j.ecolmodel.2005.01.004

Duncker, P. S., Barreiro, S. M., Hengeveld, G. M., Lind, T., Mason, W. L., Ambrozy, S. and Spiecker, H. (2012). *Classification of forest management approaches: a new conceptual framework and its applicability to European forestry*. Ecology and Society, 17(4). http://dx.doi.org/10.5751/ES-05262-170451

D'Andrea, E., Rezaie, N., Prislan, P., Gričar, J., Collalti, A., Muhr, J. and Matteucci, G. (2020). *Frost and drought: effects of extreme weather events on stem carbon dynamics in a Mediterranean beech forest.* Plant, Cell and Environment, 43(10), 2365-2379. https://doi.org/10.1002/PCE.13858

D'Andrea, E., Scartazza, A., Battistelli, A., Collalti, A., Proietti, S., Rezaie, N., Matteucci G., Moscatello S.. (2021). *Unravelling resilience mechanisms in forests: role of non-structural carbohydrates in responding to extreme weather event*s. Tree Physiology, 41(10), 1808-1818. https://doi.org/10.1093/treephys/tpab044

DeLucia, E., Drake, J., Thomas, R., et al. (2007). *Forest carbon use efficiency: Is respiration a constant fraction of gross primary production?.* Global Change Biology, 13, 1157–1167. https://doi.org/10.1111/j.1365-2486.2007.01365.x

De Marco, A., Sicard, P., Feng, Z., Agathokleous, E., Alonso, R., Araminiene, V., ... and Paoletti, E. (2022). *Strategic roadmap to assess forest vulnerability under air pollution and climate change*. Global change biology, 28(17), 5062-5085. https://doi.org/10.1111/gcb.16278

de Pury, D. G. G. and Farquhar, G. D. (1997). *Simple scaling of photosynthesis from leaves to canopies without the errors of big-leaf models.* Plant, Cell and Environment, 20(5), 537-557. https://doi.org/10.1111/j.1365-3040.1997.00094.x

de Wergifosse, L. andré, F., Goosse, H., Boczon, A., Cecchini, S., Ciceu, A., ... and Jonard, M. (2022). *Simulating tree growth response to climate change in structurally diverse oak and beech forests*. Science of the Total Environment, 806, 150422. https://doi.org/10.1016/j.scitotenv.2021.150422

del Río, M., Barbeito, I., Bravo-Oviedo, A., Calama, R., Cañellas, I., Herrero, C., Montero, G.,Moreno-Fernández, D., Ruiz-Peinado, R., Bravo, F., 2017. *Mediterranean pine forests: management effects on carbon stocks*. In: Bravo, F., LeMay, V., Jandl, R. (Eds.), *Managing Forest Ecosystems: The Challenge of Climate Change*. Springer, pp. 301–327. https://doi.org/10.1007/978-3-319-28250-3_15 .

Engel, M., Vospernik, S., Toïgo, M., Morin, X., Tomao, A., Trotta C., Steckel M., Barbati A., Nothdurft A. Pretzsch H., del Rio M., Skrzyszewski J., Ponette Q., Lof M., Jansons A., Brazaitis G. (2021). *Simulating the effects of thinning and species mixing on stands of oak (Quercus petraea (Matt.) Liebl./Quercus robur L.) and pine (Pinus sylvestris L.) across Europe.* Ecological Modelling, 442, 109406. https://doi.org/10.1016/j.ecolmodel.2020.109406

Farquhar GD, et al. (1980) *A biochemical model of photosynthetic CO_2 assimilation in leaves of C3 species*. Planta. 149: 78-90, https://doi.org/10.1007/BF00386231

Fatichi, S., Leunzinger, S. and Körner, C. (2014). *Moving beyond photosynthesis: From carbon source to sink-driven vegetation modeling*. New Phytologist, 201, 1086–1095. https://doi.org/10.1111/nph.12614

Fierravanti, A., Rossi, S., Kneeshaw, D., De Grandpré, L. and Deslauriers, A. (2019). *Low non-structural carbon accumulation in spring reduces growth and increases mortality in conifers defoliated by spruce budworm*. Frontiers in Forests and Global Change, 2, 15. https://doi.org/10.3389/ffgc.2019.00015

Fisher, R. A., Muszala, S., Verteinstein, M., Lawrence, P., Xu, C., McDowell, N. G., Knox, R. G., Koven C., Holm J., Rogers, B. M., Spessa, A., Lawrence, D. and Bonan, G., (2015). *Taking off the training wheels: the properties of a dynamic vegetation model without climate envelopes, CLM4.5*(ED). Geoscientific Model Development 8:2593–3619 https://doi.org/10.5194/gmd-8-3593-2015

Fernández-Martínez, M., Vicca, S., Janssens, I. A., Espelta, J. M. and Peñuelas, J. (2016). *The role of nutrients, productivity and climate in determining tree fruit production in European forests*. New Phytologist, 213(2), 669–679. https://doi.org/10.1111/nph.14193

Forrester, D. I., Tachauer, I. H. H., Annighoefer, P., Barbeito, I., Pretzsch, H., Ruiz-Peinado, R., Stark, H., Vacchiano, G., Zlatanov, T., Chakraborty, T., Saha S. and Sileshi, G. W. (2017). *Generalized biomass and leaf area allometric equations for European tree species incorporating stand structure, tree age and climate*. Forest Ecology and Management, 396, 160-175. https://doi.org/10.1016/j.foreco.2017.04.011

Forrester, D. I., England, J. R., Paul, K. I. and Roxburgh, S. H. (2024). *Sensitivity analysis of the FullCAM model: Context dependency and implications for model development to predict Australia's forest carbon stocks*. Ecological Modelling, 489, 110631. https://doi.org/10.1016/j.ecolmodel.2024.110631

Frank, D., Poulter, B., Saurer, M., Esper, J., Huntingford, C., Helle, G., et al. (2015). *Water-use efficiency and transpiration across European forests during the Anthropocene*. Nature Climate Change. https://doi.org/10.1038/NCLIMATE2614

Friedlingstein, P., Joel, G., Field, C.B., Fung, I.Y. (1999). *Toward an allocation scheme for global terrestrial carbon models*. Global Change Biology 5, 755–770. https://doi.org/10.1046/j.1365-2486.1999.00269.x

Friend, A. D., Stevens, A. K., Knox, R. G. and Cannell, M. G. R. (1997). *A process-based, terrestrial biosphere model of ecosystem dynamics (Hybrid v3. 0)*. Ecological modelling, 95(2-3), 249-287. https://doi.org/10.1016/S0304-3800(96)00034-8

Friend, A. D., Lucht, W., Rademacher, T. T., Keribin, R., Betts, R., Cadule, P., ... Ito, A. (2014). *Carbon residence time dominates uncertainty in terrestrial vegetation responses to future climate and atmospheric CO_2*. Proceedings of the National Academy of Sciences of the United States of America, 111(9), 3280–3285. https://doi.org/10.1073/pnas.1222477110

Furze, M. E., Huggett, B. A., Aubrecht, D. M., Stolz, C. D., Carbone, M. S. and Richardson, A. D. (2019). *Whole-tree nonstructural carbohydrate storage and seasonal dynamics in five temperate species*. New Phytologist, 221, 1466–1477. https://doi.org/10.1111/nph.15462

Genet, H., Bréda, N. and Dufrêne, E. (2010). *Age-related variation in carbon allocation at tree and stand scales in beech (Fagus sylvatica L.) and sessile oak (Quercus petraea (Matt.) Liebl.) using a chronosequence approach*. Tree Physiology, 30, 177–192. https://doi.org/10.1093/treephys/tpp105

Gifford, R. (2003) *Plant respiration in productivity models: conceptualisation, representation and issues for global terrestrial carbon-cycle research*. Functional Plant Biology. 30:171–186. https://doi.org/10.1071/FP02083

Goulden, M. L., McMillan, A. M., Winston, G. C., Rocha, A. V., Manies, K. L., Harden, J. W., & Bond-Lamberty, B. P. (2011). *Patterns of NPP, GPP, respiration, and NEP during boreal forest succession.* Global Change Biology, 17(2), 855–871. https://doi.org/10.1111/j.1365-2486.2010.02274.x

Grünig, M., Rammer, W., Albrich, K., Andrè, F., …, Seidl, R. (2024). *A harmonized database of European forest simulations under climate change*. Data in Brief. 110384, https://doi.org/10.1016/j.dib.2024.110384

Gutsch, M., Lasch-Born, P., Kollas, C., Suckow, F., Reyer, C.P.O. (2018). *Balancing trade-offs between ecosystem services in Germany's forests under climate change*. Environmental Research Letters 13. https://doi.org/10.1088/1748-9326/aab4e5

Hamilton, J., Thomas, R., & DeLucia, E. (2001). *Direct and indirect effects of elevated CO_2 on leaf respiration in a forest ecosystem*. Plant, Cell and Environment, 24(9), 975–982. https://doi.org/10.1046/j.0016-8025.2001.00730.x

Hartmann, H. and Trumbore, S. (2016). *Understanding the roles of non-structural carbohydrates in forest trees – From what we can measure to what we want to know*. New Phytologist, 211, 386–403. https://doi.org/10.1111/nph.13955

Hedstrom, N. R. and Pomeroy, J. W. (1998). *Measurements and modelling of snow interception in the boreal forest*. Hydrological Processes, 12(10-11), 1611-1625. https://doi.org/10.1002/(SICI)1099-1085(199808/09)12:10/11%3C1611::AID-HYP684%3E3.0.CO;2-4

Hidy, D., Barcza, Z., Marjanović, H., Ostrogović Sever, M. Z., Dobor, L., Gelybó, G., et al. (2016). *Terrestrial ecosystem process model Biome-BGCMuSo v4.0: Summary of improvements and new modeling possibilities*. Geoscientific Model Development, 9(12), 4405–4437. https://doi.org/10.5194/gmd-9-4405-2016

Hoch, G., Richter, A. and Körner, C. (2003). *Non-structural carbon compounds in temperate forest trees*. Plant, Cell and Environment, 26, 1067–1081. https://doi.org/10.1046/j.0016-8025.2003.01032.x

Hölttä T. and Kolari P. (2009). *Interpretation of stem CO_2 efflux measurements*. Tree Physiology, 29: 73 1447–1456, https://doi.org/10.1093/treephys/tpp073

Huang, J., Hammerbacher, A., Weinhold, A., Reichelt, M., Gleixner, G., Behrendt, T., van Dam, N.M., Sala, A., Gershenzon, J., Trumbore, S. and Hartmann, H. (2019). *Eyes on the future – Evidence for trade-offs between growth storage and defense in Norway spruce*. New Phytologist, 222, 144–158. https://doi.org/10.1111/nph.15522

Huber, N., Bugmann, H., Lafond, V. (2018). *Global sensitivity analysis of a dynamic vegetation model: Model sensitivity depends on successional time, climate and competitive interactions*. Ecol. Model. 368, 377–390. https://doi.org/10.1016/j.ecolmodel.2017.12.013.

Huber, N., Bugmann, H. and Lafond, V. (2020). *Capturing ecological processes in dynamic forest models: why there is no silver bullet to cope with complexity*. Ecosphere 11 (5). https://doi.org/10.1002/ecs2.3109.

Igarashi, S., Yoshida, S., Kenzo, T. et al. (2024). *No evidence of carbon storage usage for seed production in 18 dipterocarp masting species in a tropical rain forest*. Oecologia 204, 717–726. https://doi.org/10.1007/s00442-024-05527-w

Intergovernmental Panel on Climate Change (IPCC)(2006). *2006 IPCC Guidelines for National Greenhouse Gas Inventories*. Intergovernmental Panel on Climate Change, NGGIP Publications, IGES, Japan.

Jarvis, P. (1976). *The interpretation of the variants in leaf water potential and stomatal conductance found in canopies in the field*. Philosophical Transactions of the Royal Society of London, 273, 593–610.

Jiao, J., Su, D., Han, L. and Wang, Y. (2016). *A Rainfall Interception Model for Alfalfa Canopy under Simulated Sprinkler Irrigation*. Water, 8, 585. https://doi.org/10.3390/w8120585

Jones, H. G. (1992). *Plants and Microclimate*. Cambridge, Cambridge University Press

Kaliniewicz, Z., Tylek, P., Anders, A., Markowski, P., Rawa, T. and Andros, K. (2015). *Correlations between basic physicalparameters of nuts and the weight of common beech (Fagus sylvatica L.) seeds*. Technical Sciences, 18(1): 5–14.

Kattge, J. and Knorr, W. (2007). *Temperature acclimation in a biochemical model of photosynthesis: a reanalysis of data from 36 species.* Plant, Cell and Environment, 30(9), 1176-1190. https://doi.org/10.1111/j.1365-3040.2007.01690.x

Kira, T., & Shidei, T. (1967). Primary production and turnover of organic matter in different forest ecosystems of the western Pacific. *Japanese Journal of Ecology*, 17(2), 70-87. https://doi.org/10.18960/seitai.17.2_70

Körner, C. (1995). *Leaf diffusive conductances in the major vegetation types of the globe*. Ecophysiology of Photosynthesis. E. D. Schulze and M. M. Caldwell. New York, Springer-Verlag: 463-490

Körner, C. (2013). *Growth controls photosynthesis–mostly*. Nova Acta Leopoldina NF, 114(391), 273-283.

Kozlowski, T. T. (1992). *Carbohydrate sources and sinks in woody plants*. Botanical Review, 58, 107–222. https://doi.org/10.1007/BF02858600

Krinner, G., Viovy, N., de Noblet-Ducoudré, N., Ogée, J., Polcher, J., Friedlingstein, P., …, and Prentice, I. C. (2005). *A dynamic global vegetation model for studies of the coupled atmosphere-biosphere system*. Global Biogeochemical Cycles, 19(1), 1–33. https://doi.org/10.1029/2003GB 002199

Kuptz, D., Fleischman, F., Matyssek, R. and Grams, T. E. (2011). *Seasonal patterns of carbon allocation to respiratory pools in 60-yr-old deciduous (Fagus sylvatica) and evergreen (Picea abies) trees assessed via whole-tree stable carbon isotope labelling*. New Phytologist, 191, 160–172. https://doi.org/10.1111/j.1469-8137.2011.03676.x

Larcher, W. (2003). *Physiological plant ecology*. Berlin Heidelberg: Springer-Verlag.

Landsberg, J. J. and Waring, R. H. (1997). *A generalised model of forest productivity using simplified concepts of radiation-use efficiency, carbon balance and partitioning.* Forest ecology and management, 95(3), 209-228. https://doi.org/10.1016/S0378-1127(97)00026-1

Landsberg, J. and Sands, P. (2011). *Physiological ecology of forest production: principles, processes and models (Vol. 4)*. Amsterdam.

Landsberg, J., Waring R.H., Williams M. (2020). *The assessment of NPP/GPP ratio*. Tree Physiology, 40(6), 695-699. https://doi.org/10.1093/treephys/tpaa016

Lasch-Born, P., Suckow, F., Reyer, C. P., Gutsch, M., Kollas, C., Badeck, F. W., ... and Schaber, J. (2020). *Description and evaluation of the process-based forest model 4C v2.2 at four European forest sites*. Geoscientific Model Development, 13(11), 5311-5343. https://doi.org/10.5194/gmd-13-5311-2020

Litton, C., Raich, J., & Ryan, M. (2007). *Carbon allocation in forest ecosystems*. Global Change Biology, 13, 2089–2109. https://doi.org/10.1111/j.1365-2486.2007.01420.x

Luo, Y., Gessler, A., D'Odorico, P., Hufkens, K., & Stocker, B. D. (2023). Quantifying effects of cold acclimation and delayed springtime photosynthesis resumption in northern ecosystems. New Phytologist, 240(3), 984–1002. https://doi.org/10.1111/nph.19208

Luo, X., Zhao, R., Chu, H., Collalti, A., Fatichi, S., Keenan, T., ... & Yu, L. (2024). *Deciduous forests use carbon more efficiently than evergreen forests*. Research Square. https://doi.org/10.21203/rs.3.rs-3989566/v1

Machado, J.-L., & Reich, P. B. (2006). *Dark respiration rate increases with plant size in saplings of three temperate tree species despite decreasing tissue nitrogen and nonstructural carbohydrates*. Tree Physiology, 26, 915–923. https://doi.org/10.1093/treephys/26.7.915

Mäkelä, A. (1997). *A Carbon Balance Model of Growth and Self-Pruning in Trees Based on Structural Relationships*. https://doi.org/10.1093/forestscience/43.1.7

Mäkelä, A. and Valentine, H. (2001). *The ratio of NPP to GPP: Evidence of change over the course of stand development*. Tree Physiology, 21, 1015–1030. https://doi.org/10.1093/treephys/21.14.1015

Mäkelä, A. and Valentine, H. T. (2020). *Models of tree and stand dynamics*. Springer International Publishing.

Mahnken M., Cailleret M., Collalti A., Trotta C., Biondo C., D'Andrea E., Dalmonech D., Marano G., Mäkelä A., Minunno F., Peltoniemi M., Trotsiuk V., Nadal-Sala D., Sabaté S., Vallet P., Aussenac R., Cameron D.R., Bohn F.J., Grote R., Augustynczik A.L.D., Yousefpour R., Huber N., Bugmann H., Merganičová K., Merganic J., Valent P., Lash-Born P., Hartig F., Vega del Valle I.D., Volkholz J., Gustch M., Matteucci G., Krejza J., Ibrom A., Meesenburg H., Rötzer T., van der Maaten-Theunissen M., van der Maaten E., Reyer C.P.O. (2022a). *Accuracy, realism and general applicability of European forest models*. Global Change Biology, https://doi.org/10.1111/gcb.16384

Mahnken M., Collalti A., Dalmonech D., Trotta C., Trtsiuk V., Augustynczik A.L.D., Yousefpour R., Gutsch M., Cameron D., Bugmann H., Huber N., Thrippleton T., Bohn F., Nada-Sala D., Sabatè S., Grote R., Mäkelä A., Minunno F., Peltoniemi M., Vallet P., Fabrika M.,Merganičová K., Vega del Valle I., Volkholz J., Reyer C.P.O. (2022b). *ISIMIP2a Simulation Data from Regional Forest Sector (v.1.0). ISIMIP repository*. https://doi.org/10.48364/ISIMIP.169780

Mahnken M., Collalti A., Dalmonech D., Trotta C., Trtsiuk V., Augustynczik A.L.D., Yousefpour R., Gutsch M., Cameron D., Bugmann H., Huber N., Thrippleton T., Bohn F., Nada-Sala D., Sabatè S., Grote R., Mäkelä A., Minunno F., Peltoniemi M., Vallet P., Fabrika M., Merganičová K., Vega del Valle I., Volkholz J., Reyer C.P.O. (2023). *ISIMIP2b SImulation Data from Regional Forest Sector (v.1.0). ISIMIP repository*. https://doi.org/10.48364/ISIMIP.185401

Mäkelä A, Valentine H (2000) *The ratio of NPP to GPP: evidence of change over the course of stand development*. Tree Physiology 21:1015–1030. https://doi.org/10.1093/treephys/21.14.1015

Mäkelä, A., Pulkkinen, M., Kolari, P., Lagergren, F., Berbigier, P., Lindroth, A., Loustau, D., Nikinmaa, E., Vesala, T., & Hari, P. (2008). *Developing an empirical model of stand GPP with the LUE approach: Analysis of eddy covariance data at five contrasting conifer sites in Europe*. Global Change Biology, 14(1), 92–108. https://doi.org/10.1111/j.1365-2486.2007.01463.x

Malhi, Y. (2012). *The productivity, metabolism and carbon cycle of tropical forest vegetation*. Journal of Ecology, 100, 65–75. https://doi.org/10.1111/j.1365-2745.2011.01916.x

Marano, G., Dalmonech, D. & Collalti, A. (2024). *Modeling Forest Response to Climate Change*. Forests 15, 1194. https://doi.org/10.3390/f15071194

Marconi, S., Collalti, A., Santini, M., & Valentini, R. (2013). *Simulating Carbon cycle and phenology in complex forests using a multi-layer process based ecosystem model; evaluation and use of 3D-CMCC-Forest Ecosystem Model in a deciduous and an evergreen neighboring forests, within the area of Brasschaat (Be)*. In AGU Fall Meeting Abstracts (Vol. 1, p. 0473).

Marconi S., Chiti T., Valentini R., Collalti A. (2014). *Assessing NEE and Carbon Dynamics among 5 European Forest types: Development and Validation of a new Phenology and Soil Carbon routines within the process-oriented 3D-CMCC-Forest-Ecosystem Model*. Ms.C. Master Thesis, University of Tuscia. https://doi.org/10.13140/2.1.5065.1848

Marconi, S., Chiti, T., Nolè, A., Valentini, R. and Collalti, A. (2017). *The role of respiration in the estimation of net carbon cycle: coupling soil carbon dynamics and canopy turnover in a novel version of 3D-CMCC forest ecosystem model.* Forests, 8(6), 220. https://doi.org/10.3390/f8060220

Marks, D., J., Dozier, et al. (1992). *Climate and energy exchange at the snow surface in the alpine region of the Sierra Nevada. I. Meteorology measurements and monitoring*. Water Resources Research 28(11): 3029-3042. https://doi.org/10.1029/92WR01482

Martínez-Vilalta, J., Sala, A., Asensio, D., Galiano, L., Hoch, G., Palacio, S., ... Lloret, F. (2016). *Dynamics of non-structural carbohydrates in terrestrial plants: A global synthesis*. Ecological Monographs, 86(4), 495–516. https://doi.org/10.1002/ecm.1231

Massoud, E. C., Xu, C., Fisher, R. A., Knox, R. G., Walker, A. P., Serbin, S. P., ... and Vrugt, J. A. (2019). *Identification of key parameters controlling demographically structured vegetation dynamics in a land surface model: CLM4. 5 (FATES)*. Geoscientific Model Development, 12(9), 4133-4164. https://doi.org/10.5194/gmd-12-4133-2019

McDowell, N. (2011). *Mechanism linking drought, hydraulics, carbon metabolism, and vegetation mortality*. Plant Physiology, 155, 1051–1059. https://doi.org/10.1104/pp.110.170704

Medlyn, B.E. (1998). *Physiological basis of the light use efficiency model*, Tree Physiology, 18(3), 167–176, https://doi.org/10.1093/treephys/18.3.167

Medlyn, B.E., Dreyer, E., Ellsworth, D., Forstreuter, M., Harley, P.C., Kirschbaum, M.U., et al. (2002). *Temperature response of parameters of a biochemically based model of photosynthesis. II. A review of experimental data*. Plant, Cell and Environment 25, 1167–117. https://doi.org/10.1046/j.1365-3040.2002.00891.x

Merganičová, K., Merganič, J., Lehtonen, A., Vacchiano, G., Sever, M. Z. O., Augustynczik A.L.D., Grote R., Kyselová I., Mäkelä A., Yousefpour R., Krejza J., Collalti A., Reyer C.P.O. (2019). *Forest carbon allocation modelling under climate change*. Tree Physiology, 39(12), 1937-1960. https://doi.org/10.1093/treephys/tpz105

Migliavacca, M., Musavi, T., Mahecha, M.D., et al. (2021). *The three major axes of terrestrial ecosystem function*. Nature 598, 468–472. https://doi.org/10.1038/s41586-021-03939-9

Monsi, M. and Saeki, T. (1953). *Über den lichtfaktorin den pflanzengesellschaften und seine bedeutung für die stoffproduktion*. Japanese Journal of Botany 14: 22–52.

Monteith, J. (1977). *Climate and the efficiency of crop production in Britain, London*. Philosophical Transactions of the Royal Society 281 (980), 277–294.

Monteith, J.L., Unsworth, M.H., (1990). *Principles of Environmental Physics,* 2nd ed. Arnold, London.

Monteith, J. L. and M. H. Unsworth (2008). *Principles of Environmental Physics, 3rd Edition*. Burlington, MA, Academic Press https://doi.org/10.3832/ifor1802-009

Moorcroft, P.R., G.C. Hurtt and S.W. Pacala, (2001). *A method for scaling vegetation dynamics: the ecosystem demography model ED*. Ecological Monographs 71.4, pp. 557-586. https://doi.org/10.1890/0012-9615(2001)071[0557:AMFSVD]2.0.CO;2

Morichetti M., Vangi E. & Collalti A. (2024). *Predicted Future Changes in the Mean Seasonal Carbon Cycle Due to Climate Change*. Forests, 15(7), 1124. https://doi.org/10.3390/f15071124

Muffler, L., Schmeddes, J., Weigel, R., Barbeta, A., Beil, I., Bolte, A., Buhk, C., Holm, S., Klein, G., Klisz, M., Löf, M., Peñuelas, J., Schneider, L., Vitasse, Y., Kreyling, J. (2021). *High plasticity in germination and establishment success in the dominant forest tree Fagus sylvatica across Europe*. Global Ecology and Biogeogreography. 30, 1583–1596. https://doi.org/10.1111/geb.13320

Muhr, J., Trumbore, S., Higuchi, N., & Kunert, N. (2018). *Living on borrowed time–Amazonian trees use decade-old storage carbon to survive for months after complete stem girdling*. New Phytologist, 220(1), 111-120. https://doi.org/10.1111/nph.15302

Natali, S., Collalti, A., Candini, A., Della Vecchia, A., & Valentini, R. (2012). *Assimilation of high resolution satellite imagery into the 3D-CMCC forest ecosystem model*. In EGU General Assembly Conference Abstracts. Vol. 14, EGU2012-11736

Nielsen, B.O. (1977). *Beech Seeds as an Ecosystem Component*. Oikos. ,29(2), 268.

Noce, S., Collalti, A., Valentini, R. and Santini, M. (2016). *Hot spot maps of forest presence in the Mediterranean basin.* iForest-Biogeosciences and Forestry, 9(5), 766, https://doi.org/10.3832/ifor1802-009

Nolè A., Collalti A., ..., Valentini R. (2015). *The Role of Managed Forest Ecosystems: A Modeling Based Approach*, Chapter 5 (pp 71-85), in *The Greenhouse Gas Balance of Italy, An Insight on Managed and Natural Terrestrial Ecosystems*, R. Valentini, F. Miglietta (eds), Environmental Science and Engineering, Springer-Verlag Berlin Heidelberg, ISSN 1863-5520, ISBN: 978-3-642-32424-6, https://doi.org/10.1007/978-3-642-32424-6_5

Oddou-Muratorio, S., Davi, H. and Lefèvre, F. (2020). *Integrating evolutionary, demographic and ecophysiological processes to predict the adaptive dynamics of forest tree populations under global change*. Tree Genetics and Genomes, 16(5), 67. https://doi.org/10.1007/s11295-020-01451-1

Odum, E. P. (1969). The Strategy of Ecosystem Development: An understanding of ecological succession provides a basis for resolving man's conflict with nature. *Science*, 164(3877), 262-270. https://doi.org/10.1126/science.164.3877.262

Oleson, K. W., Lawrence, D. M., Bonan, G. B., Drewniak, B., Huang, M., Koven, C. D., ... Yang, Z.-L. (2013). *Technical description of version 4.5 of the community land model (CLM)*. Ncar Technical Note NCAR/TN-503+STR. Boulder, CO: National Center for Atmospheric Research, 422 pp

Pallardy, S. G. (2010). *Physiology of woody plants*. New York, NY: Academic Press.

Pappas, C., Fatichi S., Leunziger S., Wolf A., Burlando P.. (2013). *Sensitivity analysis of a process-based ecosystem model: Pinpointing parameterization and structural issues*. Journal of Geophysical Research: Biogeosciences 118:505–528. https://doi.org/10.1002/jgrg.20035

Parton, W.J., Schimel, D.S., Cole, C.V., Ojima, D.S., 1987. *Analysis of factors controlling soil organic matter levels in Great Plains grasslands.* Soil Sci. Soc. Am. J. 51, 1173e1179. https://doi.org/10.2136/sssaj1987.03615995005100050015x

Parton W J, Scurlock J M O, Ojima D S et al.. *Observations and modeling of biomass and soil organic matter dynamics for the grassland biome worldwide*. Global BioGeochemical Cycles. 1993 https://doi.org/10.1029/93GB02042

Parton, W.J., Ojima, D.S., Cole, C.V., Schimel, D.S., 1994a. *A general model for soil organic matter dynamics: sensitivity to litter chemistry, texture and management*. In: Quantitative Modeling of Soil Forming Processes. SSSA, Spec. Pub. 39, Madison, WI, pp. 147e167. https://doi.org/10.2136/sssaspecpub39.c9

Parton WJ, Haxeltine A, Thornton P, Hartman M. *Ecosystem sensitivity to land-surface models and leaf area index.* Global Planetary Change. 1996 https://doi.org/10.1016/0921-8181(95)00040-2

Pastorello, G., Trotta, C., Canfora, E., Chu, H., Christianson, D., Cheah, Y. W., ... and Law, B. (2020). *The FLUXNET2015 dataset and the ONEFlux processing pipeline for eddy covariance data*. Scientific data, 7(1), 225. https://doi.org/10.1038/s41597-020-0534-3

Pellicone, G., Scarascia-Mugnozza, G., Matteucci, G., Collalti, A. (2018). *Climate change mitigation by forests: a case study on the role of management on carbon dynamics of a pine forest in South Italy*. Ph.D. Thesis, University of Tuscia, 2018. https://10.13140/RG.2.2.25155.96805, https://dspace.unitus.it/handle/2067/42735

Pianosi, F., Beven K., Freer J., Hall J., Rougier J., Stephenson D., Wagener T. (2016). *Sensitivity analysis of environmental models: A systematic review with practical workflow*. Environmental Modelling and Software 79:214–232. https://doi.org/10.1016/j.envsoft.2016.02.008

Pietsch, S., Hasenauer, H., Thornton, P. (2005). *BGC-model parameters for tree species growing in central European forests*. Forest Ecology and Management 211, 264–295, https://doi.org/10.1016/j.foreco.2005.02.046

Pomeroy, J. W., Parviainen, J., Hedstrom, N. and Gray, D. M. (1998). *Coupled modelling of forest snow interception and sublimation*. Hydrological Processes, 12(15), 2317-2337. https://doi.org/10.1002/(SICI)1099-1085(199812)12:15%3C2317::AID-HYP799%3E3.0.CO;2-X

Poulter, B., Hattermann, F., Hawkins, E. D., Zaehle, S., Sitch, S., Restrepo-Coupe, N. ... and Cramer, W. (2010). *Robust dynamics of Amazon dieback to climate change with perturbed ecosystem model parameters*. Global Change Biology, 16(9), 2476-2495. https://doi.org/10.1111/j.1365-2486.2009.02157.x

Pretzsch H. (2005) *Stand density and growth of Norway spruce (Picea abies (L.) Karst.) and European beech (Fagus sylvatica L.). Evidence from long-term experimental plot*s. European Journal of Forest Research 124: 193–205 https://doi.org/10.1007/s10342-005-0068-4

Pretzsch H. (2009). *Forest dynamics, growth, and yield*. Vol. 684. Berlin: Springer. https://doi.org/10.1007/978-3-540-88307-4

Puchi, P.F., Dalmonech, D., Vangi, E. Battipaglia G., Tognetti R. and Collalti A. (2024). *Contrasting patterns of water use efficiency and annual radial growth among European beech forests along the Italian peninsula*. Scientific Reports 14, 6526. https://doi.org/10.1038/s41598-024-57293-7

Purves, D.W. Lichstein, J. W., Strigul, N. and Pacala, S. W. (2008). *Predicting and understanding forest dynamics using a simple tractable model*. Proceedings of the National Academy of Sciences 105.44, pp. 17018-17022. https://doi.org/10.1073/pnas.0807754105

Reich, P. B., Tjoelker, M. G., Machado, J.-L. and Oleksyn, J. (2006). *Universal scaling of respiratory metabolism, size and nitrogen in plants*. Nature, 439, 457–461. https://doi.org/10.1038/nature 04282

Reich, P., Sendall, K., Stefanski, A., Wei, X., Rich, R. L. and Montgomery, R. A. (2016). *Boreal and temperate trees show strong acclimation of respiration to warming*. Nature, 531(7596), 633–636. https://doi.org/10.1038/nature17142

Reyer, C. P. O., Silveyra Gonzalez, R., Dolos, K., Hartig, F., Hauf, Y., Noack, M., Lasch-Born, P., Rötzer, T., Pretzsch, H., Meesenburg, H., Fleck, S., Wagner, M., Bolte, A., Sanders, T. G. M., Kolari, P., Mäkelä, A., Vesala, T., Mammarella, I., Pumpanen, J., Collalti, A., Trotta, C., Matteucci, G., D'Andrea, E., Foltýnová, L., Krejza, J., Ibrom, A., Pilegaard, K., Loustau, D., Bonnefond, J.-M., Berbigier, P., Picart, D., Lafont, S., Dietze, M., Cameron, D., Vieno, M., Tian, H., Palacios-Orueta, A., Cicuendez, V., Recuero, L., Wiese, K., Büchner, M., Lange, S., Volkholz, J., Kim, H., Horemans, J.A., Bohn, F., Steinkamp, J., Chikalanov, A., Weedon, G. P., Sheffield, J., Babst, F., Vega del Valle, I., Suckow, F., Martel, S., Mahnken, M., Gutsch, M. and Frieler, K. (2020). *The PROFOUND Database for evaluating vegetation models and simulating climate impacts on European forests,* Earth System Science Data, 12, 1295–1320, https://doi.org/10.5194/essd-12-1295-2020

Ryan, M.G., Binkley, D. and Fownes, J.H. (1997). *Age-related decline in forest productivity: pattern and process*. Advances in ecological research, 27, 213-262. https://doi.org/10.1016/S0065-2504(08)60009-4

Rowland, L., da Costa, A. C. L., Galbraith, D.R., Oliveira, R.S., Binks, O. J., Oliveira, A.A.R., Pullen, M., Doughty, C.E., Metcalfe, D.B., Vasconcelos, S.S., Ferreira, L.V., Malhi, Y., Grace, J., Mencuccini M. and Meir, P. (2015). *Death from drought in tropical forests is triggered by hydraulics not carbon starvation*. Nature, 528, 119–122. https://doi.org/10.1038/nature15539

Running, S. W. and Coughlan J. C. (1988). *A general model of forest ecosystem processes for regional applications I. Hydrologic Balance, Canopy Gas Exchange and Primary Production Processes*. Ecological Modelling 42: 125-154. https://doi.org/10.1016/0304-3800(88)90112-3

Sala, A., Woodruff, D. R. and Meinzer, F. C. (2012). *Carbon dynamics in trees: Feast or famine?* Tree Physiology, 32, 764–775. https://doi.org/10.1093/treephys/tpr143

Sands, P.J. (1995). *Modelling Canopy Production. II. From single-leaf photosynthetic parameters to daily canopy photosynthesis*. Australian Journal of Plant Physiology 22, 603–614. https://doi.org/10.1071/PP9950603

Saponaro V., De Càceres M., Dalmonech D., D'Andrea E., Vangi E. and Collalti A. (2024). *Assessing models' sensitivity to the effects of forest management and climate change on carbon and water fluxes in European beech forests.* bioRxiv, https://doi.org/10.1101/2024.08.20.608827

Sato, H., Itoh, A., and Kohyama, T. (2007). *SEIB–DGVM: A new Dynamic Global Vegetation Model using a spatially explicit individual-based approach*. Ecological Modelling, 200, 279–307. https://doi.org/10.1016/j.ecolmodel.2006.09.006

Schiestl-Aalto, P., Ryhti, K., Mäkelä, A., Peltoniemi, M., Bäck, J. and Kulmala, L. (2019). *Analysis of the NSC storage dynamics in tree organs reveals the allocation to belowground symbionts in the framework of whole tree carbon balance*. Frontiers in Forests and Global Change, 2, 17. https://doi.org/10.3389/ffgc.2019.00017

Schwalm, C.R. and Ek, A.R. (2004). *A process-based model of forest ecosystems driven by meteorology*. Ecological Modelling, 179, 317–348. https://doi.org/10.1016/j.ecolmodel.2004.04.016

Sellers, P.J., Berry, J.A., Collatz, G.J., Field, C.B., Hall, F.G. (1992). *Canopy reflectance, photosynthesis and transpiration. III. A reanalysis using improved leaf models and a new canopy integration scheme*. Remote Sensing of Environment 42, 187–216. https://doi.org/10.1016/0034-4257(92)90102-P

Shinozaki, K., Yoda, K., Hozumi, K. and Kira, T. (1964a). *A quantitative analysis of plant form-the pipe model theory, I Basic analyses,* Japanese J. Ecol., 4, 97–105. https://doi.org/10.18960/seitai.14.3_97

Shinozaki, K., Yoda, K., Hozumi, K. and Kira, T. (1964b) *A quantitative analysis of plant form-the pipe model theory. II. Further evidence of the theory and its application in forest ecology*. Japanese J. Ecol., 14, 133–139, https://doi.org/10.18960/seitai.14.4_133

Sitch, S., Smith, B., Prentice, I. C., Arneth, A., Bondeau, A., Cramer, W., ... & Venevsky, S. (2003). *Evaluation of ecosystem dynamics, plant geography and terrestrial carbon cycling in the LPJ dynamic global vegetation model*. Global Change Biology, 9(2), 161-185. https://doi.org/10.1046/j.1365-2486.2003.00569.x

Smith, B. (2001). *LPJ-GUESS-an ecosystem modelling framework*. Department of Physical Geography and Ecosystems Analysis, INES, Sölvegatan, 12(22), 362.https://web.nateko.lu.se/lpj-guess/guess.pdf

Smith, A. M., & Stitt, M. (2007). *Coordination of carbon supply and plant growth. Plant, Cell & Environment*, 30, 1126–1149. https://doi.org/10.1111/j.1365-3040.2007.01708.x

Smith, N. and Dukes, J. (2012). *Plant respiration and photosynthesis in global-scale models: incorporating acclimation and CO_2*. Global Change Biology, 19: 45-63, https://doi.org/10.1111/j.1365-2486.2012.02797.x

Spicer, R., & Holbrook, N. M. (2007). *Parenchyma cell respiration and survival in secondary xylem: does metabolic activity decline with cell age?*. Plant, Cell & Environment, 30(8), 934-943. https://doi.org/10.1111/j.1365-3040.2007.01677.x

Stockfors J., Linder S. (1998). *Effect of nitrogen on the seasonal course of growth and maintenance respiration in stems of Norway spruce trees*. Tree Physiology, 18: 155–166. https://doi.org/10.1093/treephys/18.3.155

Taiz, L. and Zeiger, E. (2006). *Plant Physiology*. Sunderland, MA, Sinauer Associates, Inc., Publishers

Tang, J., Luyssaert, S., Richardson, A. D., Kutsch, W., & Janssens, I. A. (2014). Steeper declines in forest photosynthesis than respiration explain age-driven decreases in forest growth. *Proceedings of the National Academy of Sciences*, 111(24), 8856-8860. https://doi.org/10.1073/pnas.1320761111

Testolin, R., Dalmonech, D., Marano, G., Bagnara, M., D'Andrea, E., Matteucci, G., Noce S., Collalti, A. (2023). *Simulating diverse forest management options in a changing climate on a Pinus nigra subsp. laricio plantation in Southern Italy*. Science of The Total Environment, 857, 159361. https://doi.org/10.1016/j.scitotenv.2022.159361

Thornton, P. E. (1998). *Regional Ecosystem Simulation: Combining Surface- and Satellite- Based Observations to Study Linkages between Terrestrial Energy and Mass Budgets*. Ph.D Thesis, University of Tuscia. College of Forestry. Missoula, MT, The University of Montana. https://scholarworks.umt.edu/cgi/viewcontent.cgi?referer=&httpsredir=1&article=11555&context=etd

Thornton, P. E., Law, B. E., Gholz, H. L., Clark, K. L., Falge, E., Ellsworth, D. S., ... and Sparks, J. P. (2002). *Modeling and measuring the effects of disturbance history and climate on carbon and water budgets in evergreen needleleaf forests*. Agricultural and forest meteorology, 113(1-4), 185-222. https://doi.org/10.1016/S0168-1923(02)00108-9

Thornton, P.E. and Rosenbloom, N.A. (2005). E*cosystem model spin-up: Estimating steady state conditions in a coupled terrestrial carbon and nitrogen cycle model*. Ecological Modelling 189(1-2): 25-48, https://doi.org/10.1016/j.ecolmodel.2005.04.008

Thornton, P.E. and Zimmermann, N.E. (2007) *An Improved Canopy Integration Scheme for a Land Surface Model with Prognostic Canopy Structure*. Journal of Climate, 20, 3902-3923, https://doi.org/10.1175/JCLI4222.1

Thornton, P. E., Lamarque, J., Rosenbloom, N. and Mahowald, N. (2007). *Influence of carbon-nitrogen cycle coupling on land model response to CO_2 fertilization and climate variability*. Global Biogeochemical Cycles, 21, GB4018. https://doi.org/10.1029/2006GB002868

Thornton, P. E.: Biome BGC version 4.2: Theoretical Framework of Biome-BGC, 2010

Thurner, M., Beer, C., Ciais, P., Friend, A. D., Ito, A., Kleidon, A., …, Carvalhais, N. (2017). *Evaluation of climate-related carbon turnover processes in global vegetation models for boreal and temperate forests*. Global Change Biology, 23(8), 3076–3091. https://doi.org/10.1111/gcb.13660

Tjoelker, M., Olesksyn, J., and Reich, P. (2001). *Modelling respiration of vegetation: Evidence for a general temperature-dependent Q10*. Global Change Biology, 7(2), 223–230. https://doi.org/10.1046/j.1365-2486.2001.00397.x

Trotta, C., Collalti, A., Santini, M., Biondo, C., Regni, L., & Brunori, A. (2018). *3D-CMCC-OLIVE: a process-based model to analyze the effects of the human activities and climate changes in olive orchards*. In AGU Fall Meeting Abstracts, Vol. 2018, pp. B33E-2703.

Trotta, C., Collalti, A., Biondo, C., Pellicone, G., Matteucci, G., Brunori, A., & Proietti, P. (2019). *Estimation the olive trees traits combining Bayesian calibration, model and climatic drivers*. In EGU General Assembly Conference Abstracts, Vol. 21, EGU2019-15872.

Uusitalo, L., Lehikoinen A., Helle I. and Myrberg K. (2015). *An overview of methods to evaluate uncertainty of deterministic models in decision support*. Environmental Modelling and Software 63:24–31. https://doi.org/10.1016/j.envsoft.2014.09.017

Vacchiano, G., Magnani, F. and Collalti, A. (2012). *Modeling Italian forests: state of the art and future challenges*. IForest, 5(3), 113-120. https://doi.org/10.3832/ifor0614-005

Vacchiano, G., Ascoli, D., Berzaghi, F., Lucas-Borja, M. E., Caignard, T., Collalti, A., Mairota, P., Palaghianu, C., Reyer, C.P.O., Sanders, T.G.M., Schermer, E., Wohlgemuth, T. and Hacket-Pain, A. (2018). *Reproducing reproduction: How to simulate mast seeding in forest models.* Ecological Modelling, 376, 40-53. https://doi.org/10.1016/j.ecolmodel.2018.03.004

Vangi, E., Dalmonech, D., Cioccolo, E., Marano, G., Bianchini, L., Puchi, P.F., ... and Collalti, A. (2024a). *Stand age diversity (and more than climate change) affects forests' resilience and stability, although unevenly*. Journal of Environmental Management, 366:121822 https://doi.org/10.1016/j.jenvman.2024.121822

Vangi E., Dalmonech D., Morichetti M., Grieco E., Giannetti F., D'Amico G., Chirici G., Collalti A. (2024b). *Stand Age and Climate Change Effects on Carbon Increments and Stock Dynamics*. Forests, 15(7), 1120. https://doi.org/10.3390/f15071120

Vangi E., Dalmonech D., Collalti A. (2024c). *R3DFEM: an R package for running the 3D-CMCC-FEM model.* bioRxiv 2024.10.07.616968; https://doi.org/10.1101/2024.10.07.616968

Van Oijen, M., Schapendonk, A., Höglind, M. (2010). *On the relative magnitudes of photosynthesis, respiration, growth and carbon storage in vegetation*. Annals of Botany, 105(5), 793-797. https://doi.org/10.1093/aob/mcq039

Veroustraete, F. (1994). *On the use of ecosystem modelling for the interpretation of climate change effects at the ecosystem level*. Ecological Modelling, 75-76, 221–237.

Veroustraete, F., Sabbe, H. and Eerens, H. (2002). *Estimation of carbon mass fluxes over Europe using C-Fix model and Euroflux data*. Remote Sensing of Environment, 83(3), 376–399. https://doi.org/10.1016/S0034-4257(02)00043-3

Vicca S, Luyssaert S et al. (2012). *Fertile forests produce biomass more efficiently*. Ecology Letters 15:520–526. https://doi.org/10.1111/j.1461-0248.2012.01775.x

von Arx, G., Arzac, A., Fonti, P., Frank, D., Zweifel, R., Rigling, A., Galiano, L., Gessler, A. and Olano, J. M. (2017). *Responses of sapwood ray parenchyma and non-structural carbohydrates of Pinus sylvestris to drought and long-term irrigation*. Functional Ecology, *31*(7), 1371–1382. https://doi.org/10.1111/1365-2435.12860

von Arx, G., Arzac, A., Olano, J. M. and Fonti, P. (2015). *Assessing Conifer Ray Parenchyma for Ecological Studies: Pitfalls and Guidelines*. Frontiers in Plant Science, *6:1016*, 1–10. https://doi.org/10.3389/fpls.2015.01016

Von Bertalanffy, L. (1957). *Quantitative laws in metabolism and growth.* The quarterly review of biology, 32(3), 217-231.

Vorspernik E.M., Toigo M., Morin X., Tomao A., Trotta C., Steckel M., Barbati A., Nothdurft A., Trezsch H, del Rio M., Skrzyszewski J., Ponette Q., Lof M., Jansons A., Brazaitis G. (2021). *Simulating the effects of thinning*

and species mixing on stands of oak (Quercus petrea (Matt.) Liebl. / Quercus robur L.) and pine (Pinus sylvestris L.) across Europe. Ecological Modelling, https://doi.org/10.1016/j.ecolmodel.2020.109406

Wang, K. S. (2003). *Relationship between empty seed and genetic factors in European beech (Fagus sylvatica L.)*. Silva Fennica 37 :419-428. https://doi.org/10.14214/sf.481

Waring, R. and Landsberg, J. (1998). *Net primary production of forests: a constant fraction of gross primary production?* Tree Physiology, 18, 129–134, https://doi.org/10.1093/treephys/18.2.129

Waring, R. and McDowel, N. (2002). *Use of a physiological process model with forestry yield tables to set limits on annual carbon balances*, Tree Physiology, 22, 179–188

Waring, R. H. and S. W. Running (2007). *Forest Ecosystems: Analysis at Multiple Scales*. San Francisco, CA, Elsevier Academic Press.

Warnant, P., François, L., Strivay, D., & Gérard, J.-C. (1994). *CARAIB: A global model of terrestrial biological productivity*. Global Biochemical Cycles, 8(3), 255–270. https://doi.org/10.1029/94gb00 850

Weber, R., Schwendener, A., Schmid, S., Lambert, S., Wiley, E., Landhäusser, S. M., …, and Hoch, G. (2018). *Living on next to nothing: Tree seedlings can survive weeks with very low carbohydrate concentration*. New Phytologist, 218, 107–118. https://doi.org/10.1111/nph.14987

Weng, E. S., Malyshev, S., Lichstein, J. W., Farrior, C. E., Dybzinski, R., Zhang, T., Shevliakova,E. and Pacala, S. W. (2015). *Scaling from individual trees to forests in an Earth system modeling framework using a mathematically tractable model of height-structured competition*. Biogeosciences, 12(9), 2655-2694. https://doi.org/10.5194/bg-12-2655-2015

West, P.W., Wells, K.F., Cameron, D.M. Rance, S.J., Turnbull, C.R.A. and Beadle C.L. (1991). *Predicting tree diameter and height from above-ground biomass for four eucalypt species.* Trees 5, 30–35 . https://doi.org/10.1007/BF00225332

Wiley, E. and Helliker, B. (2012). *A re-evaluation of carbon storage in trees lends greater support for carbon limitation to growth*. New Phytologist, 195, 285–289. https://doi.org/10.1111/j.1469-8137.2012.04180.x

Wiley, E., Hoch, G. and Landhäusser, S. M. (2017). *Dying piece by piece: Carbohydrate dynamics in aspen (Populus tremuloides) seedlings under severe carbon stress*. Journal of Experimental Botany, 68(18), 5221–5232. https://doi.org/10.1093/jxb/erx342

Wythers, K. R., Reich, P. B., & Bradford, J. B. (2013). *Incorporating temperature-sensitive Q10 and foliar respiration acclimation algorithms modify modeled ecosystem responses to global change*. Journal of Geophysical Research: Biogeosciences, 118, 1–14. https://doi.org/doi:10.1029/2011JG001897

Wu, J., Larsen, K., van der Linden, L., Beier, C., Pilegaard, K. and Ibrom, A. (2013). *Synthesis on the carbon budget and cycling in a Danish, temperate deciduous forest*. Agricultural and Forest Meteorology, 181, 94–107. https://doi.org/10.1016/j.agrformet.2013.07.012

Yoda, K. (1963). *Self-thinning in overcrowded pure stands under cultivated and natural conditions (Intraspecific competition among higher plants XI.)*. J. Biol. Osaka City Univ. D., 14, 107-129.

INDEX

Regeneration	3.11
S	
Soil evaporation	4.5
Soil organic matter	3.13
Soil water balance	4.7
Snow	4.2 - 4.3
Stomatal conductance	4.4 - 5
T	
Turnover	3.8.3
V	
Volume	6.7
W	
Water budget	4
Water use efficiency	3.7